Development of Flight Test Instrumentation for Inflatable Wings and Aerodynamic Characterization Through Local Pressure Differential Analysis

DIEGO MUNIZ BENEDETTI

TESE DE DOUTORADO EM CIÊNCIAS MECÂNICAS
DEPARTAMENTO DE ENGENHARIA MECÂNICA

FACULDADE DE TECNOLOGIA
UNIVERSIDADE DE BRASÍLIA

UNIVERSIDADE DE BRASÍLIA
FACULDADE DE TECNOLOGIA
DEPARTAMENTO DE ENGENHARIA MECÂNICA

TESE DE DOUTORADO EM CIÊNCIAS MECÂNICAS

Development of Flight Test Instrumentation for Inflatable Wings and Aerodynamic Characterization Through Local Pressure Differential Analysis

DIEGO MUNIZ BENEDETTI

ORIENTADOR: CARLOS ALBERTO GURGEL VERAS

PUBLICAÇÃO ENM-DT 01/2021

Brasília, 26 de Janeiro de 2021

UNIVERSIDADE DE BRASÍLIA
FACULDADE DE TECNOLOGIA
DEPARTAMENTO DE ENGENHARIA MECÂNICA

TESE DE DOUTORADO EM CIÊNCIAS MECÂNICAS

Development of Flight Test Instrumentation for Inflatable Wings and Aerodynamic Characterization Through Local Pressure Differential Analysis

DIEGO MUNIZ BENEDETTI

Tese de doutorado submetida ao Departamento de Engenharia Mecânica da Faculdade de Tecnologia da Universidade de Brasília como parte dos requisitos para a obtenção do título de Doutor.

Banca Examinadora

Prof. Carlos Alberto Gurgel Veras, Ph.D.	(orientador)
Prof. Antônio César Pinho Brasil Jr., Ph.D.	(examinador)
Prof. Ricardo Luiz Utsch de Freitas Pinto, Ph.D.	(examinador)
Prof. Cristiano Viana Serra Villa, Ph.D.	(examinador)
Prof. Fábio Alfaia da Cunha, Ph.D.	(examinador)

Brasília, 26 de janeiro de 2021

FICHA CATALOGRÁFICA

BENEDETTI, DIEGO MUNIZ

Development of Flight Test Instrumentation for Inflatable Wings and Aerodynamic Characterization Through Local Pressure Differential Analysis. [Distrito Federal]

2021.

99p., 210 x 297 mm (ENM/FT/UnB, Doutor, Ciências Mecânicas, 2021)

Tese de Doutorado – Universidade de Brasília. Faculdade de Tecnologia.

Departamento de Engenharia Mecânica.

1. Instrumentação	2. Asas infláveis
3. Aerodinâmica	4. Sensores de pressão diferencial
I. ENM/FT/UnB	II. Título (ENM-DT 01/2021)

REFERÊNCIA BIBLIOGRÁFICA

BENEDETTI, D. M., (2021) Development of Flight Test Instrumentation for Inflatable Wings and Aerodynamic Characterization Through Local Pressure Differential Analysis. Tese de doutorado, Publicação ENM-DM 01/2021, Departamento de Engenharia Mecânica, Universidade de Brasília, DF, 99p.

CESSÃO DE DIREITOS

AUTOR: Diego Muniz Benedetti.

TÍTULO: Development of Flight Test Instrumentation for Inflatable Wings and Aerodynamic Characterization Through Local Pressure Differential Analysis.

GRAU: Doutor ANO: 2021

_____

Diego Muniz Benedetti

Correio Eletrônico: diegobenedetti@gmail.com

Resumo

Este trabalho apresenta o desenvolvimento de um sistema de instrumentação para medição *"in-situ"* do diferencial de pressão interno-externo nas superfícies superior e inferior de asas dinamicamente infláveis.

O sistema é composto por sensores de pressão diferencial, pesando cerca de sete gramas cada, alinhados em série compondo uma fita de medição que transmite dados em tempo real por meio de um protocolo de comunicação sem fio. Os testes em túnel de vento demonstraram a capacidade de leitura de baixos diferenciais de pressão na faixa de 1,0 a 120 Pa em um aerofólio do tipo ASCENDER. Os testes cobriram condições de voo representativas da operação dos principais sistemas de asas dinamicamente infláveis, com velocidades variando de 3 a 10 m / s e ângulos de ataque entre -20 e +25 graus. Foram obtidas leituras estáveis com coeficiente de variação entre 2% e 7% no envelope operacional de voo.

Os dados permitiram confirmar a existência de um limiar de inflagem e uma mudança abrupta no perfil de distribuição de pressão quando a incidência mínima é atingida. As singularidades aerodinâmicas observadas confirmaram a ocorrência de uma bolha de recirculação no bordo de ataque resultando uma queda expressiva na sustentação e aumento no arrasto. A aproximação do estol apresentou características aerodinâmicas semelhantes às asas rígidas e pode ser didaticamente evidenciada pelos dados de ensaio.

Um modelo teórico para a distribuição do coeficiente de pressão externo ao longo de aerofólios abertos foi proposto com base em estimativas da estrutura do fluxo de ar confinado. A curva de sustentação derivada do modelamento se mostrou compatível com dados anteriores e com dados do perfil rígido de referência.

A estabilidade de forma do aerofólio e os distúrbios de camada limite devido à fixação de componentes também foram avaliados, antecipando a adequação da instrumentação para aplicações em voo. Em geral, pode-se afirmar que a instrumentação pode ser aplicada imediatamente às asas infláveis, para uso como ferramenta de ensaio em voo e como sistemas de segurança que vão desde alertas de pré-colapso até sistemas complexos de aumento de estabilidade.

Abstract

This work presents the development of an advanced instrumentation system for in-situ measurement of the inner-outer pressure differential at the upper and lower surfaces of dynamically inflatable wings.

The system relied on differential pressure sensors, of about seven grams each, placed along a foil cell to transmit real-time data through a wireless protocol. Wind tunnel tests demonstrated the full capability of low-pressure differential readings in the range of 1.0 to 120 Pa at an ASCENDER airfoil. The tests covered representative flight conditions with speeds varying from 3 to 10 m/s at angles of attack from -20 to +25 degrees. Stable readings with coefficient of variation from 2% to 7% were obtained over the operational flight envelope.

Data allowed confirming the existence of an inflation threshold and an abrupt change on pressure distribution profile when inflation minimum is achieved. Observed aerodynamic singularities confirmed the occurrence of a relevant bottom leading edge recirculation bubble, which leads to expressive drop in lift and increase in drag. Stall approach presented aerodynamic characteristics similar to rigid wings, preceding the loss of shape stability.

A theoretical model for pressure coefficient distribution along open-airfoils was proposed based on estimations of the confined airflow structure. Calculated wing lift forces and loads were compatible with practical observation.

Airfoil shape stability and boundary layer disturbances due to components attachment were also evaluated, anticipating the instrumentation's suitability for in-flight applications. As a whole, the instrumentation may be applied straightforwardly to actual inflatable wings to be used as a flight test appliance and to improve their safety as a stability augmentation system or a collapse alert and prevention tool.

Acknowledgements

I would like to acknowledge the constant support of Professor Gurgel Veras, who played a fundamental role on developing the present theses, providing all the support required and working as an effective mentor.

I thank my family for the support and comprehension through the years of development, and, especially, to my first daughter, Heloisa, which is expected in our life as the most important project for the years to come.

Publications and Conferences

Benedetti, D.M.; Veras, C.A.G. ***Wind-Tunnel Measurement of Differential Pressure on the Surface of a Dynamically Inflatable Wing Cell***. Aerospace 2021, 8, 34. https://doi.org/10.3390/aerospace8020034

Contents

List of Figures

List of Tables

Nomenclature

a_κ: Internal pressure equation parameter at upper surface
AOA: Angle of attack
b: Test bench characteristic dimension - lateral
b_κ: Internal pressure equation parameter at bottom surface
c: Test bench characteristic dimension - longitudinal
C_p: Pressure coefficient
$\widetilde{C_p}$: Pressure coefficient differential
$C_{p_{max}}$: Maximum pressure coefficient
Cp_b: Pressure coefficient on the bottom surface
Cp_u: Pressure coefficient on the upper surface
g: Gravity acceleration
p: Bottom pressure coefficient equation – parametric adjustment parameter
q: Bottom pressure coefficient equation – parametric adjustment parameter
P_{atm}: Atmospheric pressure
P_e: Local external pressure
q_∞: Dynamic pressure
$\tilde{q}$: Pressure differential
r_c: Cell's cross-section equivalent radius
r_i: Area of influence equivalent radius
r_s: Sensor's surface equivalent radius
S_{tunnel}: Wind tunnel sectional reference area
t_f: Fabric thickness
V_∞: Undisturbed airflow speed
x: Chord position
W: Weight
α_b: Bottom pressure coefficient equation – parametric adjustment parameter
α_u: Upper pressure coefficient equation – parametric adjustment parameter
β_b: Bottom pressure coefficient equation – parametric adjustment parameter
β_u: Upper pressure coefficient equation – parametric adjustment parameter
δ: Deflection
$\delta_{(x)}$: Thickness of boundary layer
δ_b: Bottom pressure coefficient equation – parametric adjustment parameter
Δ_p: Differential pressure
$\epsilon_{\%}$: Sensor's resolution
γ_b: Bottom pressure coefficient equation – parametric adjustment parameter
γ_u: Upper pressure coefficient equation – parametric adjustment parameter
κ: Internal flow factor
κ_b: Bottom surface internal flow factor
κ_u: Upper surface internal flow factor
μ_c: Air kinetic viscosity
ρ_{air}: Air density (specific mass)
τ: Longitudinal stress

1. Introduction

Application of paragliders, parafoils, ram-air parachutes, and other dynamically inflatable wings increased drastically in the past thirty years [1-3]. Back to the origins of the 1960s, inflatable wings were born as deceleration systems, for which no performance or flight qualities aspects were relevant. However, evolution turned flexible wing more similar to the conventional rigid counterpart, making aerodynamic efficiency, stability, and maneuverability, essential design requirements.

Instead of merely assuring a softer landing, inflatable wings evolved into efficient, maneuverable air sport vehicles, also applied for dragging ships, running wind power generators, positioning of military troops and cargo, and recovering of launch vehicle parts. Fig. 1 below illustrates some recent applications of inflatable wings.

Figure 1: Application of dynamically inflatable wings

A recent instance can be seen in the work of Dek et al. [4] who proposed a recovery system for key components of the first stage of a heavy launch vehicle based on a particular deceleration system. As calculated by the authors, the mission could be accomplished using a parafoil with a surface area of about 836 m^2. This practical application illustrates a trend on aerospace industry. The high costs of satellite parts and launching vehicles components has been a relevant issue justifying the developments of solutions based on maneuverable inflatable wings. The flight from stratospheric heights up to a defined recovering point is challenging due to the extreme variation in wind conditions throughout the descent. Multidirectional gusts frequently result wing collapse or tangling. Therefore, designing more stable and controllable wings become a target directly associated to reducing operational cost.

Despite of the noticeable evolution on the range of applications, the development of inflatable-flexible wings is still quite empirical and the associated technology restricted to manufacturers, which means, the level of public aeronautical knowledge about the science behind these systems is very limited when compared with the wide literature about rigid wings.

There are no design manuals for inflatable wings, or public cataloged data for design optimization. Therefore, studding these wings represents an opportunity for research and innovation. Table 1 lists the main characteristics differentiating rigid and inflatable wings.

Table 1. Main characteristics differentiating rigid and inflatable wings.

	Rigid Fixed − Wing	**Dynamically Inflatable Wing**
Structural aspects	Rigid materials provide enough stiffness for all expected in-flight conditions by design.	The inflatable nature makes folding and wing collapse a constant risk imposing additional in-flight limits
Aerodynamics	Airflow characteristics are fully defined by geometry, airspeed and incidence.	Airflow is substantially affected by the air intake, the internal flow, and in-flight elastic deformations.
Flight dynamics	Six degree-of-freedom models are normally enough to fully describe wing's motion.	Relative motion between the wing and center of gravity in pendular systems adds complexity to the model.
Performance	The wide range of optimized airfoils allows reaching excellent levels of performance.	The presence of an air intake and the dynamic shape deformation imposes severe performance penalties.
Design and optimization tools	The rigid structure makes easy the use of conventional flight-test equipment and standard computational models.	The inflatable-flexible nature imposes severe restrictions to instrumentation and demands considering internal flow in computational models.
Modelling complexity	Shape stability allows using geometric-based aerodynamic coefficients for modelling the wing.	Elastic deformations and extreme flexibility limit the use of conventional aerodynamic approaches.

One of the most challenging aspects of fully flexible wings is the deforming geometry. Unlike rigid wings, parafoils and paragliders exhibit singular aerodynamic phenomena linked to their particular operational nature [5]. Of relevant concern, the in-flight shape deformability leads to constant variation on aerodynamic characteristics in flight. This makes almost impossible to derive accurate aerodynamic coefficients for performance and stability analysis, and then, it becomes unworthy to try modeling the wing based only on rigid airfoil data. It also leads to important limitations for under-design optimization using classic CFD methods, since the deformable surface plays a decisive role in the fluid-structure interaction process. As shape is profoundly modified in flight, models based on rigid airfoil data becomes unrealistic. Even a variable airfoil modelling lacks accuracy due to the absence of internal flow and fluid-structure considerations.

The shape deformability imposes also a safety issue when it culminates in collapse situations. Collapses are not rare, and can be induced by atmospheric disturbances or by command inputs. Understanding the wing's collapse mechanism is the first step to designing systems for alert and prevention.

In terms of wing performance, the air-intake openings at the leading edge of the airfoil result in a significant drawback on aerodynamic efficiency [6]. The presence of an open section at the most noble region of the airfoil results perceptible lift reduction and severe drag increase. It also add complexity to the system, by introducing an internal component of recirculation flow, absent in closed airfoils. The air intake is, of course, needed for inflation. The inflation phenomenon provides wing stiffness in flight, and this inflation mechanism imposes additional flight envelope constraints regarding the angle of attack (AOA) and speed ranges [7]. In addition to conventional aerodynamic limits dictated by flow detachment, for inflatable wings, the incidence angle and the flight speed present other limits linked to inside-pressure minimum differential.

At this point, it is already clear that inside-outside pressure distribution and shape variation plays a crucial role in flight dynamics of parafoils and paragliders. Therefore, the most efficient way to investigate the dynamically inflatable wings' in-flight behavior is through pressure distribution mapping and modeling. Which means, to abandon the attempt of finding general geometry-based aerodynamic coefficients, and to adopt a pressure distribution dynamics approach. This may allow a better understanding of how the wing behaves in flight under the different scenarios regarding maneuvering and external disturbances.

However, due to the variability experimented by the in-flight wing, experimental procedures are necessary to correlate the state of motion to pressure distribution over the wing. This basic need point to two other challenging aspects of flexible wings systems: the suitability of flight test instruments and the adaptation of safe procedures for flight tests. It is easy to see that the available set of instruments and classic flight-test theory were both developed for conventional aircrafts, however, with the recent improvement observed on sensors designed by the unmanned aircraft industry new resources are available allowing applications which might become an answer for inflatable wings flight testing.

Overcoming the challenges of measuring pressure distribution in flight, acquired data may provide tools for design optimization leading to the identification of design aspects that may increase or reduce collapse susceptibility, as well, the derivation of technical parameters for performance and stability prediction and evaluation.

1.1 Objectives

The general purpose of this work is to take a step forward to overcome the mentioned challenges by developing a suitable flight test instrumentation system, able to be used to characterize dynamically inflatable wings, and by proposing the adoption of a pressure-differential approach for inflatable wings aerodynamics characterization. The data presented is the outcome of a four years' research, carried out at the University of Brasilia, resulting a successful instrumentation system based on differential pressure sensors, which was wind-tunnel tested revealing important characteristics of the most relevant phenomena observed on dynamically inflatable wings.

It is worthy to specify the problem to be addressed, as well as, the long terms and short terms objectives of the present research, in order to set the scope of the present document, limiting the content but relating it to the final objectives of the research project.

The state of the art regarding dynamic inflatable wings aerodynamics characterization relies on simulations or laboratory tests which provide important but incomplete data. The approach following traditional external pressure coefficients evaluation to characterize the wing presents limitations regarding the inflatable nature and the existence of internal flow. This works considers the phenomena already explored by previous authors and uses a novel methodology in order to confirm these observations, evidencing the benefits of direct measurement of differential pressure, which provides an identification considering external and internal pressure simultaneously, overcoming the problem of internal flow and shape instability.

It opens a new branch in terms of methods for studying these systems and provide data for future works aligned with the following objectives:

Specific objectives (short term):

- To develop an instrumentation system able to capture low levels of aerodynamics' differential pressure encountered on the surfaces of dynamically inflatable wings with enough precision and resolution able to identifying the airfoil's pressure profile variation as a function of speed and incidence.
- To develop a methodology for analyzing pressure-differential signals as indication of airflow condition and aerodynamic limits approximation.

General objectives (long term):

- To provide a flight-test appliance able to correlate local pressure-differentials at the wing to the in-flight condition, allowing the characterization of standard maneuvers in terms of aerodynamic phenomena.
- To provide the technological and theoretical basis for the development of several safety systems based on real-time in-flight monitoring for stability augmentation and collapse prevention.

2. Literature review

The academic literature regarding inflatable flexible wings is quite limited compared to traditional aeronautical subjects as rigid wings applications. A considerable number of papers about parachutes and deceleration systems does exist, but it normally focuses on trajectory optimization, guidance, or aerodynamic coefficients indirect identification. It is not usual to find investigations about the behavior of a parachute or parafoil as a maneuvering wing, or experimental approaches to aerodynamic characterization.

The problem related to improving inflatable wings performance and reliability has gained more attention with the increasing on applications using such devices for satellite parts recovering and cargo positioning. Recently, it is possible to find a couple of papers exploring the specific in-flight characteristics of these wings. However, due to the predominance of the methods designed for rigid wings and the unsuitability of such methods to characterize dynamically inflatable wings, specific results revealing the in-flight aerodynamic characteristics of these wings are still very rare. Few experimental results related to the paraglider cell deformation can be found in the recent literature [8]. The challenges to attach reliable instrumentation to the canopy fabric make in-flight experimental measurements, either impossible or extremely difficult [6] on account of wing shape deformation and/or airflow disturbances.

A wider number of researches focused on flight dynamics aspects of parafoils and paragliders, using traditional flight mechanics modelling strategies as if it was applied to rigid airfoils. Following this strategy, several works devoted to the development of dynamic control models, guidance systems, and trajectory optimization can be found in the literature [9-16]. Even the description of the flight dynamics encounters different approaches, starting from simplistic linear models with three degrees of freedom – DOF and reaching complex 9-DOF models, which includes the particularities of relative motion between center of gravity and aerodynamic pressure center.

Recent efforts focusing on control and guidance have successfully used in-canopy motion sensors [9-12]. However, in-flight measurement of the airfoil aerodynamic characteristics remains a challenge, thus opening a fruitful field of research to verify, enhance, and correct computational or wind-tunnel based assessments. The use of inertial sensors and GPS features has expanded as a way to parameterize the basic in-flight movements. These tests are helpful

to highlight the effects of the wing's flexibility, and to demonstrate how relevant is the complex aerodynamic phenomenon governing the composition of external and internal flow, which is not present on rigid wings. Still, without a deeper understand of how the fluid-structure interactions behaves internally and externally, it is difficult to model the system allowing the design of stability augmentation systems – SAS, auto-pilot solutions, or collapse prevention features.

The aerodynamic characterization has also been performed by computational codes [6, 17-21]. The use of CFD tools to explore the characteristics of inflatable airfoils is, perhaps, the most affordable and straightforward manner to start understanding the interactions between internal and external flow, which dynamically alters the aerodynamic coefficients on an inflatable wing. However, without experimental data the improvement and application of these codes become unrealistic. Therefore, the computational approach is, without a doubt, a tool to be used for both investigation and design, but demands experimental data to fit the models.

A modest number of papers explore aerodynamic flow properties over inflatable airfoils based on experiments [22-25]. Most of them relied on wind-tunnel tests whose instrumentation is unsuitable for in-flight measurement. The main efforts using wind-tunnel applied load balances or conventional pressure gauges. Both of them faces obvious limitations to be used airborne. Even though, the results obtained by these experiments are extremely important to validate new experimental approaches, and to feed computational codes or theoretical aerodynamic models.

The present development has its roots in two specific research topics. Firstly, from the description of aerodynamic phenomena on inflatable airfoils, obtained by both simulation and laboratory test campaigns. Secondly, from the application of light, small, low-cost, onboard pressure sensors for aerodynamics investigation. The following subsections highlight some details from the most representative works toward these subjects, which allowed forming the foundation for the present contribution.

2.1 Aerodynamic Behavior of Dynamically Inflatable Wings

In 2006, Mashud and Umemura [5,7] investigated the aerodynamic characteristics of a paraglider from the aerodynamics perspective. In their work, wind tunnel experiments were conducted in an inflatable cell model designed to represent each cell's dynamic behavior along the wing. Pressure measurements relied on pressure probes connected to a digital pressure gauge. Although such a device does not apply for in-flight data collection, it was proven very

efficient in disclosing important characteristics of inflatable airfoils, including aerodynamic coefficients range and airfoil inflation as a function of the angle of attack – AOA.

The instrumentation applied for pressure measurement used pressure probes with tubes connected to a digital pressure gauge. Fig. 2 below reproduces a sketch provided by the authors:

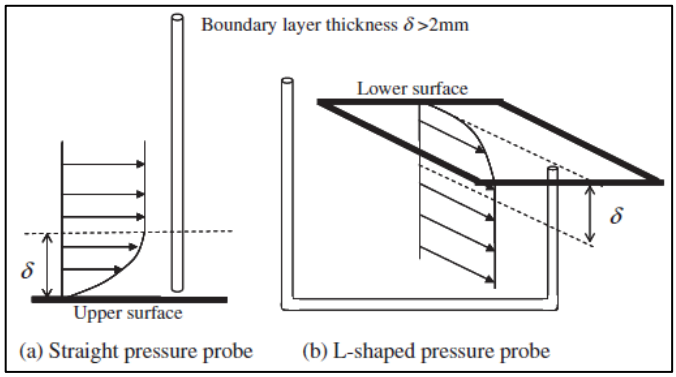

Figure 2: Mashud and Umemura [5] external surface pressure measurement method

The results show expected behavior regarding the inflation dynamics, which means, a minimum angle of attack is necessary to properly inflating the cell. It happens because at low AOA the stagnation point rests after the air intakes (ex: 0 degrees) inducing a frontal buckling. As the AOA increases, it moves toward the leading edge up to the point when it reaches the opening and the internal pressure increases drastically promoting the inflation. The experiment shows that, at AOA above 2 degrees, almost no change appears in cell model shape. In the author's own words:

> *"As the attack angle increases, the stagnation point shifts to the leading edge of the upper surface and the internal air pressure increases. At the same time, the suction pressure acting on the curved part of the upper sheet is enlarged due to the increased curvature. As a result, the leading part of the upper sheet is pushed outward and increases the opening of the air intake unless the membrane tensile force along the leading edge is not sufficient to support the deformed upper sheet. Once the air intake becomes large, the stagnation-point position is located well in front of the air intake. This is the physics underlying the dramatic change occurring at an angle of attack of 2"*

The internal pressure measurements using such scheme led to the conclusion that if the stagnation point is located in front of the air intake, the cell model inflates fully and the internal air pressure takes a close value to the stagnation pressure. Otherwise, if the stagnation point is

dislocated from the air intake, there is an external airflow passing in front of the air intake and the model is not fully inflated. The internal air pressure takes a value nearly equal to the external flow passing in front of the intake. Mashud and Umemura [5] observations about the effect of the air intake must be highlighted:

> *"A recirculating internal air, which is driven by the external air passing in front of the air intake, has a penetration length comparable to the width of the air intake. However, such a case takes place only when the air intake width is small. Therefore, the internal air flow itself cannot have any significant effect on wing formation."*

As stated by the authors, when the air intake becomes representative the intern flow becomes more representative as well. However, it is important to highlight that the method of measuring internal pressure used by Mashud and Umemura does not capture the actual condition of internal pressure distribution throughout the internal surfaces, reading only the average internal pressure. The experiments documented on the present thesis shows that, in fact, relevant effects of the internal flow can be seen at different stages of the airfoil.

The measurements of external pressure prove a commonality with the surface pressure distribution of a rigid wing at various attack angles. It corroborates some of the assumptions made by Benedetti [26] regarding the reliability of using basic catalog airfoil data for parameters estimations in paraglider's motion modeling. Fig. 3 below reproduces the data presented by Mashud and Umemura [5]:

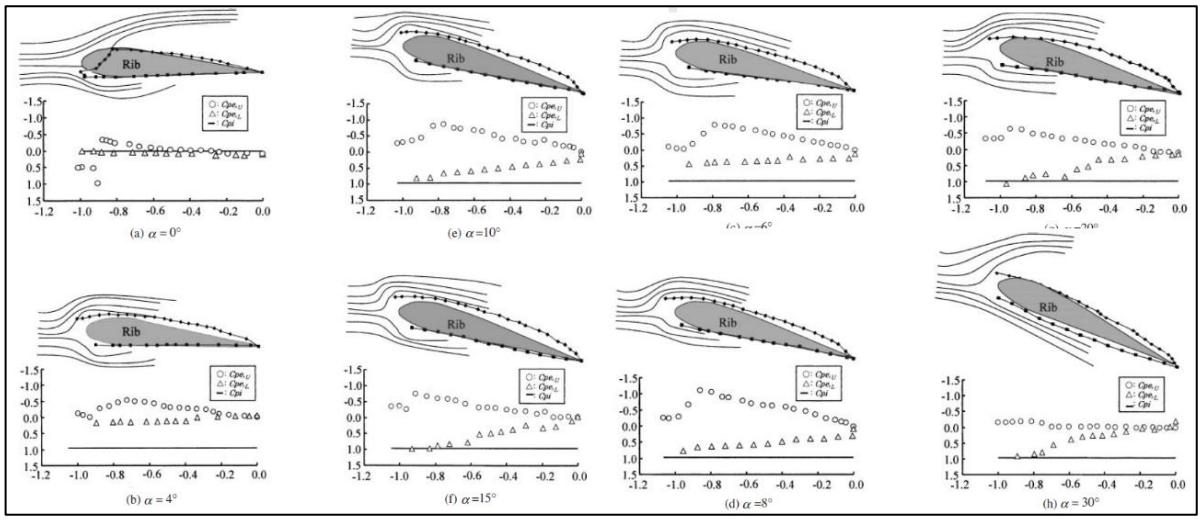

Figure 3: Mashud and Umemura [5] external pressure measurements

Applying classic aerodynamics formulation, the measured pressure coefficients provide lift and drag coefficients. The results reinforce the behavior similar to the rigid wing, especially for the correlation between lift/drag coefficients and the AOA.

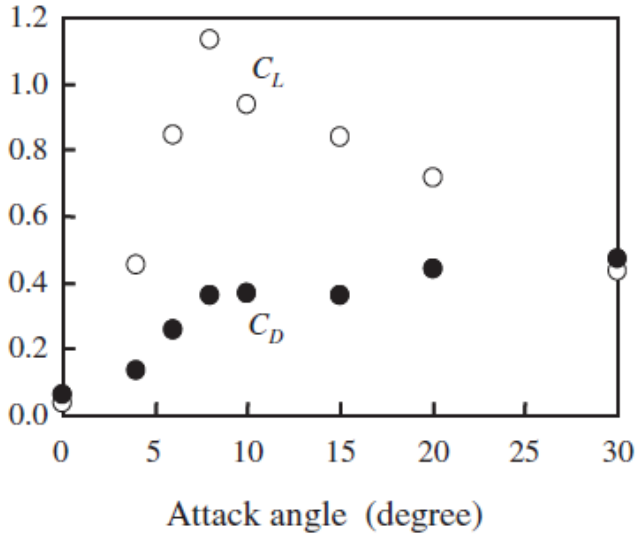

Figure 4: Mashud and Umemura [5] lift and drag coefficients data

In addition, the experiments allowed reaching conclusions toward the structural assembling of a paraglider system, as observed by the authors:

> *"At least two cables attached to the leading and trailing edges of the lower perimeter of the rib are necessary to suspend the weight for each cell. Since these cables exert a force which tends to compress the rib in the chord-wise direction, this buckling force must be cancelled by the membrane tensile force acting mainly on the upper surface"*

The statement above highlights the preponderance of the upper-surface as the lift and structural stability provider.

In their third paper, Mashud and Umemura [7] explored the three-dimensional aspect of an inflatable airfoil cell. The aim was to confirm that the surface pressure distribution over the whole cell has a similar distribution along the chord at any span station, and that the shape of the ribs consistently defines the aerodynamic characteristics.

The results show that all cross-sectional surface pressure coefficient distributions look similar along the span, which means, compared to the significant variation throughout the chord, the variation along the span is relatively small. It leads to the conclusion that three-dimensional lift coefficient of inflated cells can be estimated from the profile bi-dimensional coefficients. However, as emphasized by the authors, the three-dimensional drag coefficient

depends significantly on the air-intake size. Mashud and Umemura [7] proposes multiplying the bi-dimensional coefficients by the ratio between the area of rectangular enclosure of the air intake and the actual area of air intake opening as illustrated:

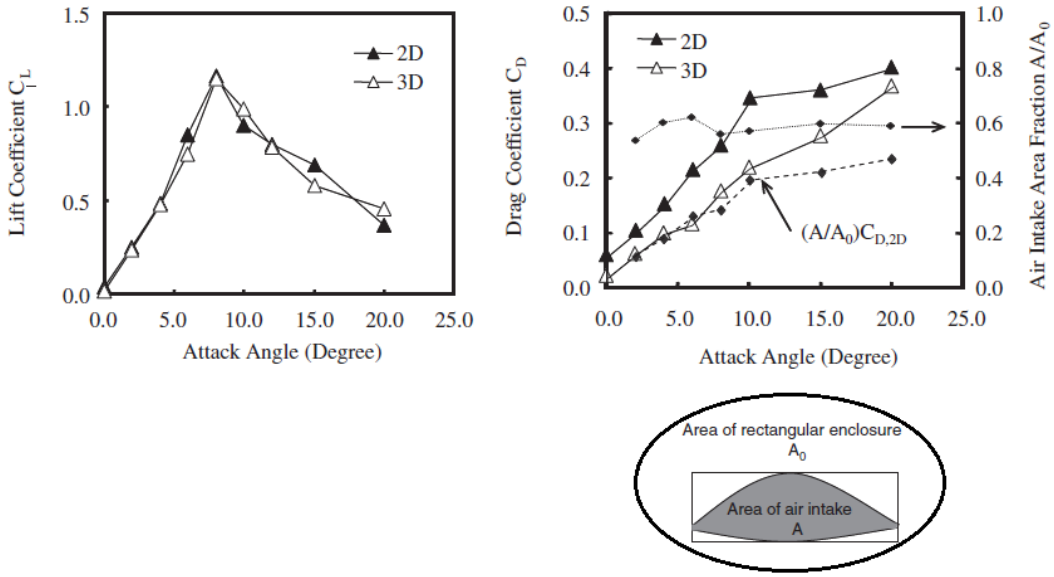

Figure 5: Mashud and Umemura [7] lift and drag coefficients – Three-dimensional effects

Overall, the presented results reinforce the theoretical idea presented by Benedetti [26] of deriving specific tri-dimensional coefficients from corrected bi-dimensional airfoil data for under design estimations. It also provides an expected range for basic aerodynamic coefficients to be used validating new approaches.

Later in 2009, following a completely different approach, Mohammad and Johari [27] predicted the flow over an inflatable wing using CFD analysis (Fluent software package) to compare the baseline airfoil with a sectioned air-intake airfoil. Besides the confirmation of the range expected for basic aerodynamic coefficients, and the observation that the external pressure distribution through the upper surface follows the baseline rigid airfoil, simulation's results suggested that the flow about the parafoil with the air-intake creates a separation bubble on the lower leading edge and an entrapped vortex near the cell opening.

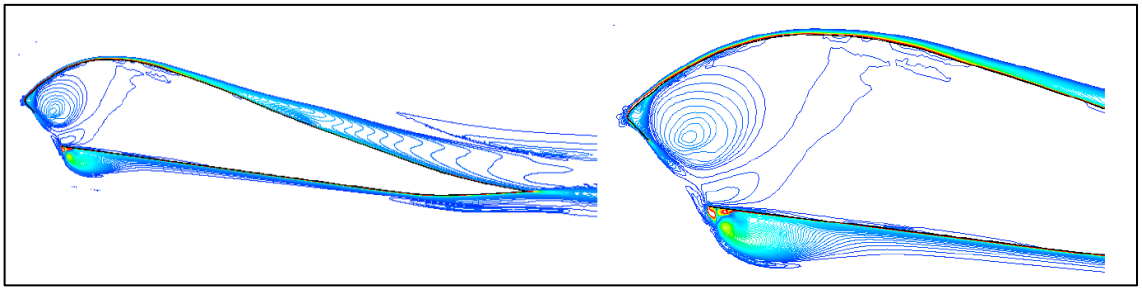

Figure 6: Mohammad and Johari [27] -Vorticity contours of the parafoil at AOA= 7º

The distinctive local flow occurring near to the air-intake and reaching the lower leading edge station forms a buff leading edge that closes the airflow profile. Both lift and drag were affected, but lift reduction seemed limited while drag was at least twice the baseline airfoil drag. In fact, experimental data documented on this thesis proves the occurrence of the predicted phenomenon and reveals the nature of the decrease in lift generated by the presence of an air-intake.

Fluid-structure interaction simulations were also developed by Fogell [6] in 2014, confirming the existence of a recirculation bubble at the bottom leading edge, causing a minimum 15% decrease in lift accompanied by a 210% increase in drag. The novelty introduced by Fogell was the execution of wind-tunnel experiments using load balances for direct measurement of lift and drag. The results confirmed that the introduction of a leading-edge cut dramatically affects the flow, by reducing the expected peak of low pressure at the upper surface. It was inferred that the flow penetrates the cell forming a large internal bubble of recirculating air, but the rear portion of the trapped air stays at pressure levels near to the expected stagnation value. This high-pressure region provides three-dimensional structural rigidity and supports the aerodynamic shape of the wing.

The author also highlights that examining changes in structure or behavior of the airflow during flight is still extremely challenging. In his own words:

> *"…the interaction of the aerodynamic forces with the parafoil are revealed to be more complicated than in the case of a structure with purely external flow. Analysis of the drag of the parafoil section demonstrated the need for the internal aerodynamic forces to be considered as part of the analysis of parafoil performance, a factor not previously acknowledged by the literature."*

Indeed, the interactions are more complicated than in airfoils with the purely external flow, requiring the consideration of internal forces, even to estimate lift. The previous observations find support on the wide discussion toward low-Reynolds-number flow [28]. Inflatable wings normally operates at Reynolds Numbers below 1×10^6, which is considerably below the normal range for conventional small aircrafts [29]. It favors the appearance of laminar separation bubbles [30], triggered by several sources, from geometric discontinuities to pressure gradients due to internal or external flow disturbances. This basic aerodynamic characteristic,

along with the specificities of the sectioned-flexible airfoil, results in a somewhat complex and necessary theme for researching.

Conclusively, the available background on aerodynamics of dynamically inflatable wings allows to infer that: for characterizing the aerodynamic behavior of parafoils and paragliders, although the external pressure distribution profile follows the pattern of the baseline rigid airfoil, it must be taken in consideration the effects of the internal flow induced by the air intake, as well as the effects of the mutable shape, which lead to a complex fluid-structure phenomenon requiring specific methods for both modelling and experimentation.

2.2 Flight Dynamics Aspects of Inflatable Systems Related to Pressure Distribution

The need for characterizing wings' aerodynamic behavior represents a means to an end. The final objective is, in fact, to predict motion and sustain shape stability. The possibility of modelling aerodynamic forces precisely, even under situations where shape varies, makes possible the anticipation of out-of-envelop situations and the design of accurate guidance systems. Therefore, a limited analysis of the aircraft dynamic aspects allows contextualizing the present research from a wider perspective.

To allow a better comprehension about the relevance of measuring pressure differentials at the wing surface, a background on paragliders and parafoils pendulum system is required. Most of the dynamic inflatable wing systems are based on pendulum stability. The vehicles are normally designed with a considerable vertical distance between the wing and the payload, which represents the center of gravity. This relative height is essential to provide longitudinal and lateral-directional stability [26].

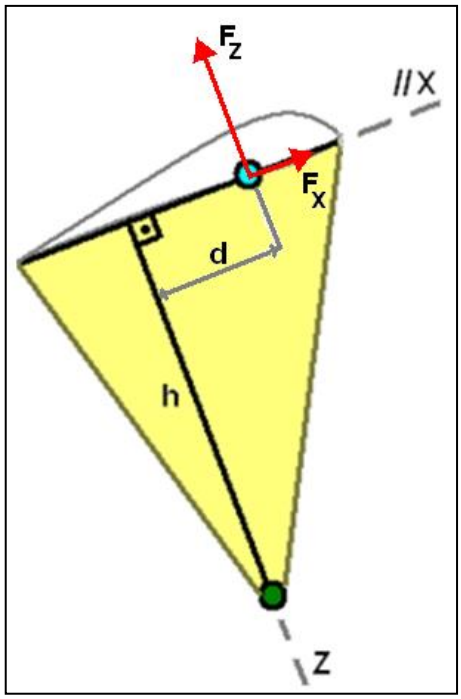

Figure 7: Benedetti [26] - Paraglider`s simplified sketch

Fig. 7 illustrates the longitudinal components of in-flight resultants. The forces are determined by relative speed and angle of attack. The speed at the wing is obviously dependent on wing's rotation, therefore, if any atmospheric disturbance causes a variation on the aerodynamic forces a resultant pitch moment will be generated. Fortunately, the system is intrinsic stable, since a diminishing on relative speed will reduce lift and provide a negative pitch, which tends to regain speed.

The steady glide is dictated by an equilibrium between speed and incidence. This is true globally and locally. Which mean, for both longitudinal and lateral-directional motions, the movement of the system occurs trying to compensate for disturbances in airflow speed or angle of incidence. This dynamic continuous cycle results constant variations on local speed and AOA.

Considering a rigid wing, if speed is known at the center of gravity, as well as the rotational speeds of the wing relatively to the C.G. local speed and AOA becomes a geometric consequence at any point of the wing's surface. Therefore, local forces can be sufficiently estimated and motion can be integrated. However, if the wing is not rigid, speed, incidence, and the aerodynamic coefficients may change locally due to flexibility or deflation.

In this way, if inside-outside pressure differential at each point of the wing can be modelled, local lift and drag can be dynamically adjusted. It does not imply that models based on rigid airfoil data should be fully discharged. In fact, the modelling of pressure distribution

is thought to work as a correction parameter. Once a steady glide coefficient is extracted for a certain airfoil type, pressure differential becomes an additional parameter defining lift and drag coefficients to be used together with global airflow speed and incidence.

It is possible to find a considerable number of published works modelling the motion dynamics of parafoils and paragliders. However, the majority of these works considers the wing a rigid wing. Which means, the dynamic models are based on geometry-based aerodynamic coefficients and do not take in account internal flow and in-flight deformations of the wing.

Among the most recent works, it is worthy to mention the approach provided by Zhang et all. [15] in which a six degrees of freedom model for a parafoils system is derived starting from classical mechanics and applying constant aerodynamic coefficients. Apparent mass corrections are applied as proposed by Lissaman and Brown [31], and a real drop test is proceeded to validate the model. Results show good results predicting general motion of the parafoils system, however, the need of further improvements related to the specific characteristics of flexible wing systems remains as stated by the authors:

> *"Owing to the fact that the parafoil is a complicated nonlinear system, it is difficult to calculate and analyze the internal dynamics of the system. The interaction of the canopy and the payload needs further studies."*

Other interesting approaches uses nine degrees of freedom models which takes in account relative motion between payload and wing. This philosophy was presented in details by Prakash [32] and a comparison between the effectiveness of using 6 or 9 DOF models for under design evaluations is full explored by Benedetti [26] leading to the following conclusion:

> *"The only relevant dynamic component neglected by the 6DOF model is a potential yawing moment due to wing twist or relative yaw. This situation is expected to happen in dynamic maneuvers or in response to violent lateral gusts. It can be identified a new internal dynamic components acting on the system, which is a reactive torque generated by the tension on the lines when twisted, and a change in aerodynamic resultants due to the sudden changing on heading and also due to wing geometric distortions. The twist moment could be modeled as a combined spring-damper component, however, would be necessary establish the physical proprieties of these idealized components, what would be very*

difficult in a conceptual design phase. Also, effects on aerodynamic coefficients due to wing geometry deformation would require additional considerations. Then, it seems not to be practical to add such considerations in a model intended for conceptual design evaluations. Finally, analyzing situations near to equilibrium or even smooth maneuvers, no relevant twist are expected to be representative. Finally, it is worthy to mention that maneuvers involving wing twist can be evaluated in a second phase when the design is already defined and experimental data can be obtained and applied in more comprehensive models focusing on specific investigations."

As can be seen, some models improve accuracy by increasing the number of degrees of freedom up to nine by considering the relative motion between the payload and the wing. However, as a matter of fact, the restrictions regarding the extremely flexible characteristic of the wing remains limiting the effectiveness of such models and leads its applicability back to basic dynamic's characteristics initial estimation. Therefore, considering the precarious accuracy of any elastic coupling parameter used for increasing complexity of dynamic models, the application of standard 6 degree of freedom models, in which the only estimation is related to the aerodynamic coefficients of the wing, works more efficiently in order to provide rational parameters needed to describe the basic in-flight characteristics of a specific wing.

Finally, comparing the different approaches found, the developments by Benedetti [26] present a distinguished advantage by parameterizing the system's geometry in a way that allows relating classical dynamic characteristics to basic design parameters. The methodology proposed to define wing's geometry and aerodynamic coefficients allows the theoretical implementation of important features like variable dihedral or aerodynamic torsion. In this work the system's geometry is defined by eighteen variables capable of representing basically any desired shape. Fig. 6 below shows the main screen of the MathLab® tool designed, in which all the design variables can be visualized.

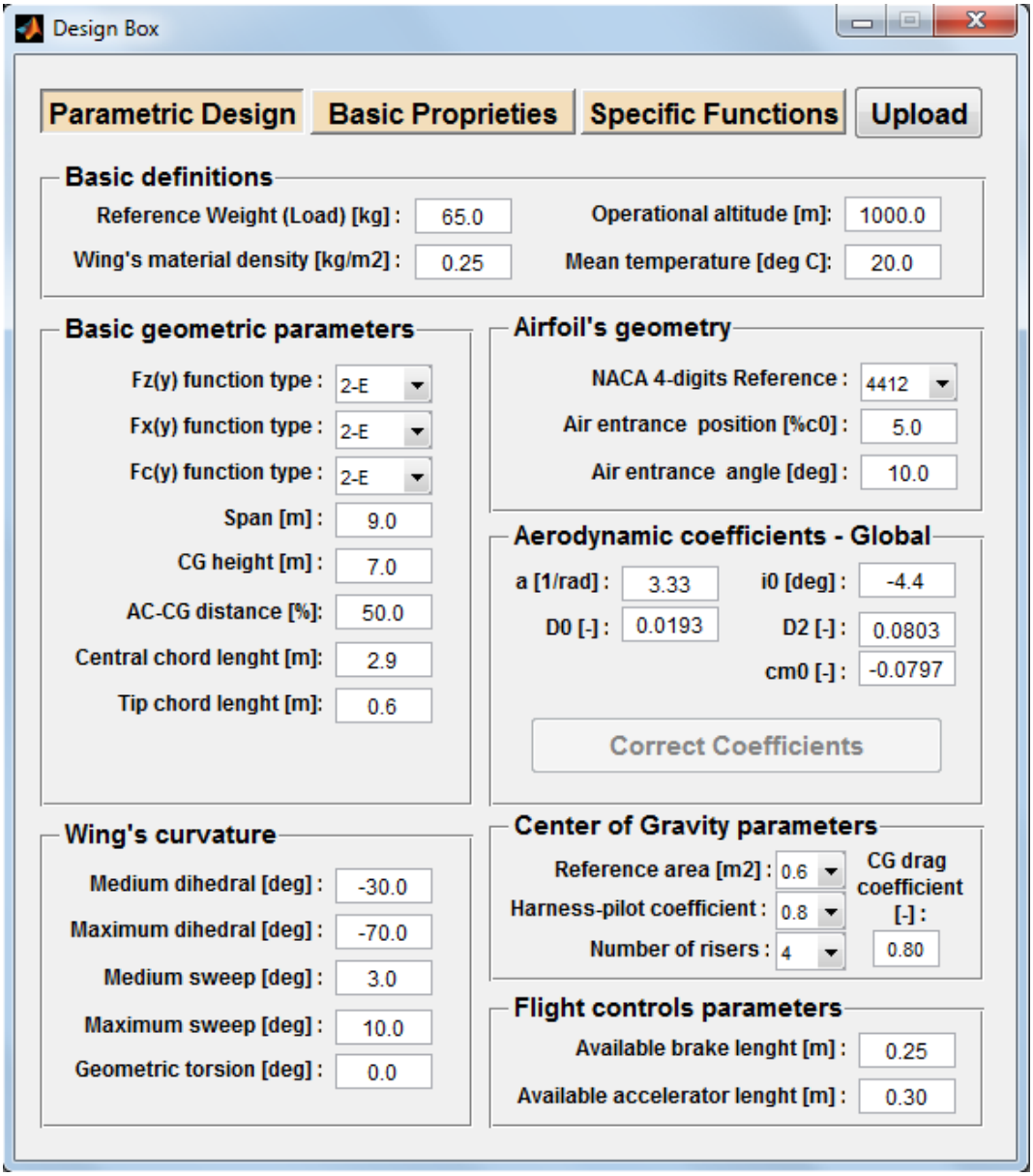

Figure 8: Benedetti [26] – Geometric and aerodynamic parameters for model evaluation.

Fig. 8 shows that an inflatable wing system can be characterized by defining the wing geometry, the C.G. position, and providing some aerodynamic data based on tested profiles. The model provided by Benedetti is capable of calculating fundamental geometric parameters and estimating basic flight characteristics for any kind of geometry. It allows a first step in design optimization, which, however, may be improved by adding considerations towards system's flexibility since the model still works with the classical rigid body assumption. Fig. 9 below presents a theoretical paraglider designed using this model and the flight characteristics calculated for it.

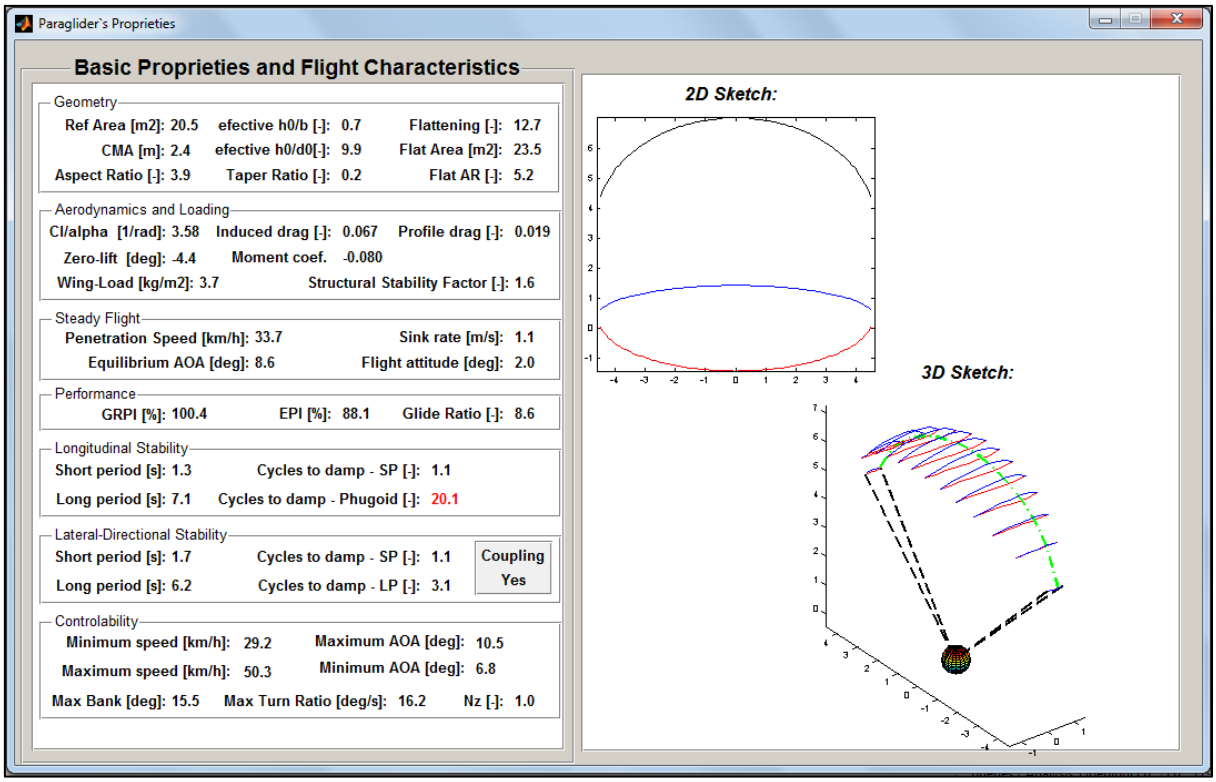

Figure 9: Benedetti [26] – Basic flight characteristics for a theoretical model.

Fig. 9 present several geometric characteristics as aspect ratio and tapper ratio, which are fundamental parameters describing the design. It also presents the aerodynamic data estimated considering a given airfoil data. Finally, it presents the flight characteristics, comprehending the equilibrium speed, incidence, and glide ratio; as well as the stability parameters. It can be noticed that the theoretical model presents a flight speed near 9m/s, an equilibrium AOA near 9º and a wing load around 4kg/m^2. All these parameters are fully coherent with values observed in real-life models.

Fig. 10 presents a simulation of the response to a 10Km/h lateral gust:

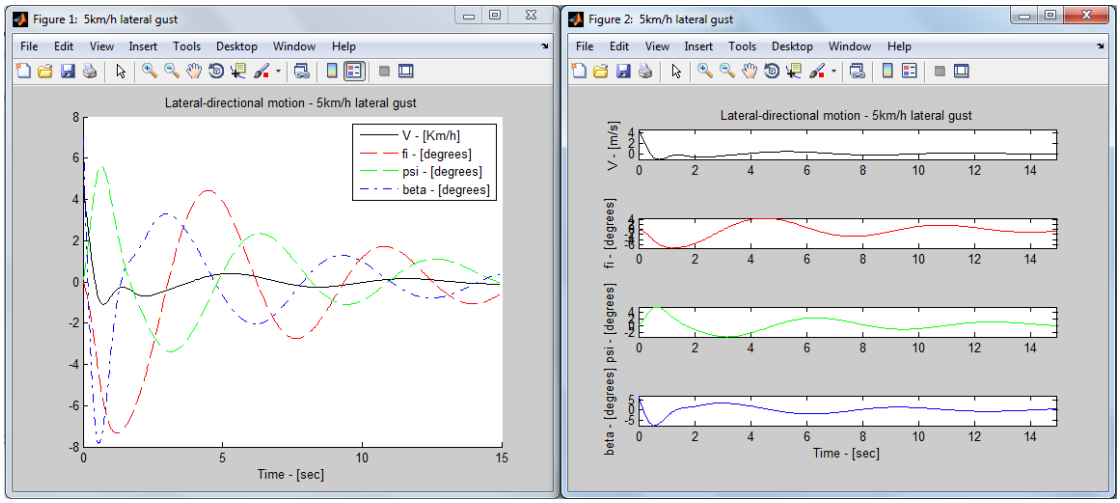

Figure 10: Benedetti [26] – Lateral gust response simulation.

As can be seen in Fig. 10, facing a lateral gust the wing banks and yaw trying to face the gust. It leads to a coupled bank-yaw dumped motion, which is completely absorbed after 15 seconds. The maximum bank experienced is around 8 degrees, which is quite low, showing that the model is strongly stable laterally. This results may be affected if a relevant pressure loss is identified at a particular point of the wing. However, working with constant coefficients such effect cannot be accounted for.

From this modelling is possible to extract stability modes periods, equilibrium speed and sink rate, glide ratio and other important characteristics. This is more than enough to be used as a first approximation, and still can be severely enhanced by adding flight test data in order to determine when the flexible characteristics starts compromising the rigid-body assumption, and, in which extent this is, in fact, relevant. However, under situations where the assumption of rigid wing becomes week the theoretical model loses utility. These situations are normally related to the limits of wing shape stability, which are: Inflation minimums, stall, and abnormal flight conditions.

There are many others models describing parafoils and paragliders. Some of them are extremely complex and accurate, and then, able to serve as the physical foundations for guidance systems programmed for specific models. Others uses traditional flight mechanics theory, providing a more practical tool to be used as a generic design tool. However, none of them are accurate for situations where the aerodynamic limits are stressed and the assumption of rigid wing is jeopardized.

Finally, it is important to highlight that, unfortunately, situations where the flexible nature of the wing overcome the stiffness provided by the pressure differential are very frequent. Therefore, the use of the presently available dynamic models becomes limited. In this way, to provide a step forward on modelling inflatable wings, it is inevitable to work with local forces, which means, to understand how pressure differential evolves inside and outside of the wing at each individual portion. Therefore, mapping differential pressure distribution defined by the aerodynamic characteristics is the core of developing the next generation of dynamic models.

2.3 Flight testing flexible wings and non-redundant systems

Once understood the aerodynamic phenomena related to inflatable wings, and the need for pressure distribution mapping for system’s modeling, it becomes clear the barrier imposed by the challenges related to flight testing. There are two main challenges in testing real size manned inflatable-flexible wings: The first one is the current limitation on flight test

instrumentation for in situ measurements, capable of capture the nuances of external and internal flow. The second one is the absence of dedicated flight test methodology capable of relating a reasonable number of maneuvers to the main aspects of the system in a safe and effective set of procedures.

Following these remarks, it is clear that there is room for improvement in terms of experimental techniques for dynamically inflatable wings. As addressed by Cochrane et al. [33], traditional sensors are neither flexible nor compatible with deformations of fabrics. The same authors present a sensor based on a Conductive Polymer Composite as a possible but costly solution. This type of approach becomes prohibitive economically and presents additional challenges to be used in aggressive environments.

Burns [34] also presented a successful data gathering prototype designed for parachutes based on optical sensors linked through wiring from the canopy to the control board at the payload point. Sensor accuracy was proven adequate. Notwithstanding, we anticipate possible vibration issues due to the use of such long wires when applied to a maneuvering parafoil. Burns successfully summarizes the challenge of inflatable-flexible wings in-flight pressure measurements:

> *"Currently, no sensor systems for low-pressure parachute measurements are available to accurately measure the low differential pressures across the parachute fabric during airdrop missions. While conventional technologies such as capacitance-based industrial pressure transmitters can provide the desired pressure range and resolution, these units are generally bulky, heavy and power-consumptive. Micromachined capacitive pressure sensors with integrated electronics offer an improved solution, although they typically fail to reach the low operating range requirements of 100 Pa (0.015 psi) or less and are not available in differential or gage pressure configurations. Low cost piezoresistive pressure sensors, which comprise the majority of pressure sensors sold today, have limited signal-to-noise ratios that prevent them from giving accurate measurements of differential pressure at low operating ranges and have relatively high power consumption. Recent innovations by other researchers of integrated capacitive pressure sensors for tire pressure sensors have produced smaller devices that are typically configured as absolute pressure sensors and as such, do not*

have the capability of measuring small differential pressures that are of particular interest in parachute monitoring. Accommodations for wireless data communications, local data storage, batteries and an antenna add size and weight to the sensor node, which can alter the flow field and distort the structural response of the parachute"

To overcome this challenge Burn's design used optically coupled resonant sensor probes connected via a lightweight optical fiber from the parachute fabric to an external interface board. The suitability of the sensor was defined as shown:

Table 2. Burns et all [34] pressure sensor specifications

Parameter	Specification
Operating Pressure Range	0 to +/-100 Pa (+/-0.015 psi) differential or gage
Accuracy	1.0%
Resolution	0.1%
Repeatability	0.1%
Linearity	±0.5% FSO
Hysteresis	±0.5% FSO
Operating Temperature Range	-55°C to +70°C
Proof Pressure	1000x rated pressure
Burst Pressure	2000x rated pressure
Pressure Port	1 mm flush hole on gage (upper) side; 1 mm OD metal tube extending 2.0 mm on lower pressure port side
Package Attachment	Attachable to 1.1 oz/yd ripstop Nylon fabric via penetration of the fabric with a protruding metal tube and retainable with a stitchable retainer covering and flush with the tube tip
Package Weight	<0.4 gms
Package Size	Package body: 10 mm x 10 mm x 4 mm high not including the protruding tube Retainer: 10 x 10 mm x 1.5 mm high Tube: flush with retainer outer surface
Sensor Excitation	Optical
Sensor Output	Intensity and frequency-modulated raw signals from sensor probe, ratiometric or formatted output from hub-embedded controller
Fiber Weight	1.0 grams/meter (1.0-mm OD POF)
Fiber Bend Radius	> 15 mm (1.0-mm OD POF)
Data Update Rate	< 1000 per second peak (sampling rate can be much less during off-peak periods; data may be stored locally for downloading at a later time; higher data rates may have lower accuracy)
Local Data Storage	> 10,000 data points including time/date stamp

And the prototype setup used is illustrated in Fig. 9 Below:

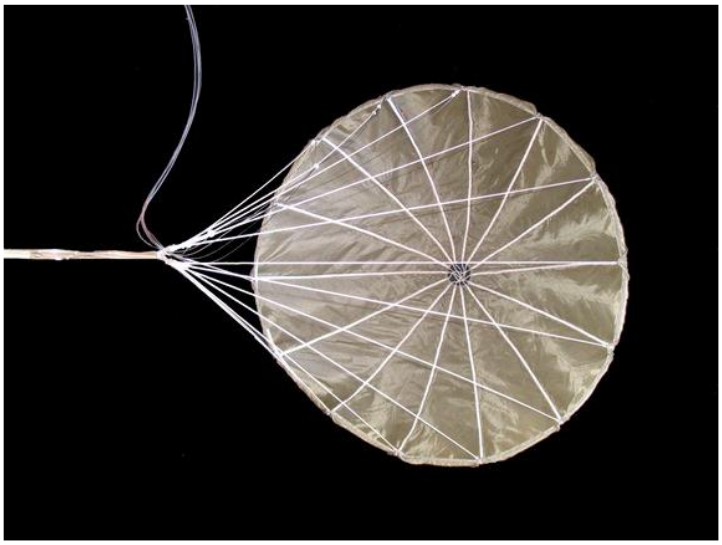

Figure 11: Burns et all [34] prototype.

Burn's results present an interesting alternative to flight test flexible wings. With a package of 10mmX10mmx4mm weighing down to 0.4 grams, the assembly of optically coupled sensors provides differential pressure measurements in a robust and accurate way for a wide range of pressure and temperature in difficult environmental conditions. However, it is important to highlight that the use of this kind of sensors and optical fibers makes the system considerably expensive. Also, the fiber connections from the canopy to the data acquisition board imposes some dynamic effects when the wing is considerably far from the board, which is the case for paragliders and parafoils delivery systems.

It is relevant, therefore, to explore the benefits of using a low cost less accurate and heavier system with a simpler mounting system if the objective is to map wing pressure distribution dynamics as an effect of maneuvering and design characteristics.

McCarthy [35] presented encouraging results on flow characterization after applying low-cost pressure sensors placed along a strip (pressure belt), which was further attached to rigid wings. It was presented a measurement system for use on a light aircraft to measure the pressure distribution over the wing surfaces. According to the author the measurement system was developed as a low-cost alternative to existing advanced measurement systems. The idea involved self-contained sensor modules with all electronic components mounted on flexible circuit board that formed the base of the modules. The total cost of the sensor modules was approximately one hundred and forty dollars for a seven sensors module. However, the level of flexibility of McCartty solution is still deficient for inflatable flexible wings. An illustration of the system is shown in Fig. 12.

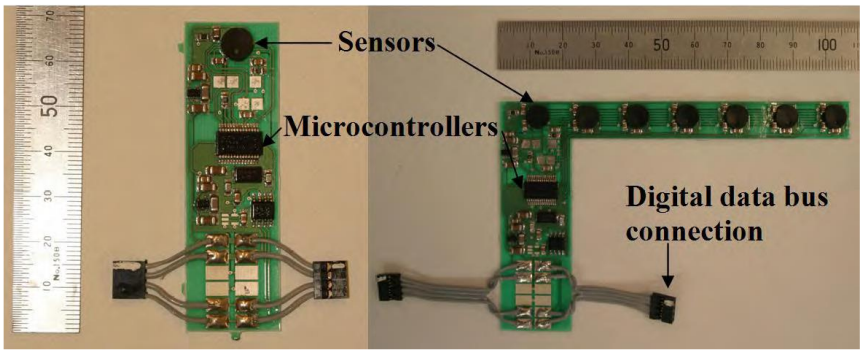

Figure 12: McCartty [35] sensors module.

McCartty contribution is very useful regarding to sensors selection in comparison with Burn's developments. He presented a set of eligible low-cost sensors as presented in table 3.

Table 3. McCartty [35] sensors options.

Sensor	Price per sensor (AUD)	Sensor size in mm (width x width x thickness or diameter x thickness)	Interface method	Sensor type	Range
Honeywell CPX05GF	$51.95	9.9 x 9.9 x 2.7	Analog	Differential	0-34.5 kPa (0-5 psi)
Honeywell CPX15A	$33.00	9.9 x 9.9 x 2.7	Analog	Absolute	0-103.4 kPa (0-15 psi)
VTC SCP1000	$25.00	7.1ø x 2.1	Digital	Absolute	30-120 kPa
Endevco 8515C	$1780.00	6.3ø x 0.76	Digital	Absolute	0-103.4 kPa (0-15 psi)
Kulite LL072	$1735.00	9.6 x 4.1 x 1.5	Digital	Absolute	0-172.4 kPa (0-25 psi)

The success of McCartty experiments proved the suitability of a VTI Technologies SPC1000 series absolute pressure transducer mounted over the wing for pressure data gathering. This is an important statement for further developments using simple low-cost sensors to measure aerodynamic pressure.

It is worthy to see from Burn and McCartty works that some basic features should be guaranteed when designing a flight test instrumentation for flexible wings: The placement of the sensors must be in a way to guarantee the integrity of the aerodynamic flow over the sensor; the sensibility of the sensor must be sufficient; and the assembling must be able to sustain the motion of a fully flexible structure.

Also, it is important to realize that most of the solutions presented up to here relies on absolute pressure measurements. No appliances based on pressure differential sensors were found. This is an important observation, since it is well stablished that inside-outside pressure differential plays a crucial role on in-flight behavior of inflatable wings. Therefore, considering all the constraints explored by previous research and the significant evolution of sensors manufacturing [36], the data documented in the present thesis presents a novel approach for aerodynamic characteristics identification on inflatable wings.

3. Developments

The present work represents the first step of a research project intended to increase safety and performance of dynamically inflatable wings. The final outcomes to be originated from the research shall provide: a deeper understanding of the in-flight behavior of inflatable wing systems; a methodology for safely flight-test inflatable wings; and, on-board instrumentation for parametric characterization, automatic stability augmentation, and collapse prevention.

The three development phases are:

1. Development and qualification of an instrumentation system for in-flight evaluation, and establishment of pressure-differential analysis as the most suitable approach for aerodynamics characterization of dynamically inflatable wings;
2. Planning and execution of flight test campaign on a paraglider prototype, and parametric identification of dynamic and aerodynamic characteristics based on in-flight pressure-differential distribution variation;
3. Development of on-board safety systems and directives for design optimization.

The present thesis documents the accomplishment of the first phase of the project.

3.1 Development background

The development of a useful instrumentation presented many challenges overcame after four years of developments which demanded the development of five different prototypes, each one with different features. Each prototype was wind-tunnel tested and discharged until the final solution.

The first fourth methods relied on using absolute pressure sensors, as observed on most of the rigid-wing methods presented on the literature; however, the alternation towards differential pressure was the breakthrough providing a functional method for characterizing the most relevant aerodynamic characteristics of inflatable wings. The use of differential pressure demonstrates to be preferable not only for resolution, but also for revealing specific and relevant aspects of inflatable wings.

Testing a paraglider in flight is a complex challenge for a number of reasons. First, the fully flexible nature of the wing severely limits the type, size and weight of the sensors to be attached. Second, the thin lines make it impossible using usual strain gauges to evaluate stress

distribution. Finally, there are limitations of weight, and the fact that attaching sensors to the system alters aerodynamic characteristics intended to be measured.

The proposed experiments for the second phase of research, for which the instrumentation has being developed, aims to investigate aerodynamic and dynamic characteristics of inflatable-flexible wings using a paraglider. Initially, the focus is on understanding in-flight pressure distribution dynamics and the wing collapse phenomena. The wing collapse is directly related to the wings pressure differential, which is intimately related to paragliders movements, since the motion characteristics defines critical alterations in speed distribution toward the span, and thus, correspondent variation on both external and internal pressure distribution. Therefore, the general objective is to investigate pressure distribution variation over and inside the wing during common maneuvers, and, derivatively, to explore the potential effects of design parameters on in-flight behavior.

In this way, the main objectives of the flight tests are:

- To relate the variation of pressure distribution around and inside the wing to basic maneuvers
- To identify the variations of pressure distribution around and inside the wing which trigger collapse

A secondary objective of the tests is to use models previously developed for under-design evaluations [26], and, verify if it is possible to corelate the established design parameters to the conditions identified as collapse triggers.

Considering the listed objectives, the data acquisition system is the first step to allow the development of the proposed investigation, however, the instrumentation itself is already an engineering challenge due to the need of several adaptations to allow good data acquisition.

The flight test instrumentation designed for the investigation relays on three principles:

1. **Low interference in flight:** System must be sufficiently light to permit the wing to inflate normally, it must avoid any kind of unnecessary aerodynamic disturbance and it must be suitable for mounting on the wing or harness without affecting the basic dynamic characteristics.
2. **Reliability and robustness:** System must be reliable and robust enough to sustain all movements of the wing without detaching or losing recording capability, even in high temperature and dusty environments.

3. **Good cost-benefits ratio:** System must be accurate enough to measure pressure and motion in a way allowing observation of the variations caused by the maneuvers in relation to a standard steady glide, and, at the same time, it must be of low cost and easy setup.

The final objective is to characterize and optimize in-flight behavior. Then, it is important to be able to relate the pressure variation with wing motion, which can be done by measuring wing's pitch, yaw and roll rates, and, of course, the most basic measurement: speed. In this way, obtaining a complete parametric identification demands, at least, the following parameters:

• Pressure at different points of the wing.

• Pitch, yaw and roll rates.

• True flight airspeed (TAS).

It is true that measuring angle of attack, stress on the lines, and even other parameters may provide additional data resources to evaluate the role system's dynamics; however, it must be taken in account the technical constraints when attaching complex hardware on an inflatable wing and the limited financial resources available. The aerodynamics and even the mechanical proprieties of the system may be compromised with the incorporation of too many sensors. Therefore, the tradeoff involved leads to the selection of small and precise sensors, applied in a strategic way to provide useful data at reasonable costs.

The measurements must focus on the dynamics, which means, the absolute accuracy is less important than the sensibility to variations. That is because the main target is to understand how the parameters change under different in-flight conditions relatively to a steady glide standard condition. The comprehension of the transient effects provoked by disturbances and maneuvering is the core knowledge that makes possible the design of systems able to anticipate and prevent dangerous situations.

There is no challenge on measuring motion or airspeed, since many miniaturized systems used in unmanned air vehicles (UAV) can be directly incorporated to any surface nowadays. On the other hand, the low level of aerodynamic pressure differentials imposes a real challenge for aerodynamic characterization. Most drones use barometric systems, pitot tubes and GPS functionalities to read speed and altitude. Unfortunately, these solutions are not suitable for capturing the aerodynamic phenomena as intended.

3.1.1 Historical results

First setup – absolute pressure sensors with light wiring

The first model proposed used absolute pressure sensors. The strategy behind this attempt was to work with conventional components attached externally to the upper-surface of the wing. This is the most basic setup and fits previously technologies used to measure aerodynamic pressure, as the one used by McCarthy [35].

The advantages of such an approach are the low cost of the sensor, the availability of comparable data, and the simplicity for deriving traditional aerodynamic coefficients. As the measurement provides a direct reading of the pressure applied at the surface, the local pressure coefficient – Cp is straightforwardly obtained, as for a rigid wing. On the other hand, the disadvantages are the lack of direct data related to internal flow, the potential disturbance of the boundary layer, and the diminished capability for reading low levels of pressure differential.

In order to proceed with this strategy a first prototype was composed by two straps, each one containing 3 LPS25H sensors by STMicroelectronics®, encapsulated on a plastic case designed specifically to provide mechanical and environment protection. The LPS25H sensor is an absolute pressure sensor which reads pressures from 260 to 1260 hPa with a resolution up to 0.1hPa at high resolution mode. The system was integrated using a standard Beaglebone Black board embarked with a Linux operational system, were data was locally recorded in a SD card.

Using absolute pressure sensors, the required range for the instrumentation is defined by the flight-envelope. Parafoil or Paraglider systems operates at speeds from 5m/s to 15m/s. At these speed, considering as atmospheric conditions a range of altitude between zero and 3000m, and a range of temperature from ISA+0 to ISA+20, minimum absolute pressure is about 600hPa and maximum stagnation pressure, considering the maximum dynamic pressure applied, is about 1020hPa.

In the same way, the minimum resolution of the sensor can be evaluated as the capability to identifying a change of 0.25 on the pressure coefficient at standard operational conditions. Considering, by design, the steady glide reference speed of 10m/s and a standard air density (specific mass) of 1.2 kg/m^3, it results a 0.3hPa variation, which is slightly above the maximum resolution of the selected sensor considering the full range.

It was decided to test the system in wind-tunnel using a rigid wing test bench based on a known NACA-4412 airfoil. In this way, pressure coefficient data could be crosschecked against cataloged data for validation. Varying the wing's incidence and flow speed the relevant flight envelope could be covered and accuracy could be checked, guaranteeing the adequacy of the instrumentation for flight test.

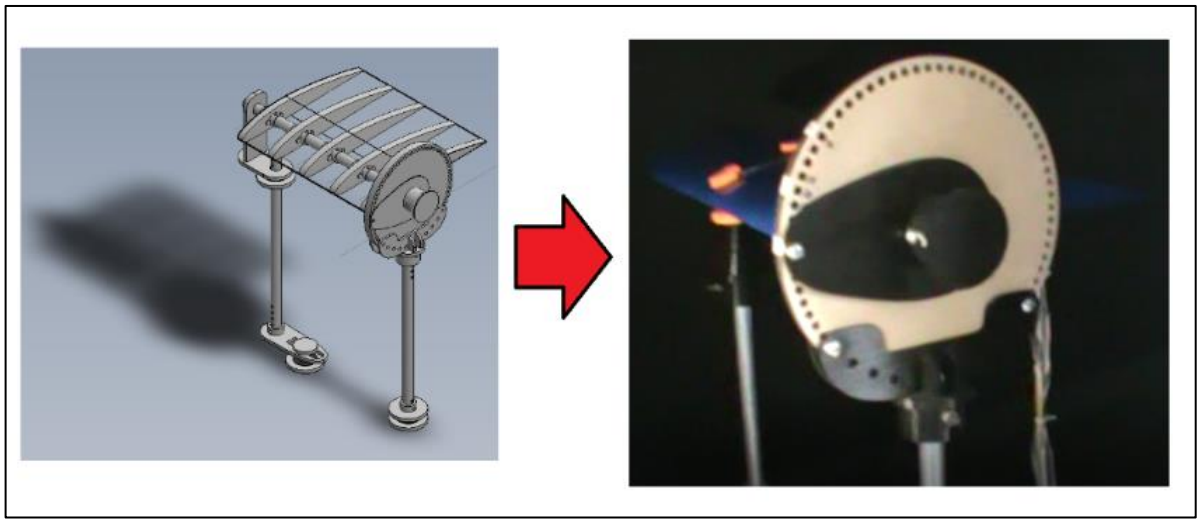

Figure 13: First test: Sensors test bench – NACA 4412 wing profile

Fig. 13 shows the model's design made in SolidWorks and the real bench installed in the wind tunnel with sensors attached. The test bench was calculated to support the aerodynamic load resulting from a maximum speed of 20m/s and maximum AOA of 40º, well above practical limits. It worked well and it is available for further tests. The sensors strip, on the other hand, presented some problems and did not meet the required performance.

Sensors were positioned at 8%, 30% and 65% of the reference chord at the upper and lower surfaces. Such a distribution was selected to cover the most important sectors of the airfoil, providing a useful pressure distribution pattern and maintaining a minimum level of disturbance of the cell structure. Sensors were numbered starting from the upper leading edge from 1 to 3 and starting from the bottom leading edge from 4 to 6.

The results from the first set of tests were considered insufficient. Although data shows that the sensors are able to read pressure variation due to speed and AOA change, high scattering on readings and some instability related to sensor's zeros were identified.

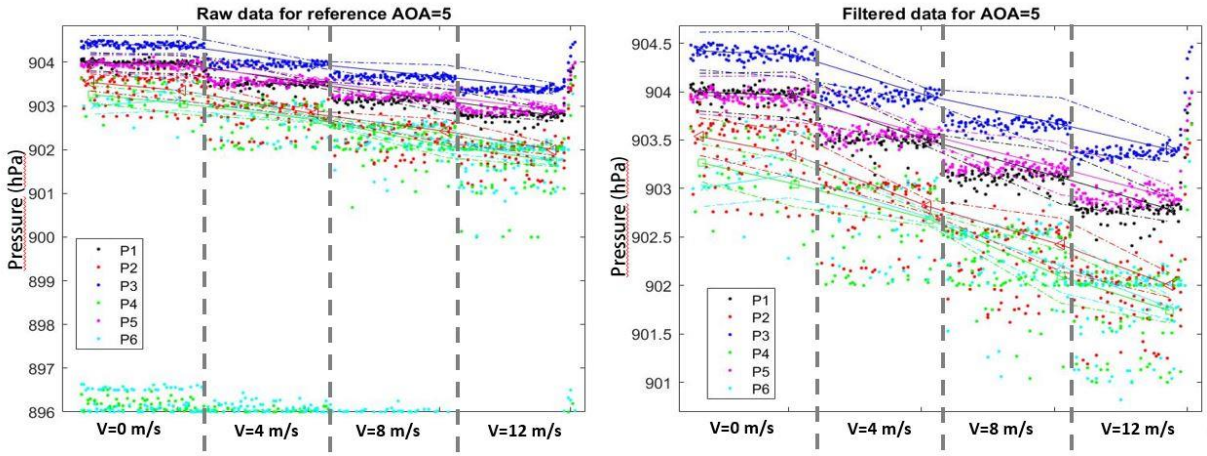

Figure 14: First test: Raw data absolute pressure measurements

Each portion of data horizontally aligned in Fig. 14 represents a different speed level of wind-tunnel airflow, which corroborates a minimum sensibility of the sensor in respect to the total dynamic pressure. However, it is possible to see that both the zero-point and scattering demonstrates poor resolution and precision to capture the low levels of aerodynamic pressure. Also, sensors at the bottom-surface extremities presented floor stability problems. It is obvious that reading oscillates far beyond the range of demanded precision (0.3hPa) reaching up to 8hPa variation. The other four sensors reading amplitude varied between 0.4hPa and 1hPa, which is still very high compared to the accuracy informed by the manufacturer (0.1hpa).

Applying a simple filter to the data to cut off the outliers results a lot more representative set of data, but still presents high level of scattering.

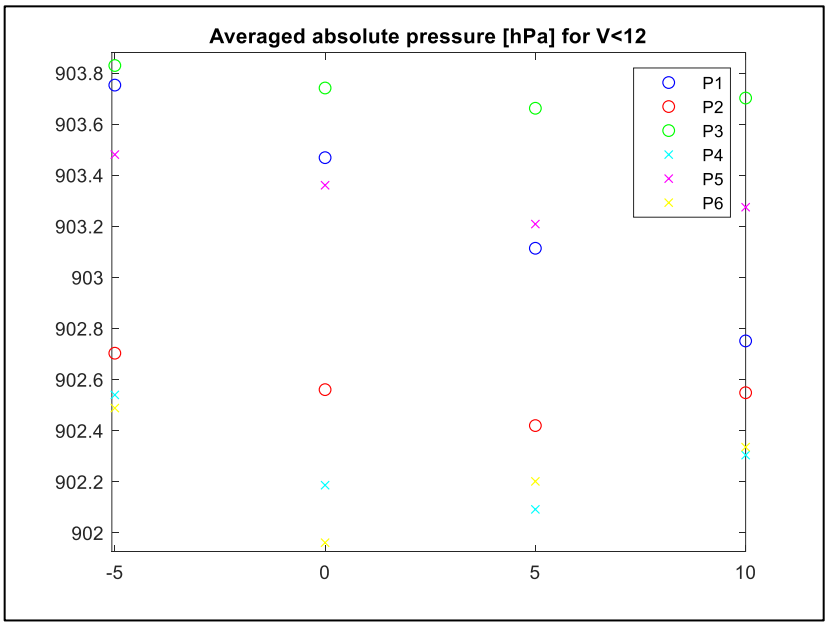

Figure 15: First test: Averaged absolute pressure as a function of AOA

Fig. 15 presents the variation of average pressure with AOA for a flow speed near to 10m/s. As can be seen, qualitatively, the general behavior is consistent since pressure on the upper leading edge decreases and pressure on the lower trailing edge increases as AOA increases. Following the same rational, Fig. 16 below shows the variation of filtered readings as flow speed is increased and AOA is kept at five degrees:

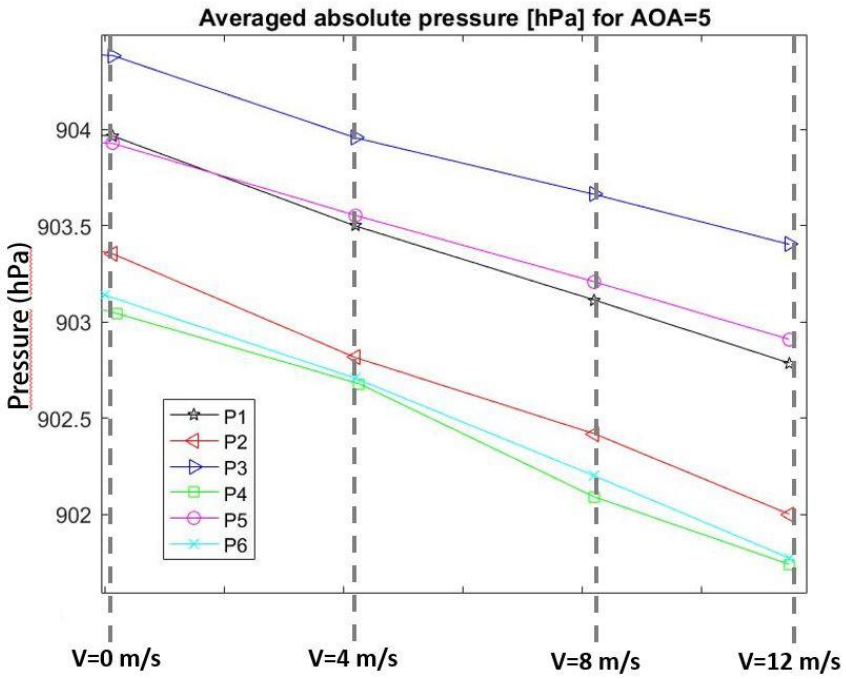

Figure 16: First test: Averaged absolute pressure as speed increase

Fig. 16, once again, shows coherent qualitative results, since the pattern of diminishing in pressure reading is sustained for a fixed AOA as flow speed is increased. However, precision is beyond unacceptable. For that reason, a new analysis toward sensors setting was accomplished and a new filtering mode was set to reduce variability and increase precision. It was observed that the first set of test did not use the high precision mode of the sensor as instructed in the manufacturer's manual. After adjusting the settings and filters an out-of-bench test showed a reduction in maximum observed variation from 0.27hPa to 0.024hPa. Even though, precision remained at an unacceptable level especially at low speed range. Therefore, it was concluded that the system architecture should be reviewed.

Second setup – absolute pressure sensors with light wiring and no protective case

In order to reduce potential disturbances to the boundary layer, which contributes to data scattering, it was decided to abandon the protective cases which might be causing too much turbulence and compromising the sensibility of the system.

As the qualitative analysis showed coherent readings and facing a substantial improvement in resolution with the correct setting of the sensors filters, it was decided to repeat the tests. However, the second attempt to test failed due to vibration problems at the welded wires. As a matter of fact, the observed problem was likely to occur on the real-size prototype where the extension of wiring would be much longer and subjected to much more severe deformations due to aerodynamic drag and wing's motion. Therefore, it was decided to change the design using wi-fi modulus in order to avoid this kind of disruption.

Third setup – absolute pressure sensors with wi-fi

A third test was made using wi-fi modulus in order to eliminate long wires of the design as illustrated in Fig. 17, however, data integrity failed. The data sent by the wi-fi modulus was clearly corrupted and the rate of readings was unacceptable reaching almost 1 second interval. Therefore the wi-fi solution was also abandoned.

Figure 17: Test bench setup with wi-fi modulus

Fourth setup – absolute pressure sensors with cables

After reconsidering some mechanical and electronic options, a fourth test was run using a more robust setup for wiring, including a cable duct to prevent vibration and going back to a local data storing strategy based on SD-card.

Figure 18: Revised bench with local SD-Card

At this time, although an improvement in stability of the readings was observed, the positioning of the sensors was disturbed by the stiffness and size of the cables, which also corrupted the boundary layer, leading to a worse level of inaccuracy and uncertainty. In many conditions pressure variation could not be noticed between sensors.

Conclusions toward system's architecture

From the first to the fourth setup, the results obtained using static pressure sensors proved to be insufficient to capture aerodynamic pressure variation as desired. It materializes some of the reasons why the previous researchers who executed successful experimental tests on inflatable cells applied conventional pressure gauges, disconnected to the wing. It also makes clear that solutions based on pressure belts, as presented by McCarthy [35] are more suitable for aircraft which flies at a superior speed range. It can be inferred that both sensors low resolution and boundary layer disturbance were the main factors determining the failure of these attempts.

The most important limitation to be highlighted is that no differentiation was perceptible between positions along the chord at most of the AOA tested. Therefore, there are strong indications that, for inflatable wings operating at low speed, the level of pressure variation due

to aerodynamic airflow requires measuring very low levels of pressure, which is more accessible through a differential pressure approach.

Finally, a decision was made to drastically change the system philosophy and development method. It was decided to base not only the flight test instrumentation, but also the aerodynamic analysis, on local differential pressure readings. It means, to work with differential pressure sensors installed inside the inflatable wing, thus, preventing any disturbance of the boundary layer and also guaranteeing pressure measurement precision.

3.2 Flight test instrumentation design and assembly

Following the recent miniaturization of small sensors applied to unmanned air vehicles (UAV), a new class of light and precise instrumentation is available to a broader range of applications [36]. Complying with the three principles stablished for designing a flight test instrumentation for in-flight aerodynamic characterization of inflatable wings, the option of applying differential pressure sensors demonstrated to be the most adequate and useful.

The systems architecture relies on reading the inside-outside pressure differential at different points on the upper and bottom surfaces by placing a group of sensors on the inside of the inflatable wing, attached to each surface. The pressure measurement units are intended to be light enough to impose minimum load at the upper-surface, not impairing inflation, and an integration board designed to be positioned at the bottom-surface near to the aerodynamic center, minimizing mechanical interference. As the sensors are inside the wing, disturbances on the boundary layer can be negligible if the shape deformation caused by the system is minimized. The use of local storage of data and protective cases guarantee reliability and robustness, as to sustain all movements of the wing without detaching or losing recording capability. Finally, the high resolution of differential pressure sensors provides the desired precision, assuring the capacity for reading the low-level aerodynamic pressure differential variations occurring over their flight envelope.

Additionally, the dynamic measurement of inner-outer pressure difference is useful to evaluate, straightforwardly, inflation stability, thus, collapse susceptibility, which is a permanent concern in inflatable wings operation. Also, pressure differential measurements may provide valuable information about the airfoil confined residual flow, which plays a vital role in pressure distribution dynamics.

The envisioned system to be developed for proceeding with the in-flight measurements defined for phase 2 is based on an assembling of four independent measurement strips as illustrated below.

Figure 19: Instrumented wing sketch

Fig. 19 illustrates the use of a total of 24 sensors distributed on four strips symmetrically attached to the wing. The system is designed to be installed on a $23m^2$ paraglider with a 12m span. The first pair of measurement strips are supposed to be placed near to the root of the wing, which correspond to a profile station at 25% of the span starting from the central profile. The second pair is supposed to capture readings at a station distant enough to characterize the pressure gradient throughout the span, but still at a point where the airfoil chord is large enough to be counted as a significant lift provider. The second strips positioned at 75% of the span is capable of reflecting the anhedral effects and the impact of torsional and flexional moments acting at the extremities of the wing influencing the local aerodynamic airflow.

It is important to take in consideration the optimum number of sensors attached, to not overload the upper surface. Therefore, at this point, it is not considered adequate to add more than 2 pairs of strips to a normal-size wing. However, for large scale parafoils, as used in cargo positioning solutions, a greater number of strips can be, for sure, considered. As the system is designed to work independently, with the data synchronization based on GPS time, any number of strips can be easily combined. In this way, the prototype built to qualifies the system represents one single measurement strip, consisting of six ordained sensors connected to a control board. For a dedicate study of the aerodynamic phenomena in a wind-tunnel, using a rigid test bench, it may be adequate to apply a strip with a much larger number of sensors, in order to fully characterize the pressure-differential profile at different flight conditions. Such an approach is scientifically relevant; however, it is unpractical and inadequate for the purpose of validating the flight test instrumentation as proposed.

Based on typical pressure coefficient distribution profiles, sensor location was planned to cover the three main portions of the airfoil, as illustrated in Fig. 20. The first pair of sensors were positioned at 8% of the baseline chord, which is the region that contributes the most for the airfoil lift. These measurements are particularly relevant to evaluate the maximum

achievable lift. The sensors installed near the aerodynamic center, at 30% of the baseline chord, cover the portion of the profile where circulation flow should be fully developed. In this case, the pressure distribution is still significantly affected by changes in the angle of attack. These measurements are especially important in revealing the wing aerodynamic characteristics as a function of flight conditions. Finally, the sensors located at 65% of the baseline chord aim to monitor the final portion of the airfoil, where pressure differentials favor stability. These rear measurements provide a relevant baseline to evaluate the pressure distribution gradient along the chord.

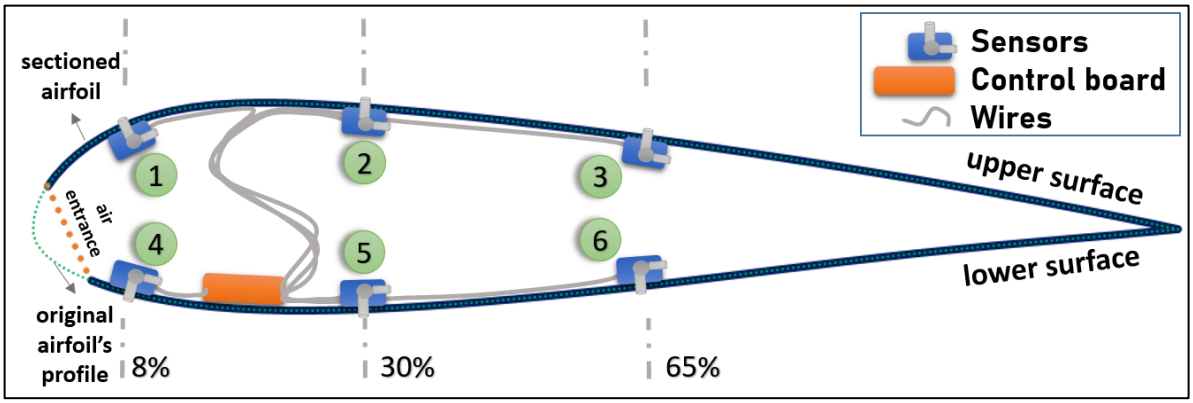

Figure 20: Inflatable airfoil instrumentation sketch.

Once defined the setup, systems specifications and limitations can be designed based on the intended application. Sections 3.2.1 to 3.2.3 details the relevant aspects of the constructed prototype.

3.2.1 Pressure range and resolution minimums

The designed system is based on direct pressure differential readings, whereas traditional aerodynamics analysis is mostly based on external pressure coefficient, which remains an important parameter to be used comparatively and for airfoil design. Therefore, establishing the correlation of pressure coefficient and pressure differentials measurement is the first step for setting the ground rules for aerodynamic characterization based on local differential pressure analysis.

Pressure coefficients at low Reynolds is obtained by the equation:

$$C_p = \frac{P_e - P_{atm}}{\frac{1}{2} \cdot \rho_{air} \cdot {V_\infty}^2} \quad (1)$$

where P_e is the external pressure at the surface, P_{atm} is the local atmospheric pressure, ρ_{air} is the air density (specific mass), and V_∞ is the undisturbed flow speed.

The inner-outer differential pressure at some given point on the airfoil surface is given by

$$\Delta_p = P_e - (\kappa \cdot q_\infty + P_{atm}) \tag{2}$$

where, $q_\infty = \frac{1}{2} \cdot \rho_{air} \cdot {V_\infty}^2$ is the reference dynamic pressure, and κ is defined as the internal flow factor, reflecting its role as an indicator of how much of the maximum available dynamic pressure is observed at each point of the internal surface.

Acknowledging the existence of a recirculation internal flow, an inner pressure distribution is established due to the flow conditions and airfoil geometry, which are also affected by airfoil thickness and the air intake design. Therefore, for a defined baseline airfoil, the internal flow factor is supposed to vary from 0 to 1 as a function of speed, angle of attack, air intake orientation and size. Therefore, the internal flow factor can also be seen as an internal pressure coefficient.

Substituting equation (1) on (2), the local pressure differential can be described as

$$\Delta_p = (C_p - \kappa) \cdot q_\infty \tag{3}$$

Equation (3) shows the direct relation between the pressure differential and pressure coefficients, highlighting the influence of the internal flow factor, a variable brought by the inflatable nature of the wing. It is important to notice that both C_p and κ are geometry-based coefficients reflecting the airfoil characteristics. For a defined flow condition (speed and incidence) the airfoil geometry will determine how pressure varies though the surfaces generating lift and drag. For closed airfoils the C_p distribution is enough, since there is no internal pressure variation to consider. A single coefficient related to differential pressure could have been defined; however, separating external and internal pressure coefficients allows a more didactic approach. Experimental data of parafoils and paragliders [5,22,24,25] using absolute pressure measurements have shown an external pressure coefficient ranging from −1.5 to 1.0. These results support computational predictions from which the C_p distribution follows the baseline airfoil pattern, with a relevant modification limited to the air intake region [6,19,27]. Considering a steady glide speed of 10 m/s, typical of inflatable wings [26], a differential pressure range of 0–150 Pa is expected throughout the surface. Then, assuming a fixed air density (specific mass) of 1.20 kg/m^3, which is the standard average air density at the site where the experiments where conducted, Eq. (3) generates data as illustrated by Fig. 21.

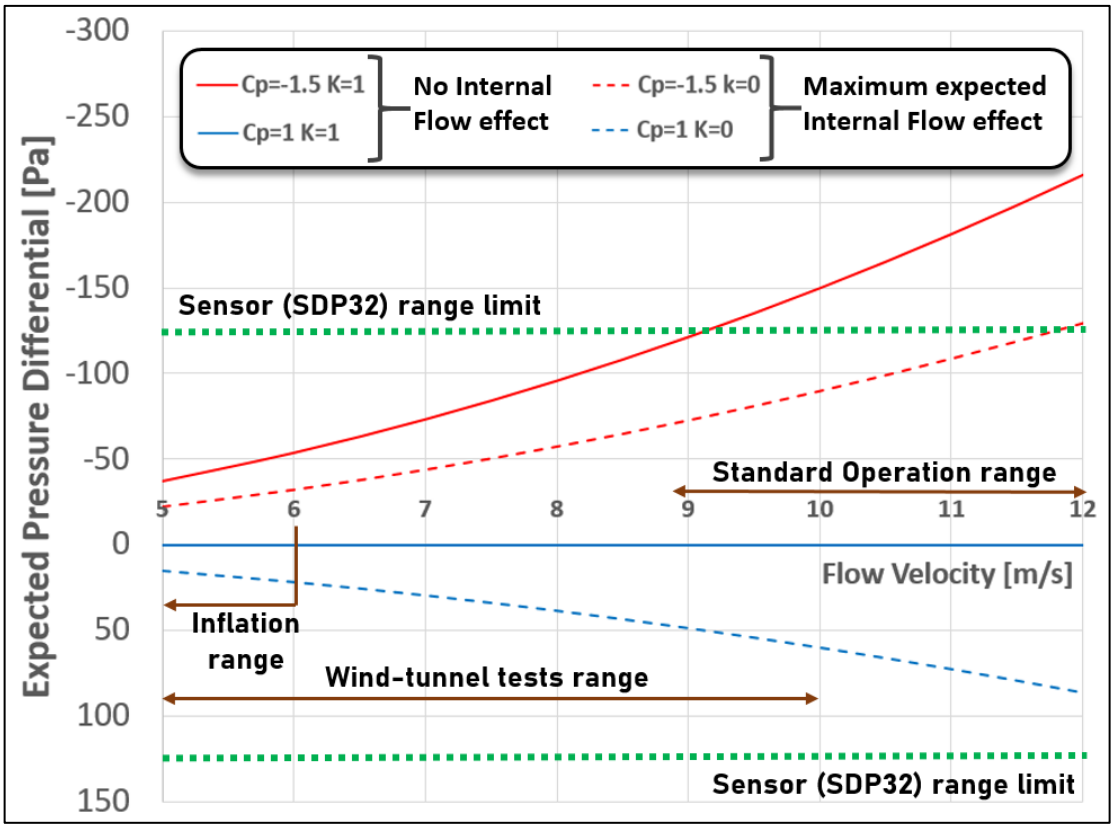

Figure 21: Pressure-differential range and the related flight regimes.

Fig. 21 shows an extended envelope useful to explore the effect of each variable. It makes clear the preponderant effect of speed on the range of measurements. It also shows that resolution requirements must be set considering low speed limits. Finally, it also reveals the importance of internal flow in reducing the maximum differential readings, if present.

The expected level of pressure differential to be measured at each condition dictates the range for sensor selection. In the same way, the capability of detecting relevant variations caused by aerodynamic phenomena dictates resolution minimums. The derivative of Equation (3) with respect to C_p reveals, for a defined airflow condition, how the pressure measurement is affected by a local variation on the pressure coefficient ($\widetilde{C_p}$). If the span accuracy of the sensor is given in terms of a constant percentage of the reading ($\epsilon_{\%}$), the derivative of Eq. 3 with respect to C_p reveals, for a defined airflow condition, the consequent uncertainty on pressure coefficient ($\widetilde{C_p}$) measurement

$$\widetilde{\Delta_p} = \widetilde{C_p} \cdot q_\infty \tag{4}$$

For the same steady glide flight speed, a 0.1 variation on C_p represents a 6 Pa variation of local pressure differential. Such a small variation is attainable for differential pressure sensors, but constitutes a real challenge for absolute pressure sensors. Looking from another

angle, Equation (4) reveals how the external pressure coefficient, indirectly measured, is affected by the sensor's precision limits, considering the internal flow factor to be unaltered. Considering that the accuracy of the differential pressure sensor is given in terms of a constant percentage of the reading ($\epsilon_{\%}$), the maximum uncertainty affecting C_p is given by:

$$\widetilde{C_p}_{max} = \epsilon_{\%} \cdot \left(\left| C_{p_{max}} \right| + 1 \right) \tag{5}$$

Equation (5) relates sensor's span accuracy to the pressure coefficient measurement potential uncertainty. It reveals that, for a 3% resolution, and an external pressure coefficient range varying from -1.5 to 0, the sensor's contribution in pressure coefficient measurement uncertainty stays between 0.075 and 0.03, which is absolutely negligible.

Finally, it is important to highlight that, in addition to the fact that differential pressure sensors present range and resolution more suitably for aerodynamic pressure levels, measuring the outside–inside local differential instead of external absolute pressure allows for the capturing of the effects of both external and internal flow simultaneously. In this way, it is possible to capture the final effect that results from aerodynamic forces without the trouble of investigating external and internal pressure separately.

3.1.2 Mechanical and aerodynamic constraints

Mechanical and aerodynamic constraints are related to adverse flow disturbances due to the presence of instrumentation. The first effect accounted for refers to the boundary layer disturbance resulting from the sensors' presence over the wing. Previous results have shown that, even for thin sensors, their attachment to the external surface may alter the boundary layer significantly [34]. It is worth mentioning that the first prototype designed for the present research used sensors attached externally to the surface of the wing and faced the same problems that are reported. This drawback was prevented by designing a system in which the sensors are attached in the inner surface, as illustrated in Fig. 20, thus preserving external flow integrity.

Wing shape deformation, due to sensors attachment at the upper surface, need also a consideration. The local pressure differential and the fabric tensile strength interactions counterbalance sensors' weight in a highly complex phenomenon. Methods for fluid-structure analysis of membrane behavior represent a particular field of research [37, 38] and is beyond the scope of the present work. Nevertheless, a simplified evaluation was developed to limit the operational mass of the sensor component .

The effect of a localized additional load was estimated with a simplistic but effective approximation considering the inflated cell as a pressure vessel [39]. For that, the minimum tension supported by the fabric should equal the longitudinal stress, as depicted in Fig. 22.

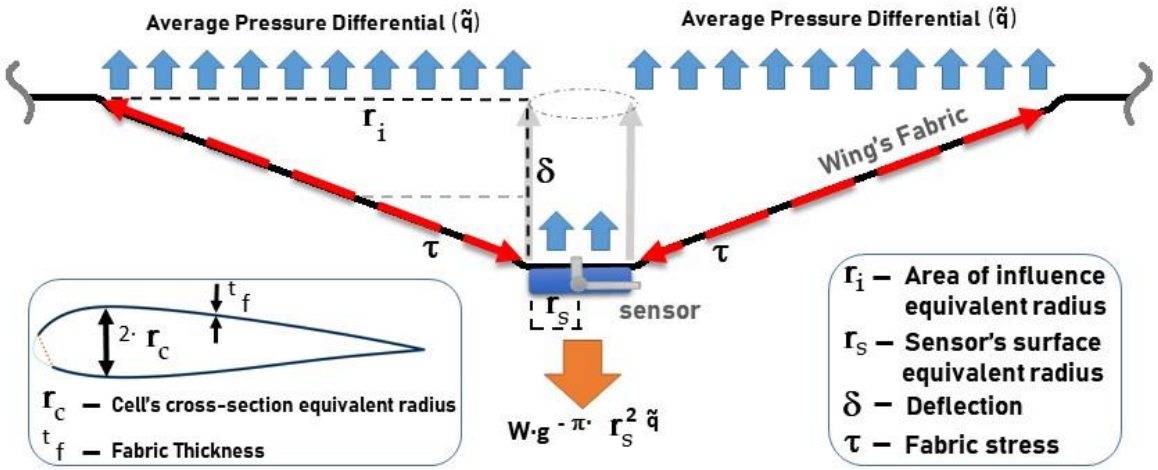

Figure 22: The simplified mechanism for sensor weight balance.

The tensile strength of the standard fabric is exceptionally high compared to the load imposed by small sensors. For very small deflections and neglecting the fabric specific weight, the weight of the sensor not sustained by the local differential pressure is compensated by the vertical component of fabric tension generated by inflation.

$$W \cdot g - \pi \cdot {r_s}^2 \cdot \tilde{q} = \pi \cdot (r_s + r_i) \cdot \tau \cdot \delta \tag{6}$$

In a conservative approach, assuming a cylindrical vessel where the diameter is the maximum height of the cell, the longitudinal stress, providing the expected minimum level of tension, is given by

$$\tau = \frac{q_\infty \cdot r_c}{2 \cdot t_f} \tag{7}$$

Equation (7) indicates that tension (τ) is proportional to the total dynamic pressure (q_∞) that inflates the cell, and to the ratio between the reference radius of the cross-section of the inflated cell (r_c) and fabric thickness (t_f).

The radius of influence can be directly determined by the area which makes the force resulting from the averaged local differential pressure ($\tilde{q}$) sufficiently high to sustain the weight (W) of the sensor unit

$$\pi \cdot {r_i}^2 \cdot \tilde{q} = W \cdot g \tag{8}$$

where

$$\tilde{q} = \left| C_{p_{(x,AOA)}} - 1 \right| \cdot q_{\infty} \tag{9}$$

Finally, from Eq. (6), the estimated deflection can be inferred as

$$\delta = \frac{2 \cdot t_f \cdot (W \cdot g - \pi \cdot r_s^2 \cdot \tilde{q})}{\pi \cdot r_c \cdot (r_s + r_i) \cdot q_{\infty}} \tag{10}$$

Equation (10) allows evaluating the potential impact of sensors attachment to the upper surface on shape stability. A criterion can be defined for each condition using basic boundary layer modelling strategies.

3.1.3 Instrumentation Schema and Measurement Chain

The measurement chain is illustrated in Figure 23 below:

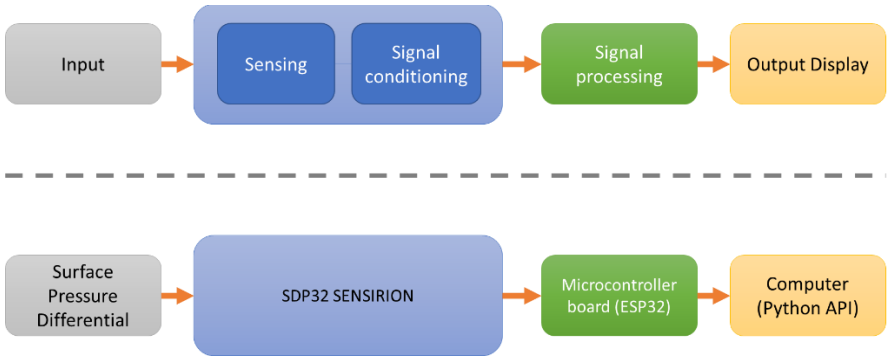

Figure 23: Measurement Chain

The sensor element is based on by-pass flow measurement and is a pre-calibrated and temperature compensated sensor, which provides differential-pressure signal interpreted by the microcontroller board, able to handle up to six sensors. The electrical signal received by the microcontroller board was converted to pressure data and stored directly in a local SD-Card and dynamically sent through wi-fi connection to a computer. The computational application (API) presents the reading chronologically using the microcontroller timer as reference. The details about the sensor and the embedded system are presented below.

Sensors selection and prototype setup

The recent boost in the UAV industry made available a whole new set of sensors potentially able to fit the designed specifications for this research. The Sensirion® SDP32-Digital [40] was found to offer the best cost-benefit for the application, after searching several options on the market. The SDP32 is a pre-calibrated and temperature compensated sensor capable of measuring pressure differentials up to 125 Pa with a zero-point accuracy of 0.08 Pa and a span accuracy of 3% (RD). It presents a typical measurement time of 45 ms, and resists

overpressure up to 1.0 bar, at a price of less than USD 30. The SDP32 also allows reflow soldering, which reduces the effective cost of the manufacturing process.

Main specifications of the SDP32 [40]:

- Measurement range: - 125 to 125 Pa
- Zero point accuracy: 0.08 Pa
- Span accuracy: 3% of reading
- Zero point repeatability: 0.025 Pa
- Span repeatability: 0.5% of reading
- Span shift due to temperature variation < 0.5% of reading per 10°C
- Offset stability < 0.01 Pa/year
- Flow step response time ($\tau 63$) < 3ms
- Resolution: 16 bit
- Calibrated for: Air, N2
- Media compatibility: Air, N2, O2, non-condensing
- Calibrated temperature range: -40 °C to +85 °C

Equation (5) reveals that, for a 3% accuracy, and an external pressure coefficient range varying from -1.5 to 0, the sensor's contribution in pressure coefficient measurement uncertainty stays between 0.075 and 0.03. These values corroborate the adequacy of the SDP32 in terms of accuracy.

Sensor's communication was made via I2C protocol, a 2-wire serial interface generally used for moderate frequencies data transmission. This protocol allows us to connect with several devices with only 2-wires, the data line (SDA) and the clock line (SCL), as shown in Figure 24.

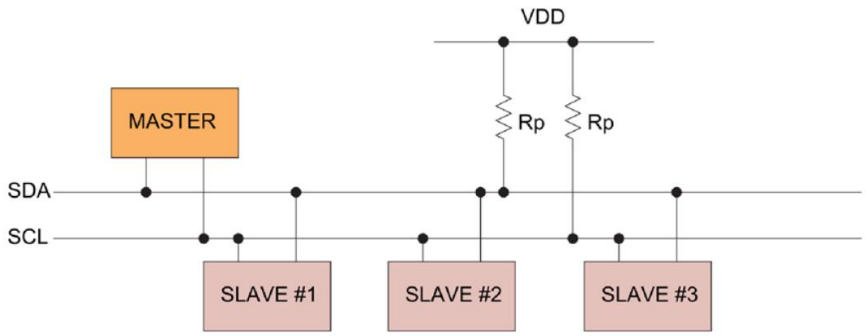

Figure 24: I2C protocol wiring [2].

In Figure 24, the Rp resistors are used to pull the lines to a high level to keep the idle state from each device and for proper operation of the Inter-Integrated Circuit (I2C) communication. For a brief understanding of this protocol, let's assume a single data package transmission. At the start of the packet, a master device takes control of the bus by driving the Serial Data (SDA) low while the Serial Clock (SCL) remains high. This initiates data package transmission. Next, a 7-bit address is transmitted followed by an R/W bit to indicate whether the master wants to read (1) or write (0) instructions. The addressed slave device then transmits an Acknowledge (ACK) bit by pulling down the SDA line. The address of each sensor can be set by an external resistor, as shown in Figure 4. The SDP32 sensor allows only 3 different addresses. For this reason, an I2C expander is necessary, which expands up to 6 different slaves. By using the expander (TCA9548APW), the address is kept fixed. The “0x21” was chosen.

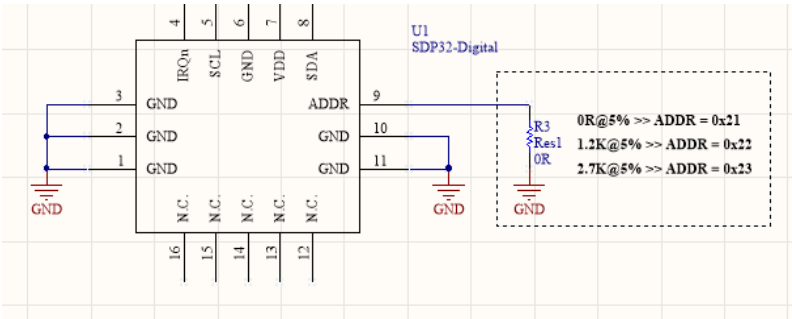

Figure 25: Address configuration with resistor value.

For the resistor packages, the 0402 size code was chosen by default, except for the resistor labeled “R4”, which is a jumper used to avoid vias on the Printed Circuit Board (PCB). In this case, the package used was 1206, which allows for routing optimization and compact design.

The connector chosen for this application is the compact FI-S5P-HFE. This connector has 5 positions, in which two are used for I2C bus lines, and the other three for power signals.

Microprocessor Board

For the microprocessor, the ESP32 module was found to be the best Integrated Circuit (IC) for this application, due to its extended functionality, high speed, low price and manly for the fact that it comes with an integrated Wifi/Bluetooth transceiver, which makes the design even more compact. Furthermore, this module has an integrated antenna, and additional circuit conditioning, which allows for a clean and simple design procedure.

The main characteristics of this IC are listed below:

- 80-240Mhz clock;
- 2 CPU cores;
- 2.7 to 3.6V power supply range;
- 80mA current consumption;
- SD card interface, Ethernet, I2C, UART, among others;
- Wifi integrated;
- Bluetooth integrated;

For ESP32 to be operational and stable, it is necessary a clean DC power supply, which is difficult to meet with a single Li-ion battery. A single-cell li-ion battery may vary its nominal voltage from 2.7V, when it is discharged, to 4.2V at full charge capacity, exceeding the absolute maximum rating. This behavior could damage the ESP32 module and other components on the board.

For the voltage to be regulated to a defined value, most IC´s use a feedback loop, which senses the output voltages and amplifies the error employing the duty cycle via a Pulse Width Modulation (PWM) controller. For this project, the IC TPS63060 was chosen, for its size, current capability and efficiency up to 93%, which extends the requirements defined previously. Its schematic is shown below.

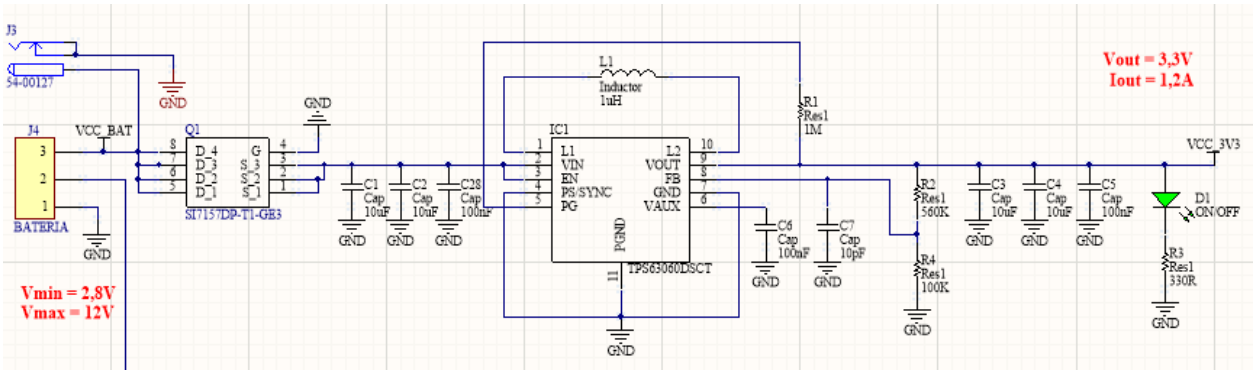

Figure 26: Buck-boost converter circuit with TPS63060.

To validate this topology, a simulation was made on TINA®, a simulator provided by the manufacturer. By varying the input voltage from 2V up to 4V, we simulate a battery voltage variation under the nominal level. The result is a regulated DC output voltage of 3.3V, as shown in Figure 27.

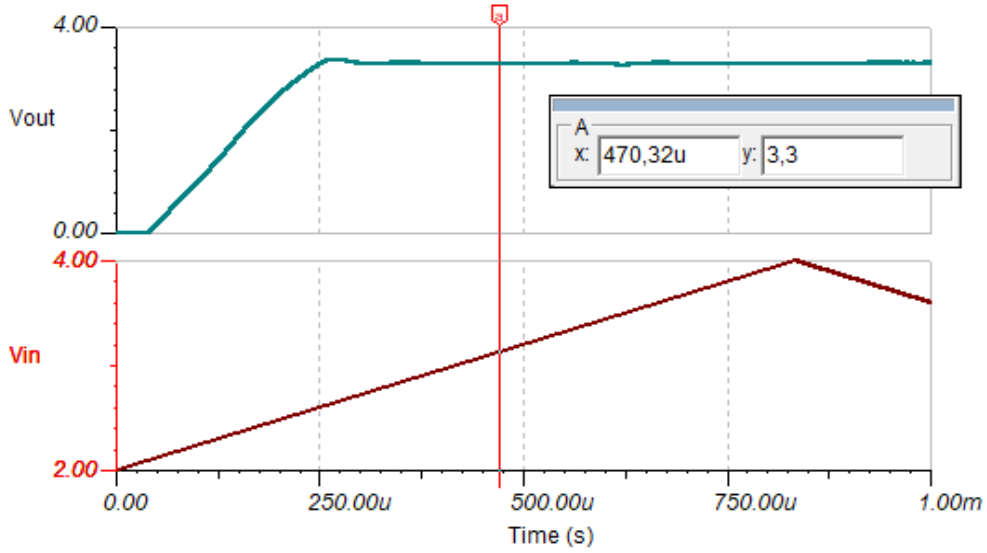

Figure 27: Simulation of a triangular wave input on the buck-boost TPS63060 Topology.

As a characteristic of switching power supply, a little ripple of ~25mV is expected. For this to be eliminated, a Low-Dropout (LDO) regulator is often placed after the DC-DC regulator. In this case, it was not needed since the voltage ripple was well below this value.

For the microcontroller (ESP32) to be programmed, it is also needed a circuit that converts the USB voltage levels into a conventional UART communication. For this purpose, the IC FT232RL was used, together with the topology depicted in Figure 28.

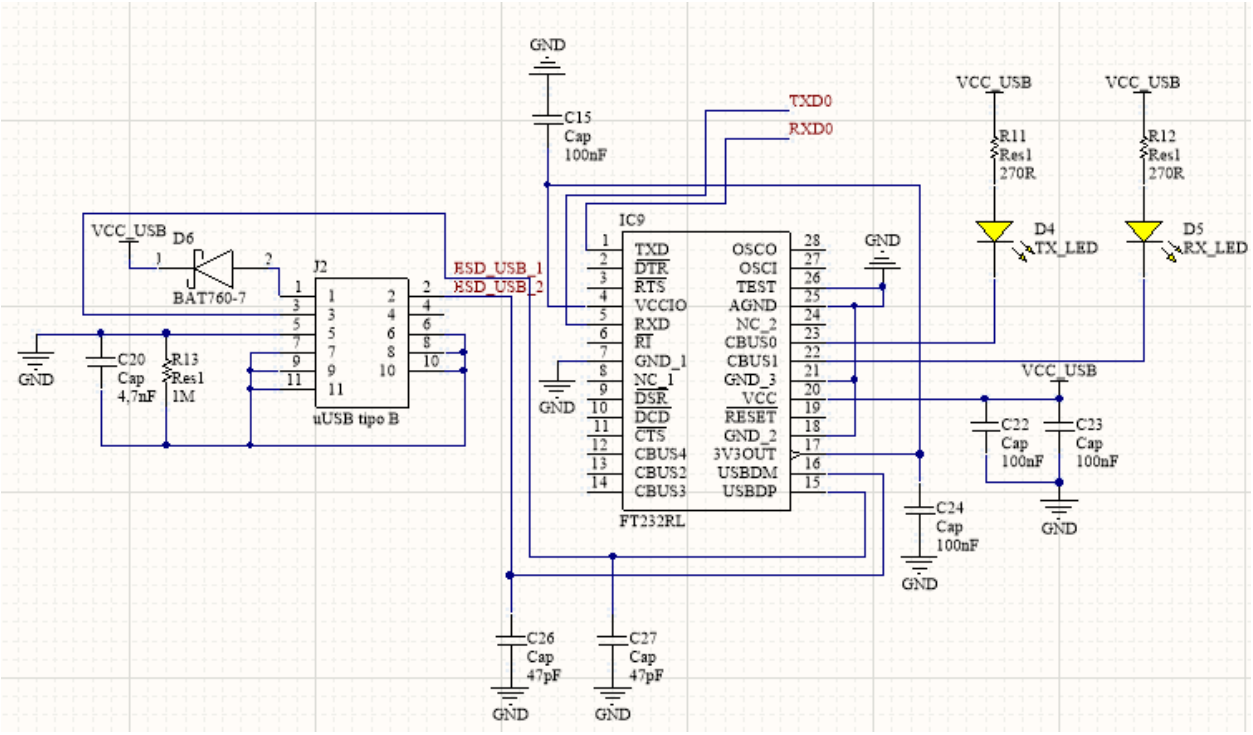

Figure 28: RTC Circuitry.

Employing this topology, the board is now able to connect with any USB host device. The LED´s presented in this circuit (D4 and D5), indicates if data is being transmitted or not. To protect this circuit against short-circuit or voltage polarity reversing, the Schottky diode BAT760-7 was used.

For the RTC circuit, the one that sends and stores the current time/date value, it was preferred IC´s that used I2C protocol, the same protocol used to communicate with the sensor modules. By that, it would facilitate the layout design and save a few GPIO pins, which could be used later by other applications. The IC chosen for this purpose is the DS3231, a high precision RTC clock. It integrates battery management and with only 2 ppm variation, accounting for 1 minute variation a year.

Finally, for the ESD protection, needed for applications where there is much human interaction between the board connectors, the IC´s PUSB3FR4 was placed between all the connectors connection, except for the SD card connector, which was used the CM1624 IC, which integrates EMI filters and TVS diodes for ESD protection. The final layout is illustrated in Figure 29.

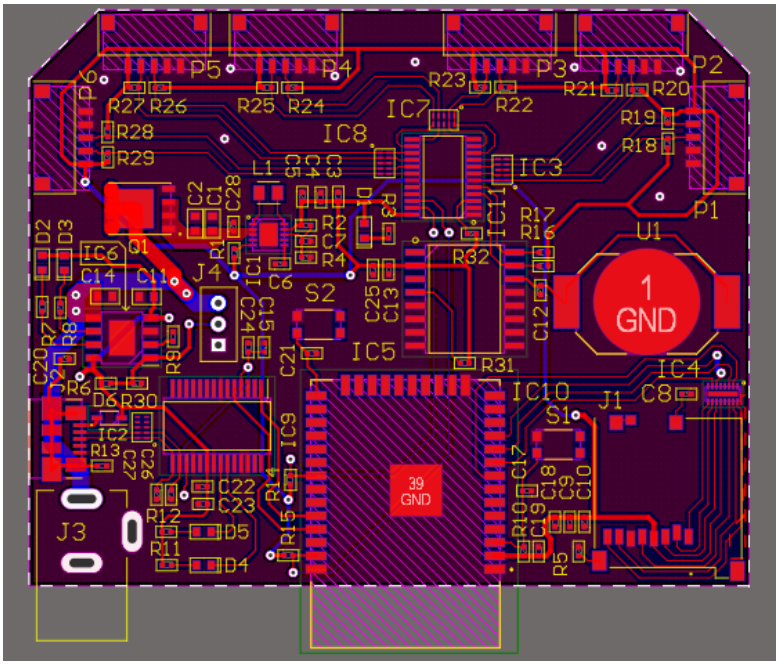

Figure 29: Final layout of the microcontroller board.

Measurement strip

As illustrated in Fig. 20, the instrumentation strip integrates six sensor units to an ESP32 microprocessor module, which comes with WIFI/Bluetooth transceiver and antenna. A single 3.7 V Li-ion battery cell was used to supply the microcontroller's power and the set of sensors. Sensors were connected to the control board using lightweight cables, freely disposed inside the airfoil cell to minimize confined flow disturbances. Data was recorded directly into a local SD-card and simultaneously sent via WIFI for remote monitoring.

The sensor unit was mounted inside a 3D printed ABS plastic case designed to be glowed or sewed to the wing's fabric, providing perfect attachment to the airfoil surface and motion resistance. Fig. 30 illustrates the designed sensor unit.

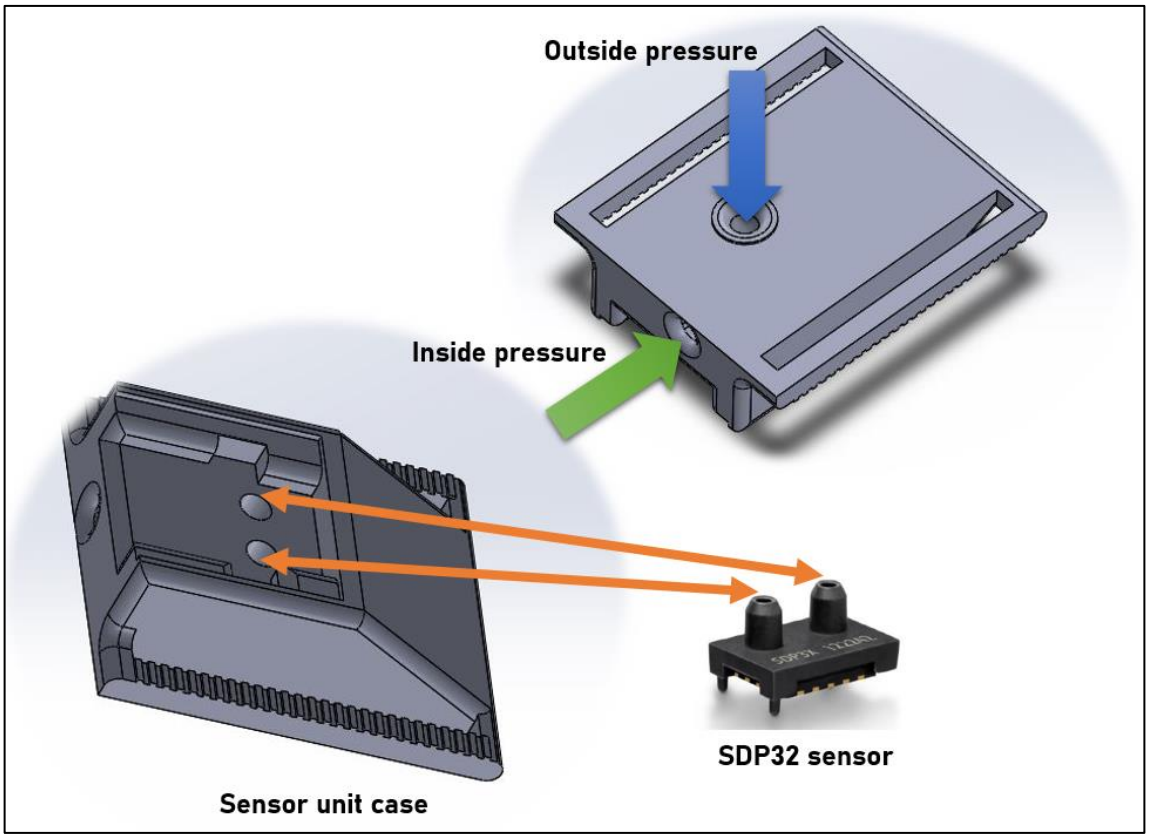

Figure 30: Sensor Unit.

Fig. 30 shows the two separated intakes leading to sensor's input pin. For the external pressure the access was fully vertical and unobstructed, whereas for internal pressure access, a transverse duct was used. Although the duct diameter is much higher than the input pin, a reduction on internal pressure readings is expected when internal flow is present. Hence, the uncertainties on internal pressure distribution may increase. When internal flow is relevant, a correction for the inner pressure may be applied taking in to account the case geometry.

The complete sensor unit weighted 7.0 g distributed over a 2.6 cm x 2.9 cm surface, resulting in a 0.93 g/cm^2 load. The cell had an 8.76 cm maximum cross-section height, and was made with a nylon fabric with 0.6 mm thickness. Equation (10) suggests that, for the worse situation when $C_p = 0$, and V_∞ = 5 m/s a wing surface deflection of 0.6 mm is expected. For the same situation the minimum boundary layer thickness can be calculated as suggested by Ferreira [41] using

$$\delta_{(x)} = 4{,}64 \cdot \sqrt{\frac{\mu_c \cdot x}{V_\infty}} \tag{11}$$

At 5 m/s air speed, considering a standard air kinetic viscosity of 14 m/s^2, a 2.2 mm boundary layer thickness is anticipated at the location of the first sensor (8%). It demonstrates

that the predicted deflection is far below the boundary layer thickness even at pre-inflation speeds. As speed increases, deflection decreases rapidly, providing an additional margin relative to the boundary layer thickness. For speeds inside the operational flight envelope (≈9 m/s), the predicted deflection approaches 0.2 mm, which is completely unable to affect aerodynamic characteristics or measurements.

The predictions suggest that, even at low speeds, the sensor unit causes a negligible deformation on cell's shape, which is not supposed to affect aerodynamic characteristics. Exploring design limits, Fig. 31 uses Eq. (10) and Eq. (11) to reveal how the potential disturbance increases with sensor's weight if everything else is hold constant.

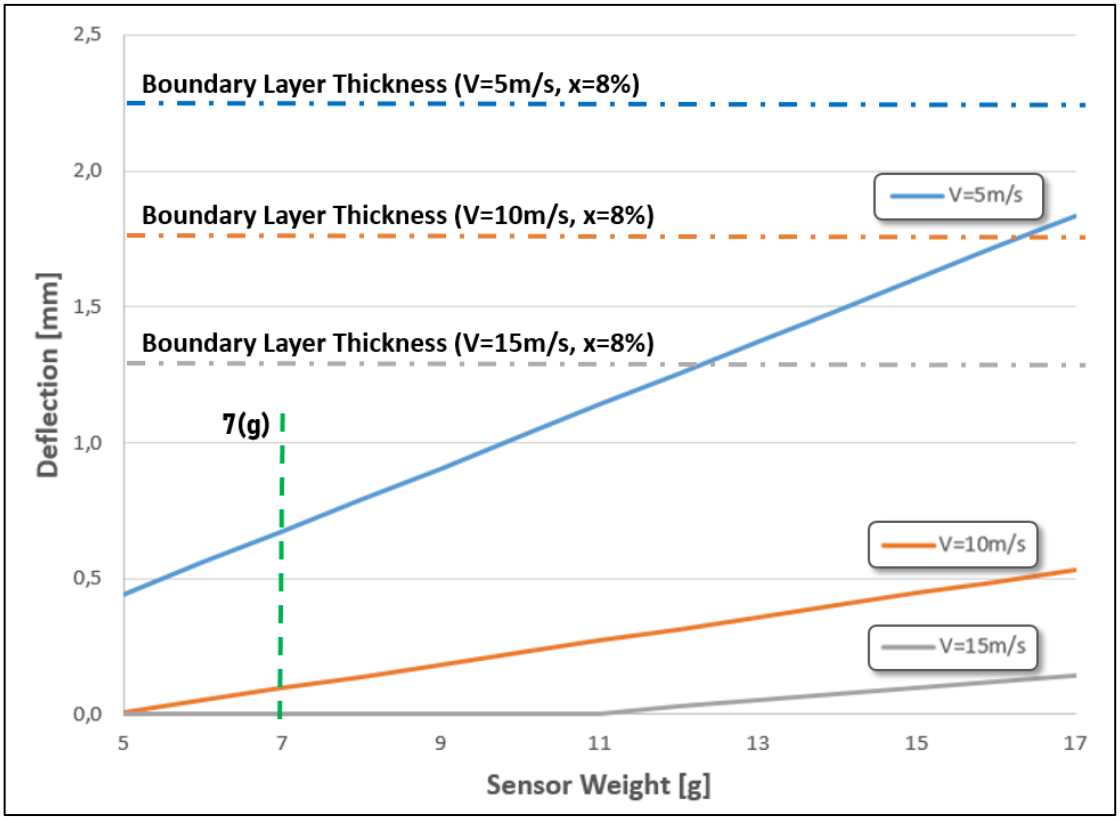

Figure 31: Potential deformation due to the weight of the sensor.

In Fig. 31 the distance between the boundary layer thickness threshold and the line representing the relation between deflection and sensor's weight for each speed represents an assurance margin for airflow integrity. It indicates that the designed instrumentation meets the basic requirements for aerodynamic non-disturbance, since for a 7 grams sensor the expected deflection stays far below the expected boundary layer thickness for the entire speed range. It suggests that the potential deflection caused by the sensor unit is negligible considering the extension of the aerodynamic flow effect.

Final measurement uncertainty

Following the basic metrological concepts, error is the difference between the measured value and the ‘true value’ of the thing being measured. Therefore, without a viable standard reference, it is extremely difficult to evaluate and to measure error. In this way, it is often more useful to evaluate measurement quality in terms of uncertainty. Uncertainty is a quantification of the variation, or the doubt about the measurement result. Such an information is much more practical, and also, much more adequate to evaluate comparative measurements.

The problem at hand is addressed by comparing the differential-pressure readings obtained at the surface of the wing for several flight conditions in comparison to a steady flight condition (design point). Taking in consideration the many variables involved:

- Wind-tunnel effects on local flow speed
- Wind-tunnel instrumentation error
- Test-bench structural and “finite-wing” effects on aerodynamic flow characteristics
- Pressure-differential instrumentation error
- Environmental variations on static pressure and temperature

Without a more robust instrumentation associated to multiple parametric corrections related to the many variables, each one demanding specific experimental data, it is unlikely to obtain an accurate result or even estimate error precisely for calculated parameters. On the other hand, for the pressure-differential signal, the sensor’s resolution minimum represents a fair estimation of accuracy and the coefficient of variation of the stabilized measurements provides a fair indication of measurements’ uncertainty.

It is especially important to consider the use of the data. If differential-pressure signal is being used to identify changes in flow characteristics due to in-flight conditions variation, the absolute value of speed, density or pressure coefficients are secondary information. The important data is the relative change on pressure-differentials observed. Therefore, the coefficient of variation is the best parameter to be used evaluating the capability of the designed instrumentation.

3.3 Wind-tunnel tests

Wind-tunnel tests demonstrated the capability and limitations of the pressure measurement instrumentation. They provided data necessary to characterize the aerodynamic behavior of inflatable wings at several combinations of speed and angle of attack. The

ASCENDER profile [42] was chosen as the baseline airfoil because it has been employed in previous studies of paragliders. Also, the ASCENDER geometric characteristics were suitable for test-bench construction and instrument implementation in a laboratory environment.

The open-circuit wind tunnel from the Laboratory of Energy and Environment of the University of Brasília was employed for the test campaign. It has a 2 m long test chamber with a 1.2 m x 1.2 m cross-section and can deliver airflow speeds up to 20 m/s. The wind-tunnel has been used for several academic purposes. As detailed by Macias [43], free-flow speed is adjusted by an integrated Pitot-static tube, providing speed-accuracy of 0.3%. The sensor was positioned 20 cm inside the chamber at the upper right corner, distant 14 and 10 cm from the lateral and superior walls, respectively.

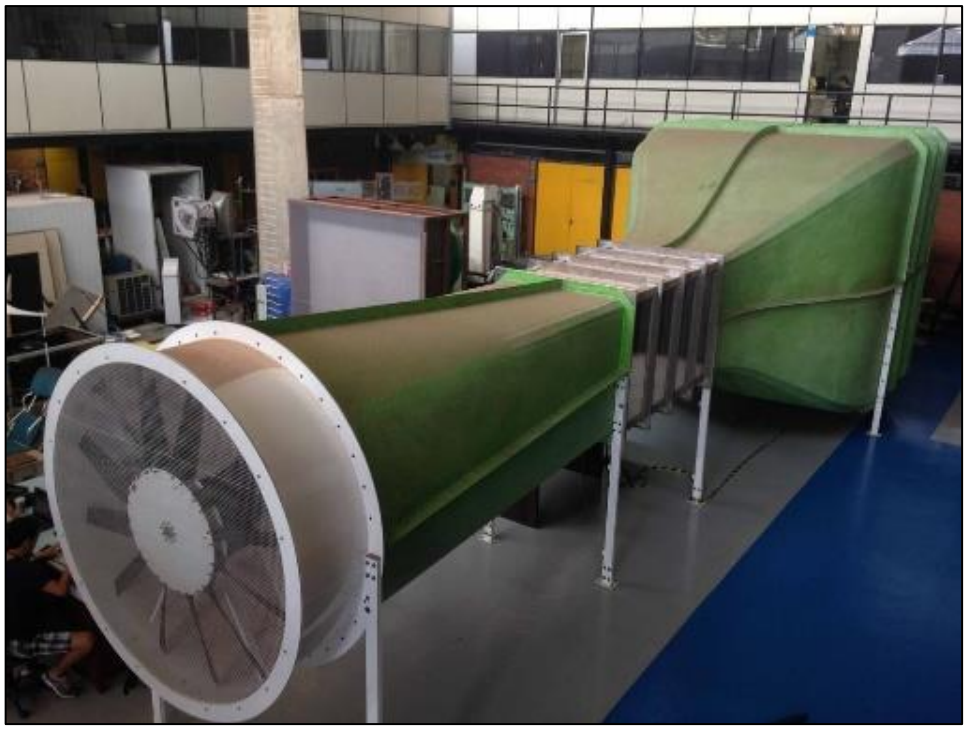

Figure 32: The Laboratory of Energy and Environment wind-tunnel.

3.2.1 Test-bench design and setup

The test bench was built as a three-cell wing with zero anhedral angle, representing the central portion of an inflated wing. It included a pulley mechanism to allow changing the incidence angle from outside the tunnel. Fig. 33 presents the designed prototype. The wood rib's chord was 80 cm long, and each cell was 12 cm wide, resulting in a 36 cm span. The rigid skeleton was covered with a lightweight paraglider's fabric named Porcher Sport Skytex weighing 38 g/m^2.

Figure 33: Test bench skeleton.

Sensors were attached in the middle of the wing, as sketched in Fig. 20 covering the three main regions of the airfoil at 8%, 30%, and 65% of the chord. The sensor units were glowed and sewed to the upper and lower surfaces to represent real flight test conditions. The units must be carefully attached to the wing in a way that even abrupt collapse folding would not cause detachment. The control board, representing the most massive component, was positioned near the aerodynamic center at 25% of the chord on the lower surface. This unit weighted 66 g distributed in a 7 cm x 6 cm surface, resulting in a 1.57 g/cm^2 load. Fig. 34 shows pictures of the final prototype displaying the assembly and the sensor units' attachment details.

Figure 34: Test bench with instrumentation installed.

A semi-rigid structure has been used to qualify the instrumentation system in order to allow for the reaching out-of-envelope conditions. Without a rigid skeleton, it would not be possible to explore regions of pre-inflation speed, negative AOA or post-stall situations. These scenarios are of great relevance to judge the capability of the system measuring pressure differentials under extreme situations like collapsing. Nevertheless, the system was fully designed to operate airborne and both the theoretical assessments of mechanical constraints and the wind tunnel tests practical observations assured the suitability of immediate in-flight application. The only additional consideration made necessary by the test bench structure was related to the effects of the horizontal bar used to fix the ribs on the internal flow.

As demonstrated by Zovatto and Pedrizzetti [44], the flow over a confined cylinder leads to a circulation vortex, altering the surrounding pressure distribution. As the bar is located at the aerodynamic center, at 25% of the wing, it stays close enough to the middle sensors to be able to cause a perceptible disturbance at the inner pressure around this region in case of significant airfoil confined recirculation flow. The combined factors of undetermined internal flow patterns, sensor cases geometry features, and test-bench horizontal bar made it clear that internal pressure readings can be the main source of uncertainties. Nonetheless, this potential inaccuracy is mostly relevant for pressure coefficient estimations. Monitoring local differential pressure helped reveal the state of the external flow related to the internal one at specific regions of the wing. Then, even if the air inside the wing is not at rest, the important information was whether the differential is sufficiently negative (pressure effort from inside to outside) and how it evolves throughout the chord. The presence of the bar could alter the internal flow leading to perceptible changes to the readings of sensors S2 and S5; however, analyzing the variations throughout the range of AOA and speed tested, no relevant effect has been identified.

3.2.2 Wind-tunnel test procedures

The wind-tunnel tests covered most of the flight envelope expected for common inflatable wings. Static tests were carried out by selecting angles of attack (AOA) from −20° to 25° in 5° steps and free-flow airspeeds of 3, 6, 9, and 10 m/s for each AOA as summarized in table 4.

Table 4. Wind-tunnel testpoints

	-20º	**-15º**	**-10º**	**-5º**	**0º**	**5º**	**10º**	**15º**	**20º**	**25º**
3 m/s	#1	#5	#9	#13	#17	#21	#25	#29	#33	#37
6 m/s	#2	#6	#10	#14	#18	#22	#26	#30	#34	#38
9 m/s	#3	#7	#11	#15	#19	#23	#27	#31	#35	#39
10 m/s	#4	#8	#12	#16	#20	#24	#28	#32	#36	#40

3.2.2.1 Measurement procedures:

Two separate procedures were applied for capturing static readings and dynamic readings. For the static readings, the following steps were stablished:

1. Set the "nominal" AOA by fixing the lateral wheel on the test bench - At this point, it is important to clarify that the AOA measurement was obtained considering the angle between the direction of free flow and the direction of the profile's geometric chord. It means that no corrections were applied related to the zero-lift line. Therefore, as the ASCENDER profile is not symmetric, there is a difference between the angle obtained from this reference and the one obtained with reference to the geometric chord. However, it does not demand any corrections, and, in fact, dealing with the angle between flow speed and the geometric reference is better, since assuming the zero-lift line position on a sectioned airfoil would be something completely arbitrary.
2. Set the flow speed by introducing on the synoptic tool a value sufficiently bellow the target and progressively increase the speed input monitoring the pitot-tube speed measure up to reaching a stable flow – Flow is considered stable when both the reading at the wind-tunnel instrumentation presents no perceptible variation and the readings from the sensors are stabilized for at least 3 seconds.
3. Record data from sensors for 10 seconds monitoring flow stability – Flow stability is considered in terms of wind-tunnel instrumentation data and differential-pressure instrumentation data. Both signals must be stable for 10 seconds.
4. Increase speed target and repeat steps 2 and 3 up to 12m/s or up to reaching sensors' range limit – Sensors range limit can be reached in different levels of speed depending on the angle of attack.
5. Repeat steps from 1 to 4 covering all the planned AOA spectrum.

For the dynamic readings, a single speed of 10m/s was used. This speed was selected to make sure that the combination of rotational speed with the free-flow speed would not impair the dynamic measuring due to local extrapolation of pressure-differential reading limits. the following steps were stablished:

1. The wing-cell was kept free to rotate and held at zero degrees AOA – Using the geometric chord as reference.

2. Speed was set in 10 m/s as indicates on step 2 above.
3. Pulling the control lines attached to the lateral wheel, a first round of excursions from zero to 25 degrees and back to -25 degrees was executed at a rate of approximately 0.4 rad/sec – Average rotation rate was obtained after the test using the video of the test to extract the time to cover the excursions.
4. A second round of excursions was executed following steps 1 and 3 at a rate of approximately 0.9 rad/sec.

3.2.2.2 Test environment considerations and analysis

Due to the sensor's pressure range limitations, speeds higher than 10 m/s were out of consideration. It does not impair flight envelope coverture, since for high speeds above 10m/s AOA will naturally adjust to low values, and then, aerodynamic pressure is sustained inside the expected range.

Dynamic excursions, at low and high speeds, were executed by varying AOA to evaluate the system's capability to capture dynamic changes in pressure distributions during maneuvers and to evaluate instrumentation integrity. It is worth clarifying that the operational range concept is related to normal flight conditions, which is limited to speeds between 9 to 12 m/s and AOA from 0° to 10° [26]. For most paragliders and parafoils, the steady glide is maintained at speeds near 10 m/s and AOA around 5°. Wing motion and maneuvering leads to global variations attaining speeds between 6 m/s and 12 m/s and AOA between 0° and 15°, but local variations can be much higher. Situations outside these limits are transient, and then, considered as the exploratory range. It comprehends pre-inflation situations, which are represented by speeds below 6 m/s, and pre-collapsing situations, which are represented by negative incidences or an AOA above 15°.

The Reynolds Number (Re) is an important parameter in the aerodynamic study of aircraft systems. For inflatable wings, the low-Reynolds number becomes a relevant aspect linked to the occurrence of flow separation and reattachment during the wind-tunnel tests. Considering the test-bench geometry and the conditions tested, Re varied from 1.6 × 105 to 5.6 × 105. The range is inside the envelope of $104 < Re < 106$, defined by King [30] as that subjected to laminar separation bubbles. The Re assessment from wind-tunnel measurements needs no corrections since it corresponds to the same range of actual-flight operation. Therefore, no scale effects are supposed to affect the validity of experimental results.

It is worthy highlighting that measurements at speeds near or under 6 m/s were useful, especially to set inflation thresholds, as well as measurements at negative AOA and at AOA above 15°, which were useful to characterize collapse and stall. However, the data acquired under conditions inside the interval of 9–10 m/s and 0–15° AOA are especially relevant to demonstrate the capability of the instrumentation to monitor the pressure differential variations that are relevant for the dominant flight conditions. Speeds above 10 m/s are achievable in flight, however, sensor's range limit prevented tests at higher speeds. It does not impair any evaluation, since the important task to be accomplished by the instrumentation is to capture relevant variations at low-pressure levels. At higher levels wing is certainly fully inflated and fly far from any aerodynamic limit. Additionally, sensor overpressure capability up to 1 bar (105 Pa) guarantees that no expected acceleration could ever reach levels that may damage the sensors.

The free-flow speed collected from the wind-tunnel embedded system was recorded manually after stabilization. Data from the pressure measurement system was monitored remotely via WIFI and recorded automatically into the SD-card. The error contribution associated with pressure measurement is intrinsic to the sensor's characteristics as there was no static pressure influence. However, the contribution regarding flow speed must be considered taking into consideration the blockage effect.

Becker and Paul [22] highlights that, as no previous studies define specific corrections for parafoils, a viable strategy is to keep blockage ratio low to minimize the effect up to a point at which it could be neglected. Therefore, following Choi and Kwon [45] suggestion, a blockage ratio under 5% was considered sufficient for the present research. Applying the test-bench and wind-tunnel dimensions in Eq. (12) for the range of AOA tested, the chart in Fig. 35 was obtained.

$$\frac{b \cdot c \cdot sin(AOA)}{S_{tunnel}} = \frac{0.36 \cdot 0.80}{1.2^2} \cdot sin(AOA) \tag{12}$$

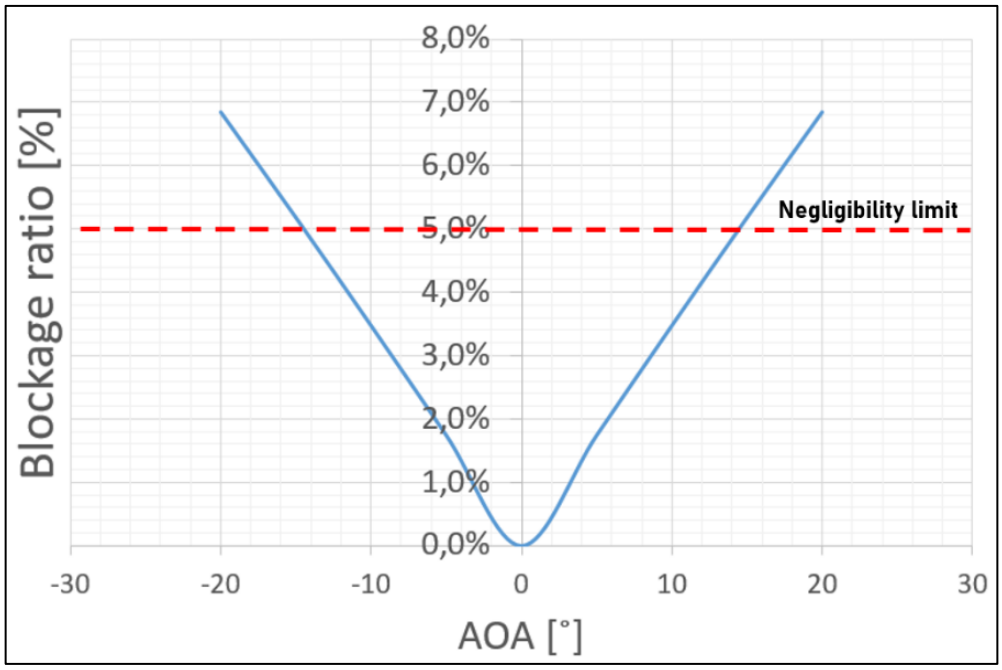

Figure 35: Blockage ratio negligibility limit.

Fig. 35 indicates that for AOA up to 15˚ blockage effects are negligible. For angles above 15˚ a dedicated analysis could be recommended depending on data uniformity evaluation. However, after evaluating readings stability it was clear that no relevant effect appears overpassing this threshold.

Still, a dedicated discussion is necessary about the wind-tunnel variables and the test-bench scale aspects. The test-bench represents a real size wing, which is an important aspect to consider fitting the instruments to a real system. It makes the model somewhat big for the tunnel chamber, but it is the best option for anticipating any possible effects induced by the attachment of the instrumentation on the wing's surfaces.

It is important to highlight that, any eventual uncertainty about the exact value of flow speed due to the blockage effect, and also a deviation in terms of air density, which was not directly measured, could lead only to a drift on the data, unable to compromise any conclusions about the phenomena or relevance of measurements. It must be considered that by varying flow speed from zero up to the sensors' limit value and varying AOA from pre-inflation to post stall the only consequence of a potential error on speed or density values is to shift the dynamic pressure reference value. Although it might be interesting to be analyzed in future works, it does not compromise, in anyway, the analytical evaluation of pressure profile variation and parametric identification of flow conditions through differential-pressure local readings.

At each procedure, surface conditions were closely monitored and no perceptible deflections on the fabric due to instrumentation attachment were noticed for speeds above 6m/s. There were no indications of deformation, vibration or flow detachment that could anticipate the restrictions for immediate on-board installation. Additionally, a visual windsock test was performed using dummy weight cases representing the total weight of the instrumentation. It was observed that even using a windsock, with no rigid parts, the inflation at speeds above 6 m/s was stable and had no visible signs of deformations due to the presence of the weights. At 3m/s it is possible to notice vibration at the surface. It corroborates that, at this speed, there is no sufficient pressure differential to provide sufficient wing stiffness. For higher speeds at negative angles of attack, a general small deflection was evident at the upper-leading edge, evidencing the tendency of buckling.

The differential pressure readings were stable and consistent for all test points, including the dynamic excursions and the static situations out of envelope. Even when vorticities resulted a progressive scattering on data, the data processing showed no adverse behavior. In general, the testes allow to affirm that no adverse measurement behavior was identified during the entire experiment. Neither from mechanical or electronic point of view.

The results obtained in the wind tunnel qualify the instrumentation for both static and dynamic readings and demonstrate basic phenomena occurring on inflatable wings with no perceptible elastic deformation. These results are immediately applicable to stable conditions, since size and speed are both representative of real operational wings. In-flight, dynamic elastic deformations will affect the differential pressure measurements, revealing local reactions due to the aerodynamic load. The capacity of identifying these reactions is assured based on the instrumentation performance verified by the wind-tunnel campaign. Following the next step on the research, moving to a wing prototype, any relevant elastic deformations are captured as local pressure differential variation. Parameterizing these variations based on a set of defined flight-test maneuvers allows for the characterizing of the wing in terms of responsiveness and stability.

4. Results

The wind-tunnel test campaign proved the instrumentation system's suitability for in-flight measurements of aerodynamic pressure distribution over dynamically inflatable wings. It shows that the designed instrumentation may be used as a development toll, as well as, the core component for a collapse alert and prevention system.

Data obtained demonstrated essential aspects of inflatable wings aerodynamics. It confirmed previously identified characteristics and revealed novel singularities and proprieties directly related to differential pressure distribution, which allows mapping in-flight behavior and anticipating flight envelope limits approximation situations.

The analysis was conducted separately for operational and exploratory ranges. The operational range represents conditions expected from inflation up to a stable flight, encompassing speeds from 5 to 12 m/s and angles of attack (AOA) from zero to 15˚. The exploratory range deals with pre-inflation speeds, negative incidence, or higher angles of attack, which are supposed to indicate unstable conditions in-flight, which are helpful for wing dynamic evaluations.

At the operational range, the relevance of data is obvious, and, cheerfully, the aerodynamic behavior follows the basic principles observed in rigid wing's airfoils. However, the system exhibits relevant singularities induced by the presence of the air intake and the resulting flow in the wing cavity.

At the exploratory range, the inflatable nature of the wing overcomes all typical characteristics, considering that in-flight collapse may occur. However, although out-of-envelope conditions may be uncommon, it emphasizes the significant changes on pressure distribution observed when limits are trespassed. The test-bench rigid skeleton allowed to explore the pressure distribution even at negative angles of attack and at angles way above stall, allowing to relate pressure distribution evolution with the trend to exceed the operational aerodynamic limits imposed by the inflatable nature.

4.1 Instrumentation performance

An initial measurement with no flow speed was conducted to evaluate sensors setting at zero speed. The sensors presented stable readings under 1.0 Pa ±0.03. Another measurement at 12 m/s, representing the maximum speed, was executed and the range limit of the sensors was

reached as expected (125 Pa ±3.75). A total of 12 conditions were tested inside the operational range, AOA of 0, 5, 10, 15 degrees, and wind velocities of 6, 9, 10 m/s. No adverse measurement behavior was identified in any condition.

Static measurements were evaluated in 10 seconds stabilization intervals. The coefficient of variation observed was consistently around 2% of the reading for most of the sensors, with the exception of the bottom-front sensor at low angles of attack, which displayed an average coefficient of variation of about 7%, three-fold higher than the others. This higher deviation is related to Fogell's observation [6] about the occurrence of a recirculation bubble at the bottom leading edge of the wing due to the air intake. Figs. 36 and 37 summarize the observations.

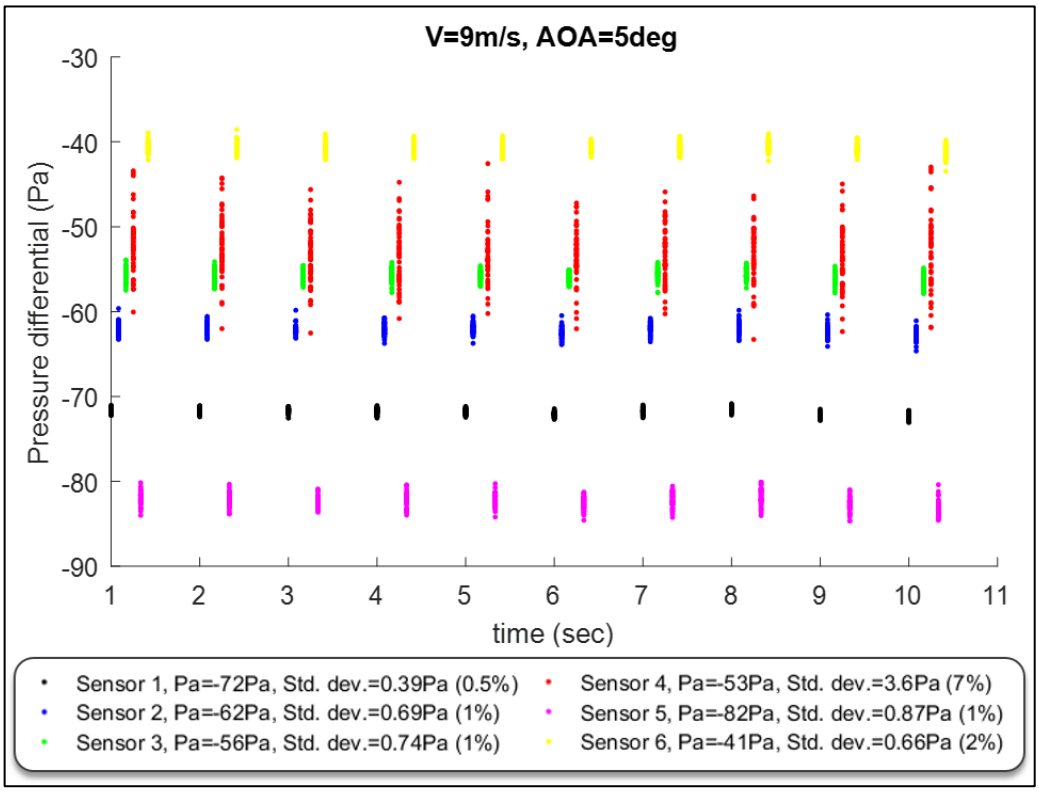

Figure 36: Test data for AOA=5° and V=9m/s.

Fig. 36 shows the significant scattering of data from sensor 4, positioned at the bottom-front of the cell as indicated in Fig. 20. This is one of the signs of the recirculation bubble acting in this region. The same behavior is seen throughout the operational range. It became even more noticeable by inspecting Fig. 37, which presents the evolution of coefficient of variation with AOA.

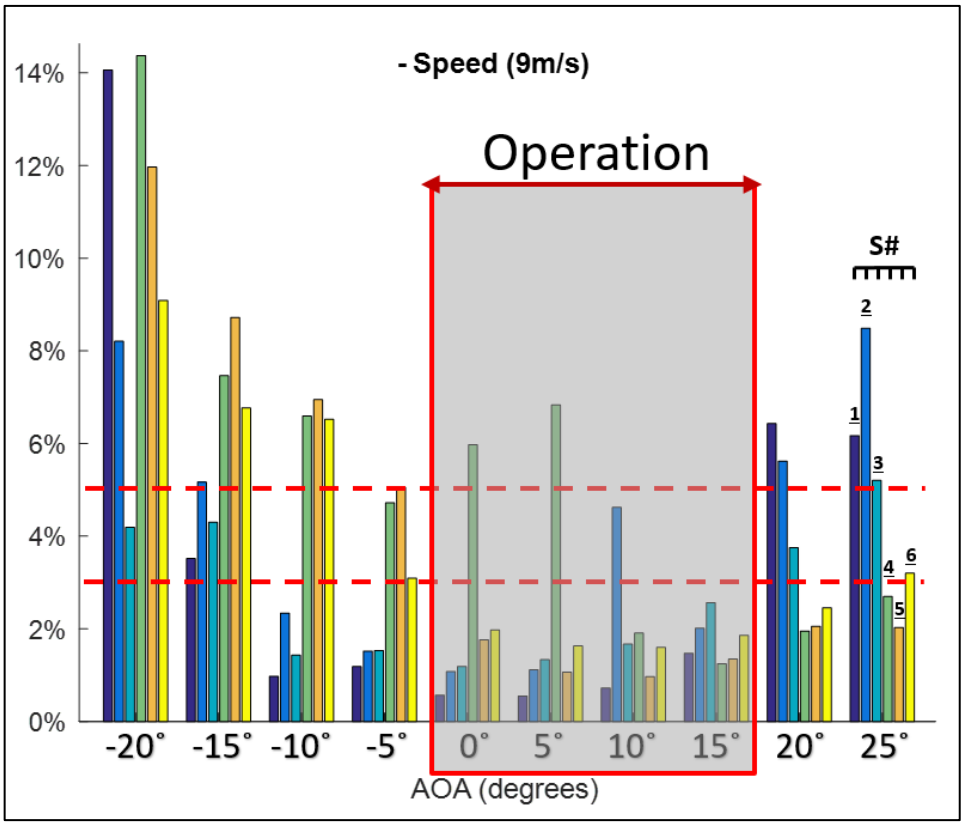

Figure 37: coefficient of variation with AOA for *V*=9 m/s.

Fig. 37 evidences that coefficient of variation follows a path driven by the position of the vorticities. At positive low AOA, the recirculation bubble is located near to the air intake; no other relevant effect is perceptible. As AOA increases, the bubble moves along the chord, slightly approaching the fifth sensor region. At the same time, flow detachment starts to generate vortices at the upper surface, as a sign of stall approximation. The data not only corroborates previous conclusions about the formation of a recirculation bubble at the bottom of the air intake, as it reinforces sensors' capability to represent flow characteristics at several flight conditions.

The recirculation bubble is an effect driven by the air intake. It involves a set of geometric and aerodynamic variables. When air approaches the wing, instead of finding a solid and well defined stagnation point, as in a rigid airfoil, it encounters a pressure gradient formed by the interaction of external and internal flow. Part of the flow circulates back, forming a vortex as illustrated in figure 6. This phenomenon causes an unlikely rising on inside-outside pressure-differential, which would not be seen on a closed airfoil. Therefore, the evidence is not simply data scattering, but the combination of data scattering and the abrupt augmentation on pressure differential at the bottom leading edge as presented in figure 38.

Such a dynamic situation will concentrate a small vortex of recirculation near to the air intake, which will result a drop on the local pressure at the external bottom-surface. The extension and the exact positioning of this vortex will depend on the air intake size and shape, as well as, on AOA and flight speed. It can be inferred that, a lower air intake or a higher AOA tends to drive the recirculation bubble further to the middle of the chord. Also, a small air intake and a high speed airflow tends to reduce the manifestation of the recirculation bubble. However, it is important to highlight the tradeoff balanced by the air intake design, which defines the equilibrium between aerodynamic performance and inflation stability.

Considering the exploratory range, 26 additional test points, including a pre-inflation speed of 3 m/s combined with angles of attack from -20˚ to 25˚, revealed sensor unit's capability to record pressure differentials from 1.0 to 125 Pa with coefficients of variation from 1% to 23%. For the operational range, precision was kept near to the sensor's resolution (3%), and consistently below 5%, except for the bottom-front sensor.

For pre-inflation speeds and angles of attack outside normal operation, a perceptible change on the scattering profile occurs due to flow disturbance. At negative angles of attack, an expressive jump on data scattering starts at the bottom surface sensors, evidencing flow detachment at that side of the wing. As the wing continues to pitch down, the vorticities reaches the upper surface. It is easy to understand that, at aggressive negative incidence, the dynamic pressure imposed by the flow is trying to flip and collapse the wing, and the upper surface is now acting like a simple physical barrier.

For excessive positive angles, the upper surface is, correctly, the first to show signs of flow detachment, starting by the upper-rear sensor and, followed by the middle and frontal sensors respectively. Interestingly, from 15º to 20º it becomes clear the change on the relative level of data scattering between the upper-surface sensors when the flow detachment is fully configured. It didactically illustrates the stall.

The considerations up to here are more than enough to assure the capability of the instrumentation to accurately capture the relevant changes on airflow regime through the identification of vorticities and general flow instabilities reflecting on data scattering. However, system must be also capable of reading significant pressure differential throughout the operational and exploratory range, registering the variations caused by wing motion. Fig. 38 illustrate the pressure differential measurements variation with AOA demonstrating the fully capability of the system for characterizing changes on flight conditions.

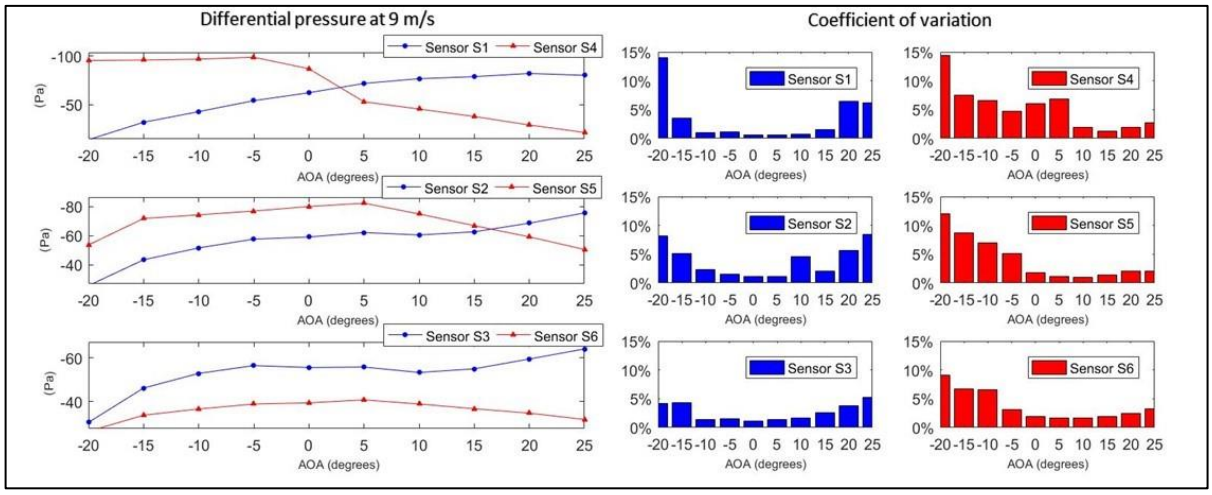

Figure 38: Differential pressure data for *V*=9 m/s.

Fig. 38 present the data obtained at 9 m/s grouped by airfoil regions. As can be seen, differential pressures varied from less than −10 Pa to about −100 Pa. The upper-front (S1) and the bottom-front (S4) sensors present a wider range, as expected, since lift is concentrated at the initial portion of the airfoil. For the same reason, the upper-rear (S3) and the bottom-rear (S6) sensors present a more stable pattern. The upper-middle (S2) and bottom-middle (S5) sensors present the intermediate conditions linking the leading and trailing edges, which reveals a distinctive behavior at the bottom surface, which is strongly affected by the air intake. It is worth reaffirming the intention of working with pressure differentials and not with traditional external pressure coefficients, since the direct measurement of pressure differentials reveals the combined effect of external and internal flow dynamics, which are crucial for inflatable wings.

The coefficient of variation (CV) consistently shows increased data scattering outside the operational flight envelope (0° < AOA < 15°). At negative incidences or at angles above stall CV up to five times higher. It demonstrates the system's capability of indicating detachment vortex formation. For angles of attack inside the operational envelope, the coefficients of variation were very close to the sensor's resolution (3%), as informed by the manufacturer, except for the bottom-front sensor at low angles of attack, which have reached about 7%. The significant data scattering from sensor S4 materializes the effect of a vortex linked to the recirculation bubble acting on that region. It becomes even more noticeable by inspecting the change on sensor S4 measure pattern after entering the operational envelope. This effect is linked to both the low Reynolds number regime and the existence of an air-intake at the leading edge.

Another didactic way of looking into the data is taking the pressure differentials at the rear sensors (S3 and S6) as a baseline. These readings are supposed to be more stable in respect

to AOA and to reflect the pressure-differential potential provided by the flow speed. Table 5 represents data extracted from Fig. 38 for the operational flight envelope measured as a percentage of the baseline pressure differentials:

Table 5. Relative pressure differential readings at 9 m/s and angle of attack between 0° and 15°.

AOA	$\left(\frac{S1}{S3}-1\right)\%$	$\left(\frac{S2}{S3}-1\right)\%$	$\left(\frac{S4}{S6}-1\right)\%$	$\left(\frac{S5}{S6}-1\right)\%$
0°	12.5	6.4	120.8	103.5
5°	28.7	11.4	30.4	102.2
10°	43.9	13.5	17.7	93.1
15°	43.2	14.0	3.9	82.7

At 9 m/s, the average pressure measured by S3 and S6 are, respectively, 55 Pa and 39 Pa at 65% of the chord, revealing enough of a pressure differential to sustain inflation and a difference of 16 Pa between pressure differentials at the upper and lower surfaces, indicating lift at that region. These measures are almost unaffected by AOA variation inside the operational flight envelope, presenting standard variations of ±1.7 Pa and ±1.1 Pa, respectively. However, the frontal and middle sensors' readings vary considerably with AOA. In the same way, it is made clear how perceptible is the pressure-differential variation throughout the chord at both upper and lower surfaces for each flight condition. These observations are extremely important because it shows that the measurement of local pressure-differentials at the selected regions of the cell can provide an effective way of characterizing flight condition. For instance, increases in the pressure gradient at the upper surface, together with the decreasing in pressure gradient at the lower surface, between the second and third lines in Table 5, clearly indicates a pitching up from 5° to 10° AOA.

The pressure-differential distribution profile defines a standard in-flight signature for a particular wing model. Measuring the differential pressure profile at the steady glide condition provides a baseline, which can be used to identify in-flight dynamic reactions through pressure profile variation. As the inflatable wing will be dynamically deformed by aerodynamic loads originating from maneuvering or atmospheric disturbances, local variations on the pressure differential readings will be perceived, revealing reactions that can be linked to wing motion. Therefore, the wing can be characterized by correlating its motion, using standard accelerometers and inertial sensors, to the aerodynamic loads captured as pressure differential variation.

An additional consideration must be done about the values presented by the measurements. In fact, the readings are fully coherent with the expected level of pressure to be encountered. As stated by Benedetti [26], paragliders and parafoils present wing load near

$4kg/m^2$ (≈±40Pa). Although this is an average parameter, the fact that data in Fig. 38 is consistently above this level, and at the same range, reveals that the range of measurement is compatible with practical observations. It must be taken in account that three-dimensional effects like the anhedral and the aerodynamic tip vortex will reduce the final available lift. Also, the measurements presented are at each point of the surface, and the final local resultant must be integrated by combining the effects at upper and lower surfaces. An estimation using simple interpolation of the data for V=9 m/s and AOA=10º reveals a value near 40Pa for the difference between upper and lower pressure-differential.

It is also important to highlight that, the precision level demonstrated by the coefficient of variation, combined with the sensors' accuracy data revels implied uncertainties varying from 3% to 8% at the operational range, which reflects the coefficient of variation range with minimum adjustments. Therefore, further considerations about error propagation on differential pressure data were considered unnecessary.

Finally, to demonstrate the capability of the system to efficiently capture pressure differentials variation during wing motion, Fig. 39 presents a dynamic AOA excursion at 10 m/s from zero degree to the lower and the upper limits of the test bench.

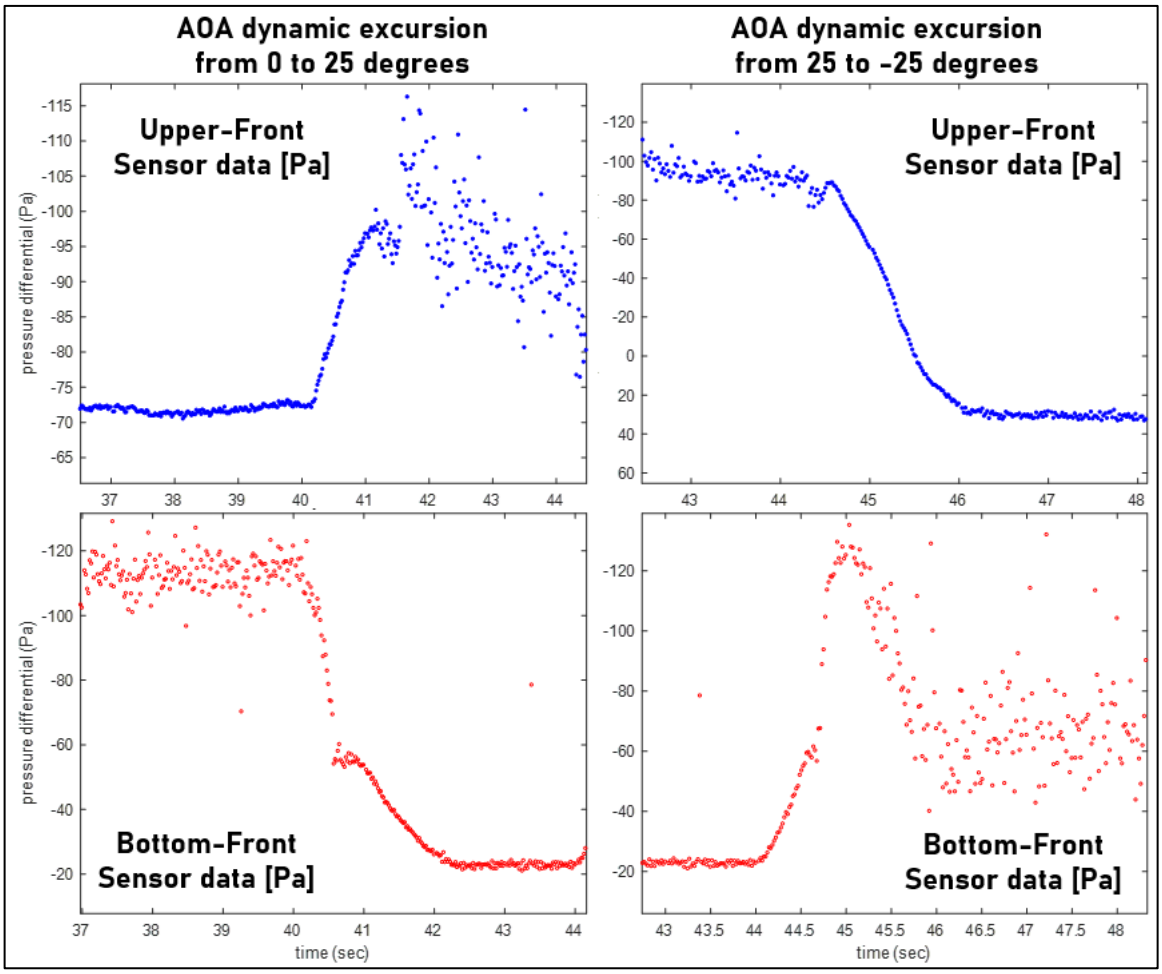

Figure 39: Dynamic AOA excursions.

On the left side, the increase in AOA captured by the sensors is absolutely stable and consistent with static data up to the stall. The final scattering didactically characterizes the stall phenomenon. The initial condition shows a fixed pressure differential at the upper surface, most related to the existence of confined air inflating the wing and not to aerodynamic components, and the vorticities at the bottom surface. As wing is pitched up it encounters a "flying condition" and the aerodynamic effect becomes evident. The pressure differentials rise at the upper surface and decay at the bottom surface almost coordinately until the stall is reached.

In the same way, on the right side, when the wing is pitched down, pressure differential over the upper surface is inverted, becoming positive, and a vortex at the bottom surface can be detected. The observed values remain fully consistent with those obtained for the stabilized conditions, proving that the readings are precise at dynamic and stabilized conditions.

It is interesting to point out that the bottom-front recirculation bubble disappears when the wing if fully pitched up, and the readings become stabilized at a considerably low value. It ascertains the source of the scattering systematically observed for sensors 4 and 5, the local

bump in differential pressure, and proves the occurrence of the phenomenon previously suggested. When the wing is fully up there is no recirculation flow creating the phenomenon.

Overall, the instrumentation was shown to be efficient for in-flight measurements. It was capable of capturing pressure differentials levels much lower than those expected during maneuvers, as well as the differences between pressure differentials from one point to another on the wing surface. There were no concerning signs of aerodynamic or mechanical interference due to the installed instrumentation.

4.2 The inflation phenomenon

The phenomenon representing the very nature of an inflatable wing manifests itself when a stiff structure able to sustain substantial load is formed from a previously shapeless peace of tissue. The occurrence of such a phenomenon imposes some conditions, which becomes flight envelope limits, since it dictates the existence of an aerodynamic surface able to provide lift.

By being able to identify when the wing approaches such a limit, abrupt loss of shape is prevented and controllability is maintained. Therefore, it is of first relevance to identify the aerodynamic signs preceding deflation.

Data analysis revealed a substantial change in pressure differential distribution when the angle of attack goes from zero to five degrees, characterizing the point of inflation of the cell, and confirming what was previously observed by Mashud and Umemura [5,7].

As illustrated in Fig. 40, and Fig. 41, the increase in AOA up to a point where the stagnation point coincides with the air intake substantially increases the internal pressure and makes the cell potentially stable.

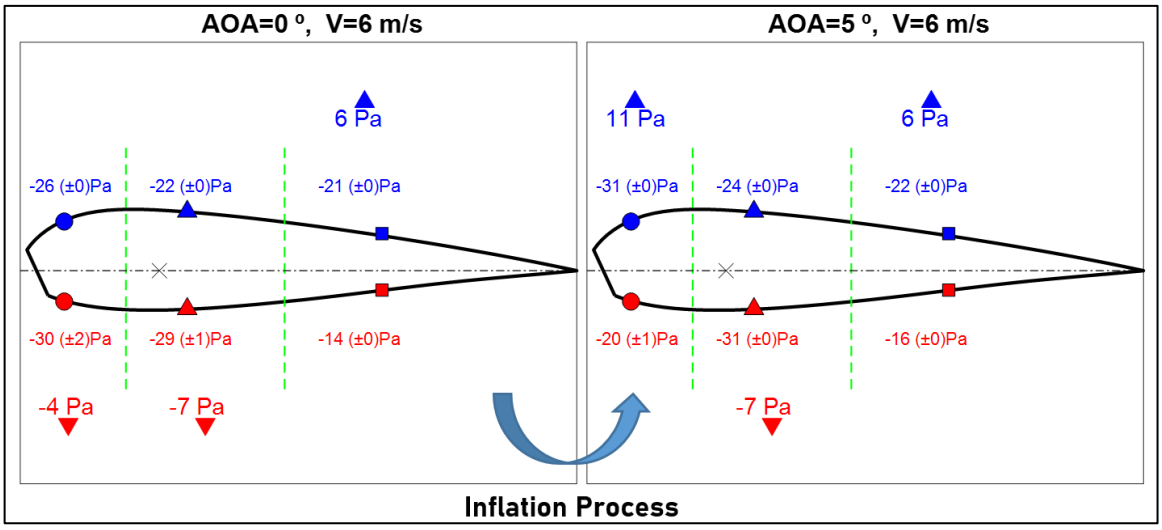

Figure 40: Cell inflation dynamics.

Fig. 40 presents the sensor's punctual readings and the difference between up and bottom pressure differentials in the three sectors of the chord. The difference between the upper and bottom measures would represent the local resultant pressure differential at the airfoil sector only if there were no internal flow, which is not the case. Even though, these differences are sufficient to indicate how pressure distribution throughout the cell varies with AOA.

It makes clear that, for negative angles, or even for a very small AOA depending on the air intake's geometry, the airfoil condition is unstable, because the higher-pressure differential at the bottom leading edge tends to rotate the cell downwards, leading to a frontal collapse. On the other hand, after incidence is increased above the point where internal pressure is sufficient, the relationship between upper and bottom pressure is inverted. The frontal lift tends to rotate the airfoil clockwise, providing stability. Equilibrium will be established by the combination of pressure distribution throughout the cell. In-flight, the pendulum mechanism automatically adjusts speed and AOA [26], reaching the stable glide condition. In a wind-tunnel, the supports or actuators will balance the resultant pitching moment.

As known from classic airfoil theory, the frontal part of the airfoil is responsible for most of the lift, which means, variations on relative proportions of upper and bottom pressures at this region drive airfoil's behavior. Fig. 41 expands the data from Fig. 40 covering angles from -15˚ to 20˚, to improve the understanding of the phenomenon.

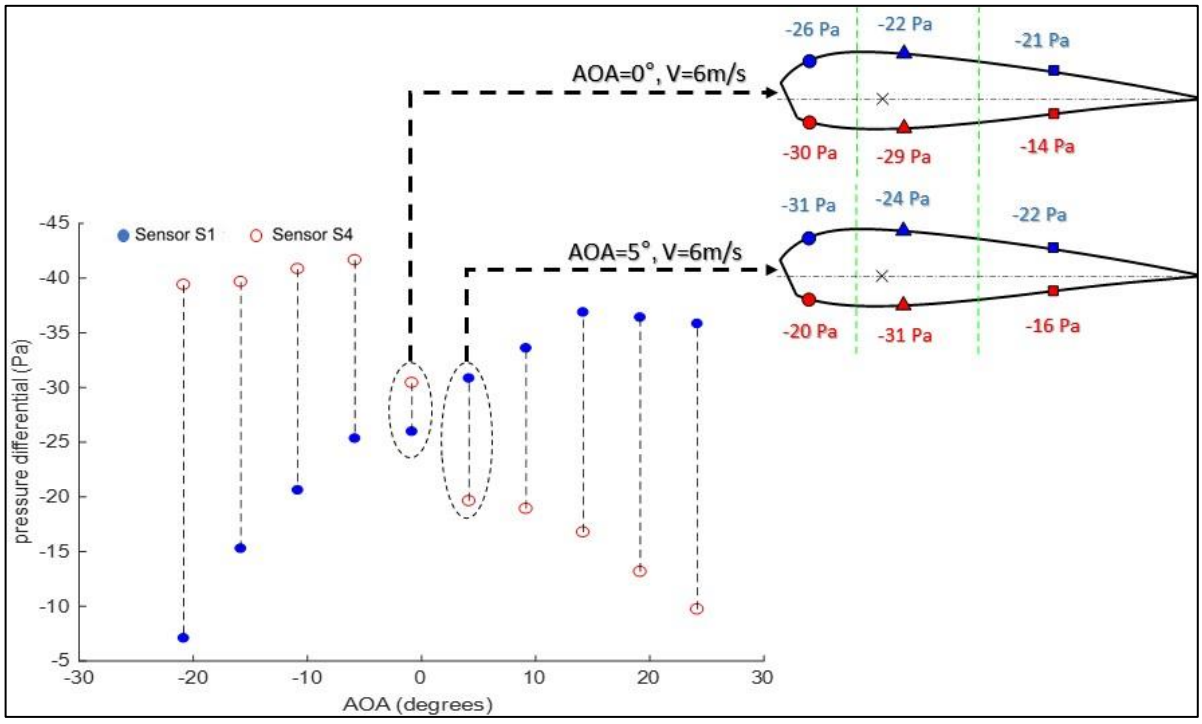

Figure 41: Pressure differentials at the inflation range.

Fig. 41 shows the upper-front pressure differential rising steadily with AOA up to the stall, and the bottom-front pressure differential going through an abrupt reduction at the inflation range. It provides a clear sign characterizing an inflation threshold.

The high level of pressure differentials at the bottom leading edge for negative incidence is explained by the fact that, when the wing is pitched down, the flow accelerates through the upper surface, absorbing most of the dynamic pressure imposed by the flow, sustained by the test-bench ribs. Such a situation is unsustainable in flight since it would result in an immediate frontal collapse. The bottom surface is, then, exposed to a low-pressure vortex, as illustrated in Fig. 39. When AOA increases to a point where air faces efficiently the cavity of the cell, and the inside pressure is sufficient to provide structural stiffness, the flow over the airfoil becomes stable as in a rigid wing. Both internal and external pressure at the bottom leading edge are entirely reconfigured. Table 6 present data for 6 m/s between −10° and 10° AOA, illustrating the abrupt change in the pressure gradient at the leading edge of the airfoil:

Table 6. Pressure differential readings at 6 m/s and an angle of attack between -10° and 10°.

AOA	$\boldsymbol{S1}$ $[\boldsymbol{Pa}]$	$\boldsymbol{S4}$ $[\boldsymbol{Pa}]$	$\boldsymbol{S1 - S4}$ $[\boldsymbol{Pa}]$
−10°	20.6	40.8	−20.2
−5°	25.3	41.6	−16.3
0°	26.0	30.4	−4.5
5°	30.8	19.6	11.2
10°	33.6	18.9	14.7

For the tested airfoil, a linear interpolation based on the frontal pressure differentials indicates that inflation occurs near to 1.43˚, which is almost the same value (2º) previously found by other researchers for different inflatable airfoils [5,7]. It is a fact that air-intake geometry will change the AOA for inflation, however, it is expected a range from zero to not more than 5º. It is important to mention that speed itself plays an important part in inflation. Tests at 3 m/s proved that, even at favorable AOA, speeds lower than 6 m/s do not provide sufficient airfoil stiffness, resulting in shape instability, visual fabric deflections, vibration, and consequently, unrepresentative data.

It is clear that the monitoring of the ratio between pressure differential at upper and lower leading edge can be directly used as a control parameter to avoid deflation by preventing further reductions on AOA. The same signal may be also used as a comparative under-design parameter revealing the magnitude of lift potential of the wing.

4.3 The stall approximation condition

Stall is a common aerodynamic limit to every kind of wing. Stall is reached when the angle of attack is so high that airflow is not able to follows the profile detaching from the surface and abruptly compromising lift and increasing drag. Flow detachment is also characterized by the appearance of vorticities at the upper surface of the airfoil, as illustrated in Fig. 39. For inflatable wings, stall add some interesting effects as revealed by practical observation and confirmed by the test data.

There are different stages of stall approaching. At first, the increase in AOA causes some turbulence at the upper trailing edge. As the incidence increase, flow detachment expands up to a point where all the upper surface is compromised. At this stage it is said that stall is complete. The idea of progressive stalling is an ancient concept in aeronautics, which explains why some aircraft present clear signs of stall approximation and others abruptly stalls with no perceptible warnings.

From the wind-tunnel tests the full stall condition is indicated by a sudden increase in data scattering at the upper-front of the cell. This effect is clearly shown in Fig. 39. Numerically, the coefficient of variation obtained in stabilized conditions for the upper-front sensor jumps from 1% to 6% when AOA goes from 15˚ to 20˚, revealing the detachment vortex that characterizes the stall.

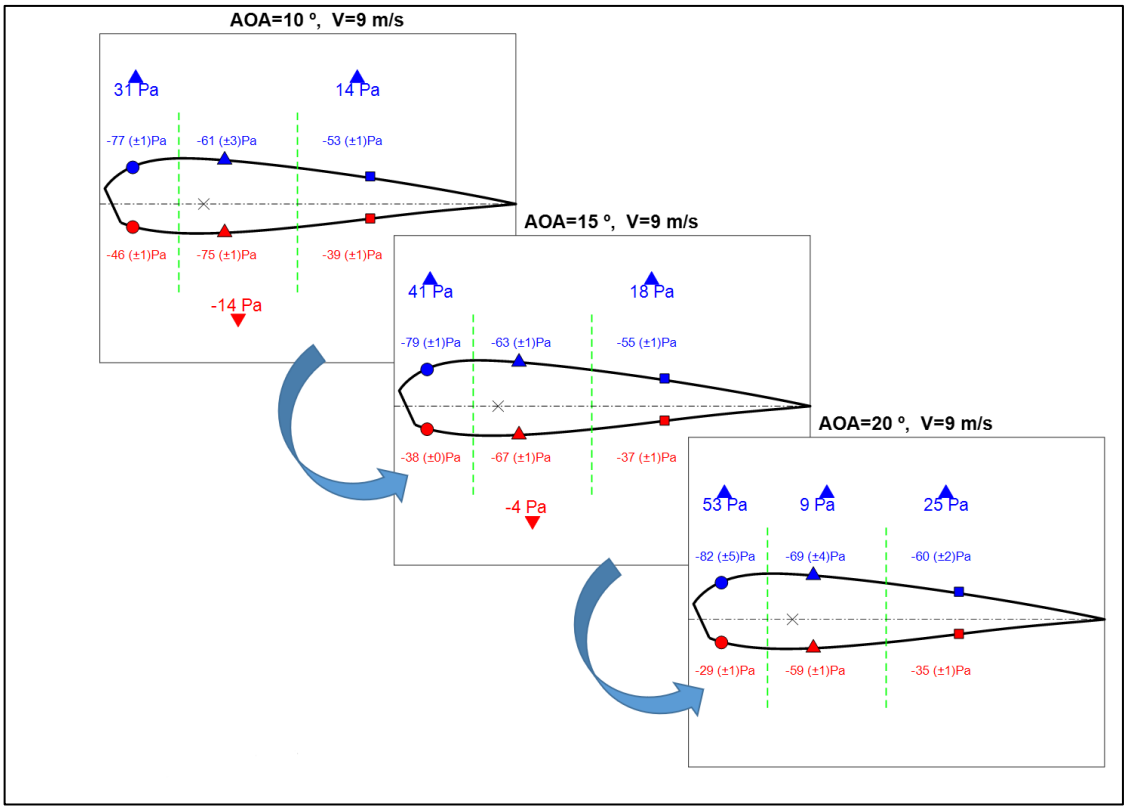

Figure 42: Inflatable wing stall dynamics.

Fig. 42 shows a consistent decrease in the bottom surface pressure differentials combined with a consistent increase in the upper surface differentials, resulting a substantial increase in lift and drag. The increase in both lift and drag leads to a progressive decreasing in speed up to a point where inflation is jeopardized, and collapse is imminent.

It is essential to highlight that the aerodynamic stall does not directly cause collapse, but has a major effect on it. As represented in Fig. 38 and Fig. 39, when a stall condition is reached, the low-pressure vortex formed at the upper surface can sustain inflation even if the flow is detached. However, such a situation will abruptly increase drag, driving speed down very fast, to a point where dynamic pressure is too low to sustain inflation. This observed time lag between stall and collapse can be explored to build collapse prevention systems.

An auxiliary evaluation that took in account the evolution of the pressure differentials at the upper-middle portion of the wing revealed an important stall characterization tool. Fig. 43 presents pressure differentials evolution at the stall range, allowing better visualization of the phenomenon.

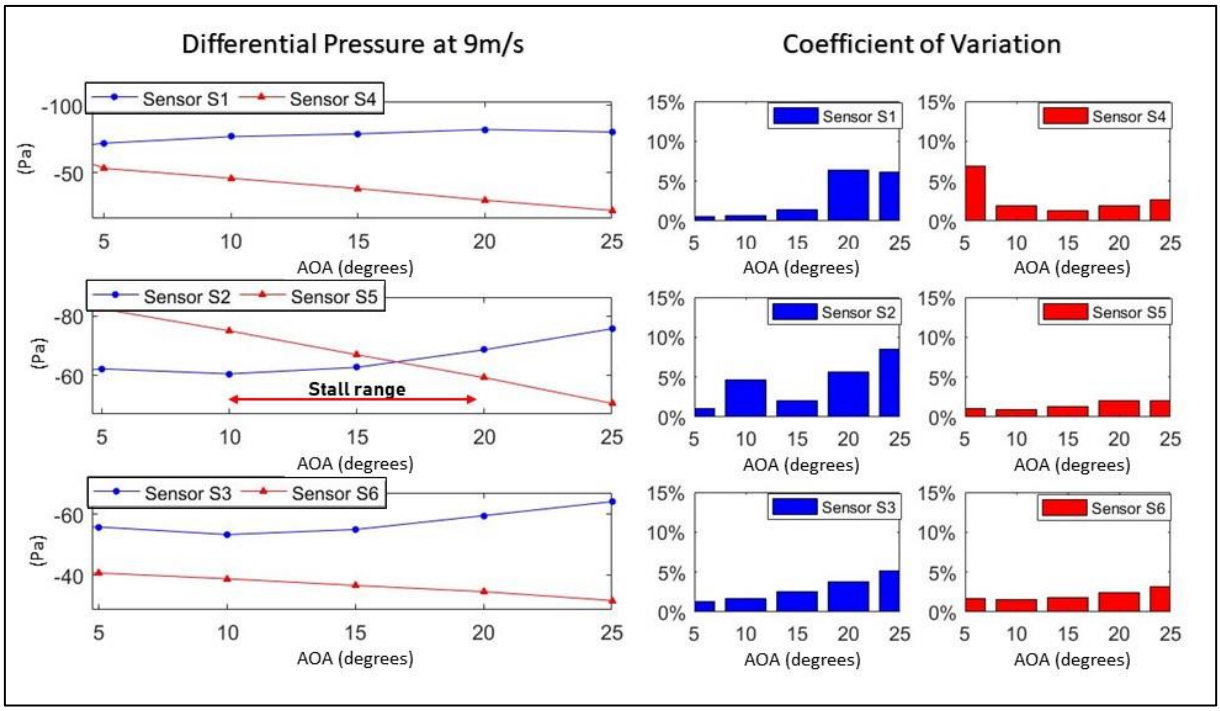

Figure 43: Pressure differentials up to wing stall.

Fig. 43 shows that, throughout the operational range, the upper-middle pressure differential is quite stable, up to a point where it starts rising, revealing the progressive formation of a detachment vortex. At the same time, bottom-middle differential decreases uniformly as a direct result of the wing's pitching up, due to the progressive increase in bottom pressure imposed by the airflow.

The change in upper-middle readings rate of variation between 10˚ and 15˚ confirms previous findings [22, 23, 27] indicating that, for paragliders and parafoils, stall effects are triggered above 9 degrees and are fully characterized above 13 degrees. The rate of variation of the upper-middle pressure and the difference between up and bottom middle readings are relevant aspects for the central portion of the cell. The first one reveals lift evolution and the second one reveals the pressure gradient at the middle of the profile. Setting a reference at the steady glide condition (V = 9m/s and AOA = 5°), it is possible to judge stall eminence by monitoring the climbing in upper-middle readings (S2/S2std) and the difference between upper-middle and bottom-middle readings. The first parameter reveals whether the characteristic of the flow has changed perceptibly, and the second parameter reveals how far from the inflation condition the system might be. Table 7 illustrates the use of these parameters.

Table 7. Stall monitoring parameters at 9 m/s and an angle of attack between 5° and 25°.

AOA	$\left(\frac{S2}{{}^{*}S2_{std}} - 1\right)\%$	$\left(\frac{S2 - S5}{{}^{*}S2_{std} - {}^{**}S5_{std}}\right)\%$	$CV(S1)\%$
5°	0	100	0.5
10°	−2.7	70	0.7
15°	0.8	20	1.4
20°	10.4	−50	6.4
25°	21.7	−120	6.2

* $S2_{std}$ (V = 9m/s; AOA = 5°) = 62.2 Pa; **$S5_{std}$ (V = 9m/s; AOA = 5°) = 82.3 Pa.

Finally, the sharp variation of values on Table 7 demonstrates that stall approximation can be efficiently identified using these parameters, which opens the path to a stall alert and prevention system based on local pressure-differential monitoring.

4.4 Collapse triggers and shape stability

Collapses are phenomena particularly important for inflatable wings. Naturally, there are several levels of wing collapse, starting from perceptible loss of internal pressure, which might evolve into partial transient deflations, and then into a complete loss of wing's shape and stiffness. Fig. 44 presents different levels of collapse:

Figure 44: Levels of wing collapse

Three primary triggers might lead to collapse situations. One is a negative incidence resulting in an angle of attack below inflation. A second one is an excessive incidence resulting in a full stall. The third refers to the relative speed drops, which may be caused by maneuvering and atmospheric disturbances.

The situations directly linked to AOA limits were already explored in previous subsections dealing with the inflation and stall phenomena. However, there may be conditions where, even at an operational AOA, a general reduction on internal-external pressure differential results in a noticeable loss of wing's stiffness (upper-left corner photo on Fig. 44). For instance, when a tailwind gust hits the wing, the relative speed is suddenly reduced with a

perceived pressure loss. The lift reduction will cause the wing to accelerate regaining equilibrium. Notwithstanding, the reactions are not instantaneous, resulting in a period in which the low inner-outer pressure differential causes perceptible shape instability. The disturbance may be transient, but a high-speed drop may lead to stall or to an intense pendulum reaction that leads to negative incidence. Then, it is interesting to evaluate the level of pressure differentials captured by the sensors at different levels of flow speed tested.

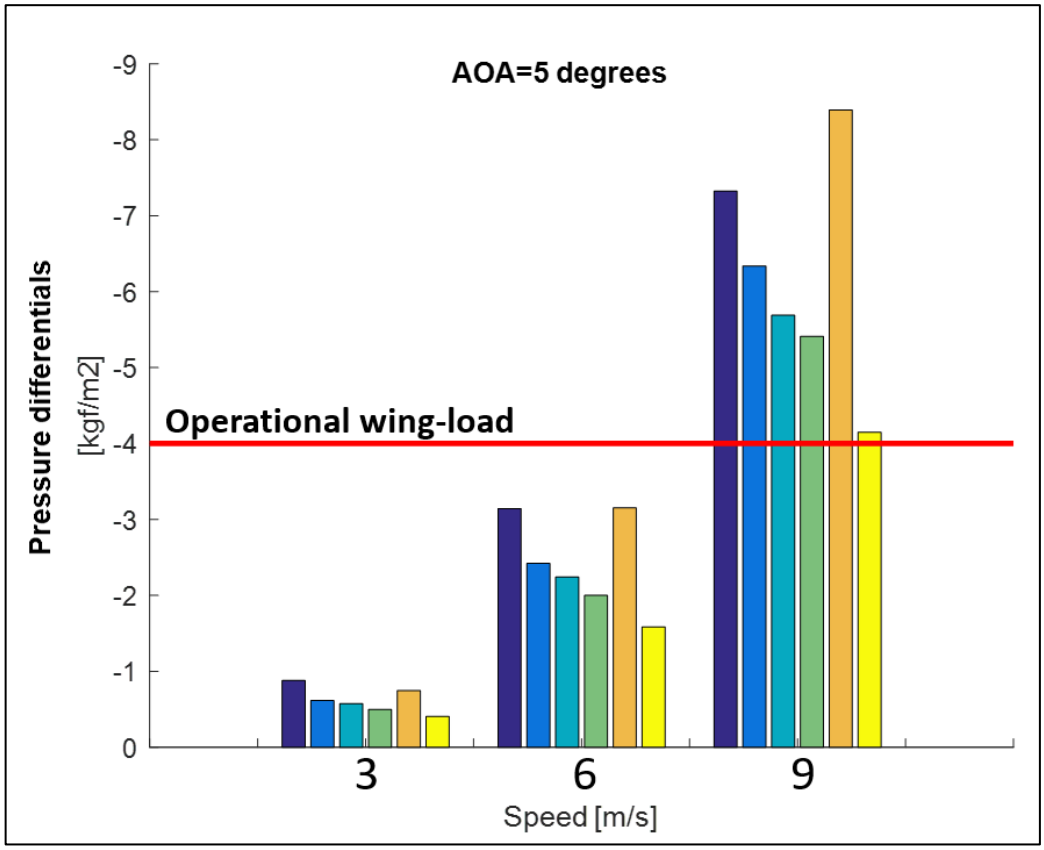

Figure 45: Pressure differentials range (AOA=5˚).

Fig. 45 presents the pressure differentials measured at 3, 6, and 9 m/s for an AOA of 5 degrees. The output is presented in force per unit area (kgf/m2) to allow a comparison with a demanded average wing-load, a design parameter. Common paragliders present wing-load around 4 kg/m2 [26]. The collected data show that general readings at operational speed are consistently above this limit. At inflation speed, pressure differentials are much lower but still far higher than the wing's fabric specific weight (38 g/m^2). Table 8 presents the mean value obtained with the readings from the six sensors at 5° AOA for an unsustainably low speed (3 m/s), an inflation speed (6 m/s), and an operational speed (9 m/s):

Table 8. Pressure-differential readings at 5° AOA for different speeds.

$V[m/s]$	$S1$ $[Pa]$	$S2$ $[Pa]$	$S3$ $[Pa]$	$S4$ $[Pa]$	$S5$ $[Pa]$	$S6$ $[Pa]$	$\frac{1}{6}\sum S$ $[Pa]$
3	8.6	6.0	5.6	4.9	7.3	4.0	6.1
6	30.8	23.7	22.0	19.6	30.9	15.5	23.8
9	71.8	62.2	55.8	53.1	82.3	40.7	61.0

Table 8 reveals that the level of pressure-differentials change perceptibly with speed, and the mean value can be used to characterize the level of available dynamic pressure. It should also be noticed that the general level of pressure-differential measured is directly related to the wing load, a factor traditionally used as a design parameter. None of these values correspond to the final wing load, which requires integration throughout the surface, but they are a fair indicative based on local evaluations. Considering that common paragliders and parafoils present wing-loads around 40 Pa [26], the collected data show that the average reading at operational speed (9 m/s) is substantially above this value, whereas, at inflation speed (6 m/s), the average differential pressure is much lower.

More important than defining certain levels of desired pressure differentials is to identify general pressure drops. This can be done by taking the average value of differential pressure measurements all over the wing as a composed parameter. Setting a standard at the design point, which means the steady glide condition, it is possible to identify relevant disturbances which may jeopardize wing stiffness.

Consequently, a calibrated system can dynamically monitor wing stiffness using the average differential pressure, and its time derivative sign, to provide an alert preventing further reductions in speed.

4.5 Pressure Coefficient (Cp) distribution and the internal flow adjustment model

One of the main objectives of the present work is to sustain the use of local pressure differential measurements to characterize inflatable wings instead of using classic approaches based on external pressure coefficients or global lift and drag coefficients. The use of geometry-based aerodynamic coefficients for wing design encounters relevant limitations even in cases where the wing is fully closed. For example, dealing with inflatable-wing drones for planetary exploration, as discussed in the work by Hassanalian et al. [46], the same issues originating from elastic deformation can be anticipated. For these situations the use of local differential

pressure monitoring can, as well, represent a more suitable approach, since it provides information about the external pressure field and the wing stiffness simultaneously. However, Cp assessments can still be useful with the only purpose of comparing data obtained from previous experiments and numerical simulations, demonstrating that the pressure differential approach generates consistent results and, at the same time, provides important information about the internal flow, which is a major player for inflatable wings.

Equation (3) provided the fundamental relation between external and internal pressure coefficients. It reveals that, considering the external pressure distribution expected for a defined airfoil geometry, if an internal flow exists a drop on the differential pressure felt on the surface is expected. Therefore, the differential reading is, in fact, a composition of external and internal flow.

An accurate characterization of the internal flow can be supported by combining differential and absolute pressure readings. By such means, one can extract the actual pressure at each point on the inner surfaces. However, the multiplicity of measurement devices encounters obvious limitations for in-flight applications. A future laboratory work to fully characterize the behavior of internal and external pressure coefficients on open airfoils constitutes a welcome effort. It can be done by substantially increasing the number of sensors on the surface, and, combining absolute pressure measurements to extract the C_p and κ coefficients accurately. Such a work would contribute for a better characterization of the aerodynamic phenomena in place. In this work, however, the demand for a practical flight test instrumentation is the priority. Therefore, the present analysis about external and internal flow is simply an approximation intended to support system's usability.

Previous studies show conflicting conclusions regarding the confined flow structures. Some researchers claim that relevant flow occurs inside the cell [22, 27], leading to significant effects on global lift and drag, whereas others [5,7] affirm that the encapsulated air is mostly stationary along with the cell, being slightly affected at low angles of attack. Data obtained from pressure differential readings indicated that the inner flow is a relevant phenomenon. It is important to highlight that most of the experiments used to capture internal pressure in the cited references applied methods where an inspection tube was placed somewhere at the middle of the wing to capture pressure. Therefore, it is easy to understand why such experiments suggested a pressure near to stagnation. It is important to remember that aerodynamic pressure

differentials are naturally low, therefore, such a method would not capture local effects of aerodynamic internal flow, which results relevant variations at the inner surface.

From basic aerodynamic theory, it is expected that the pressure at the upper surface should be consistently lower than the pressure at the bottom surface for positive AOA. If the inner pressure were constant and near the stagnation level, upper-pressure differentials should be considerably higher than the bottom pressure differentials in this same region. However, as illustrated in Fig. 38, the bottom-middle pressure differential was consistently higher for a considerable range of operational AOA. Also, at low AOA, the difference between upper and bottom pressure differentials at the middle diminishes as AOA increases, which is an unnatural response. The logical explanation of such behavior comes from the internal pressure gradients. This means the cell's internal flow increased the pressure at the inner bottom surface more than that at the inner upper surface around the initial portions of the cell.

When the air intake is perfectly aligned with the incoming air, the inflation process is more productive through the ram effect. It is also important to realize that the recirculation bubble observed at the bottom leading edge is linked to the internal flow, thus affecting its extension and magnitude. At the virtual origin of the reference chord, the internal flow factor is almost null, since there is no airfoil surface and the incoming flow is nearly undisturbed. At the end of the cell, on the other hand, where the air was already contained, and the internal pressure gradients were dumped, the pressure approaches its stagnation value.

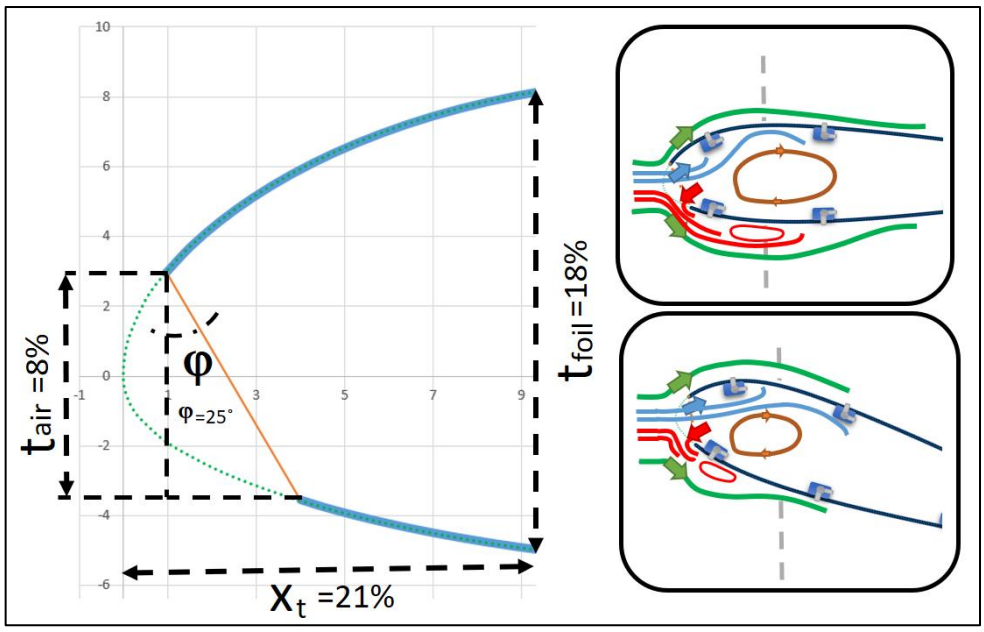

Figure 46: Internal flow sketch near to the air intake.

As the flow circulates near to the air intake, at positive AOA, the bottom flow is supposed to decelerate much faster than the upper flow, which may be even in acceleration when filling up the airfoil internal space. The expected result is a complementary behavior between upper and bottom inner pressure coefficients, which rise from zero to one following a different pattern. The bottom pressure rapidly increases, whereas the upper flow only starts a definitive pressure rise after passing the maximum thickness of the airfoil. Therefore, as a theoretical model, the following correlations are proposed for the internal flow factor, at the upper and bottom surfaces, respectively:

$$\kappa_u = \frac{e^{\frac{x}{a_\kappa}} - 1}{e^{\frac{1}{a_\kappa}} - 1} \tag{13}$$

$$\kappa_b = \frac{ln\left(1 + e^{b_\kappa \cdot x}\right)}{ln\left(1 + e^{b_\kappa}\right)} \tag{14}$$

An accurate characterization of the internal flow can be achieved by designing additional experiments combining differential and absolute pressure readings as discussed. Such an approach is scientifically relevant but moves away from the objective of minimizing instrumentation to deliver a suitable on-board system. An alternative way of separating the effects of internal flow using only differential pressure is to rely on computational simulations, setting averaged parameters (a, b) for Equations (13) and (14). Considering airflow speed of 10 m/s and AOA varying from 5° to 15°, simulation data revealed that, where the thickness is maximum (x = 0.21), the inner bottom pressure coefficient should be near 80 ± 5%, and the upper-pressure coefficient should be around 10 ± 5%. It allowed for the defining of the theoretical curve for the internal flow factor (a = 0.35, b = 6.25), associated to the ASCENDER airfoil at 10 m/s and 5° < AOA < 15°.

Equations (13) and (14) where obtained by assuming an exponential and a logarithmic rising profile for internal pressure at the upper and bottom surfaces respectively. The curves' parameters were, then, fit to the conditions established through computational simulation. This fully theoretical model materializes the hypotheses made about the inner flow.

For the external pressure coefficient, considering the baseline airfoil, a wide number of traditional methods are available providing the Cp distribution curve, which can also be averaged for a defined AOA range. Equations (15) and (16) present the mathematical modeling reflecting the Cp distribution observed on the same computational simulations:

$$Cp_u = \gamma_u \cdot x^{(\alpha_u - 1)} \cdot (1 - x)^{(\beta_u - 1)} \tag{15}$$

$$Cp_b = \gamma_b \cdot x^{(\alpha_b - 1)} \cdot (1 - x)^{(\beta_b - 1)} + \delta_b \cdot e^{\left(-\frac{x-p}{q}\right)} \quad (16)$$

The type of mathematical functions used to describe the external coefficient profile is traditional, except by the term added to the bottom coefficient, which was included using a normal distribution curve to represent the "bump" on pressure differential observed on the bottom leading edge. While Equations (15) and (16) define the type of curve representing the Cp distribution based on the characteristics observed computationally, the specific parameters were numerically adjusted to fit the model to the experimental data based on Equation (3). It means that, the C_p distribution curve is obtained by fitting the theoretical model defined for κ to the experimental data. The results applying the suggested model are illustrated in Fig. 47, and the specific values were obtained by adjusting the parameters to the experimental data, as presented in Table 9.

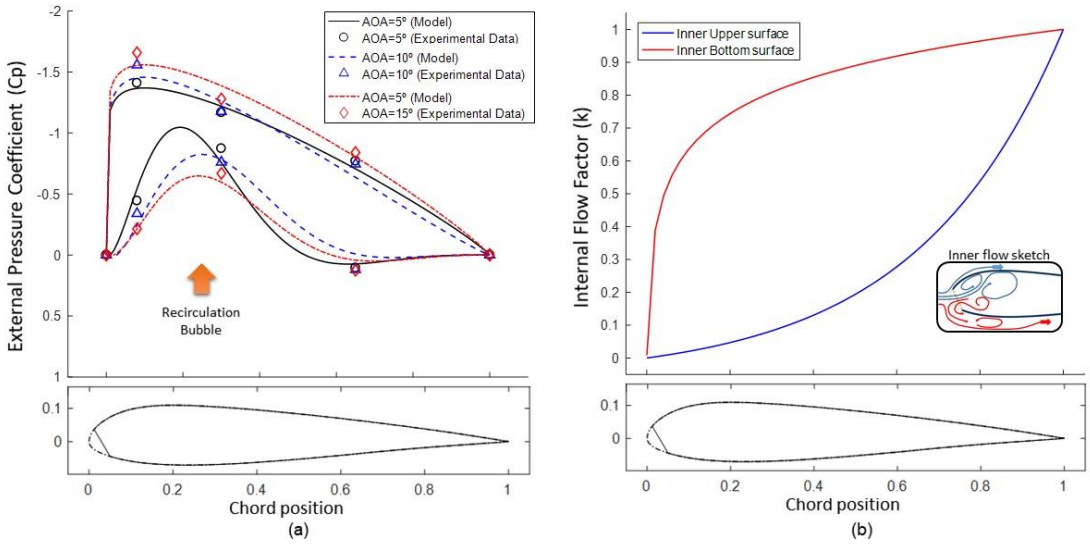

Figure 47: (a) External Pressure Coefficients; (b) Internal Flow Factor -(V=10 m/s, 5° ≤ AOA ≤ 15°)

Table 9. Model parameters for the ASCENDER airfoil at 10 m/s and an AOA between 5° and 15°.

AOA	γ_u	α_u	β_u	γ_b	α_b	β_b	δ_b	p	q
5°	1.10	1.90	−1.89	2.0	4.00	4.00	2.70	7.80	−102.63
10°	1.12	2.12	−2.18	2.0	4.00	4.09	2.75	6.25	−64.37
15°	1.10	1.90	−2.16	2.1	3.57	2.93	2.85	6.55	−61.02

The distribution calculated using the proposed model to fit experimental data reveals an upper-surface Cp distribution pattern fully compatible with Cp distribution obtained theoretically for the same baseline airfoil. It also presents levels of Cp that are fully coherent with previous experimental results [5,7], as obtained by completely different methods.

The most distinct observation brought up by Fig. 47 is the singularity present at the bottom surface resulting from the recirculation bubble at the bottom leading edge. This phenomenon, which was already observed following a completely independent rationale, presents itself as a major player that helps explain the significant reduction in lift and the increase in drag informed by several researches.

4.6 Lift and Drag estimation

The most common use of any pressure coefficient distribution model is to estimate aerodynamic forces. Combining the external Cp estimation and the airfoil geometry, it is possible to integrate lift coefficients for different AOA. Drag was not calculated, since the pressure coefficients would provide only a small component of the total drag, which is highly affected by parasites and induce drag. These two components require force measurement methods, which are out of scope of the present experiments. Nonetheless, the estimated CL is useful to characterize the wing and to corroborate the methodological adequacy.

The CL-Alpha curve plotted in Fig. 48 is fully compatible with the results obtained by previous researchers [27] for sectioned airfoils. Further, the resulting wing load range from 30 Pa to 50 Pa corresponds precisely to the expected range previously calculated [26]. Therefore, parallel observations seem to lead to consistent results, reinforcing the usefulness of the differential pressure measurement approach, and the relevance of the inner flow

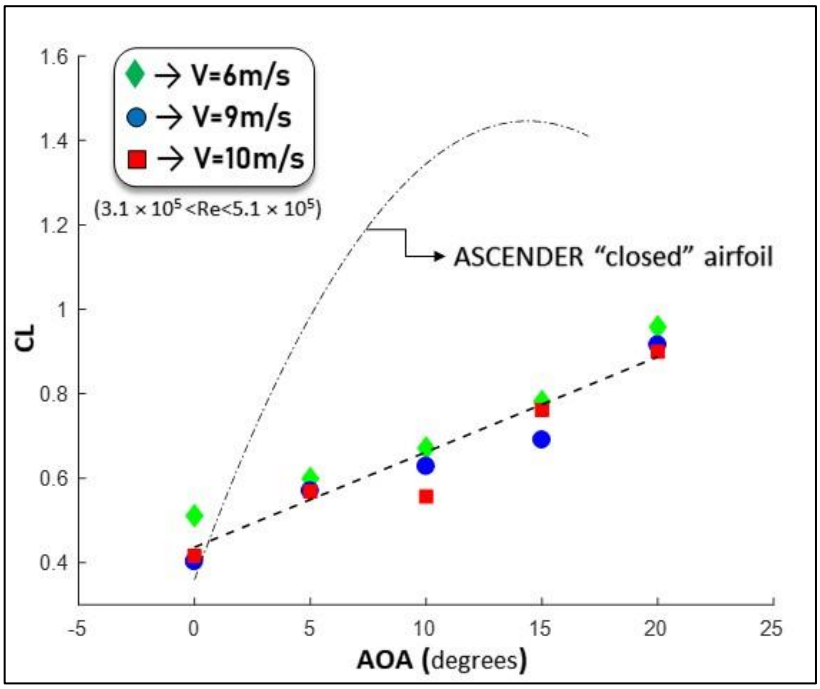

Figure 48: Lift Curve (CL-Alpha) as a function of angle of attack.

It is important to observe that, considering the speed of 10 m/s and operational AOA (5˚ to 15˚), the lift coefficient range resulted in a wing load range from 3 to 5 kg/m2, which is precisely the operational range as discussed in Fig. 45. Therefore, parallel considerations seem to lead to consistent results. It, once more, cohoborates the utility of the model for under-design investigations.

The comparison with the "closed" airfoil reference curve shows that lift penalty increases with AOA. It also shows up to 45% potential lift loss at high angles. However, the data must be interpretated carefully. It is important to understand that the reference curve was obtained computationally considering the bi-dimensional reference profile. Therefore, when subjected to three-dimensional effects a considerable reduction on lift is expected.

It is never enough to emphasize that the external pressure coefficient, the internal flow factor, and the lift coefficient were derived to provide a classic representation of the observed characteristics, allowing useful reflections about the collected data. However, no theoretical model was used for analyzing the main characteristics in Sections 4.1–4.4, but only the differential pressure data directly measured. Therefore, the potential uncertainties related to modeling pressure coefficients distribution profiles do not impair the main objective, which is demonstrating that a pressure-differential approach is more suitable for inflatable wing analysis and can be used to characterize the wing and to prevent undesirable in-flight conditions

Finally, the modelling based on differential pressure assessments represents an entire field for research. Once established the use of differential pressure sensors as the basic element for inflatable wing aerodynamic characterizations, a variety of models can be developed to expand the use of such a data. Up to this point, the demonstration of the capabilities of the instrumentation system based on differential pressure and the provision of simplistic methods to correlate data to conventional pressure coefficient data are sufficient to support the successful finalization of the task proposed for the first phase of the research.

5. Conclusions and perspectives

This work presented the development of a flight-test instrumentation system, applied to dynamically inflatable wings, for outer-inner differential pressure measurements at the upper and lower surfaces of the airfoil. Data gathered from a wind-tunnel test campaign allowed to describe aerodynamic phenomena, including inflation and stall approximation. Data analysis confirmed previous findings regarding the existence of a minimum AOA for inflation and the appearance of a recirculation bubble at the bottom leading edge that significantly affects airfoil performance.

The existence of significant internal flow was confirmed in the first half of the cell. A theoretical model for pressure coefficient distribution along open-airfoils was proposed based on estimations of the confined airflow structure. Calculated wing lift forces and loads were compatible with practical observation.

Airfoil shape stability and boundary layer disturbances were also evaluated, anticipating the instrumentation's suitability for in-flight applications. As a whole, the instrumentation may be applied straightforwardly to actual inflatable wings, as a flight test appliance, and to improve their safety as a collapse alert and prevention tool.

Considering the previous investigations toward the subject, it is possible to say that the present work contributes to the discussion in three different ways. First, it confirms through a completely different method the findings regarding the singularities observed on dynamically inflatable wings and offers a parallel approach for open airfoils aerodynamic characterization. Secondly, it provides a viable and capable instrumentation system to be used in-flight, opening a wide range of possibilities of practical investigations using real-size prototypes. Finally, it points to the use of local pressure differential signal monitoring as the core for safety systems design.

The combined use of the proposed instrumentation with computational and wind-tunnel data may improve parafoils and paragliders' design techniques by providing new modelling strategies based on local differential pressure dynamics. Existent models may by update to account for the effects described and to consider parameters not previously envisioned.

It was shown that differential pressure sensors may also allow further investigations regarding fluid-structure interactions considering the fabric tensile efforts. It may be useful to improve researches linked to material specifications and structural analysis. It was also

recognized that the results are very limited in terms of accurate characterization of flow characteristics, due to the small number of sensors applied and the lack of multiple instrumentations to identify coupled parameters. However, respecting the defined scope, the results are encouraging for further laboratory tests. Using additional instrumentation and varying the airfoil tested a lot can be discovered about the nature of flow over open airfoils. This is, by itself, an entire field for research.

The next step will be to instrument a real manned paraglider and execute a complete flight test campaign to characterize the pressure differential variations during typical maneuvers and collapse situations. The results shall provide important data for design optimization and safety systems conception.

At the present stage, the results proving the value of working with pressure differentials, and the capability of the instrumentation system, already constitute an important scientific and technological step.

Bibliography

[1] Lingard, J.S. Precision Aerial Delivery System—Ram-Air Parachute Design. In Proceedings of the 13th AIAA Aerodynamic Decelerator Systems Technology Conference, Clearwater Beach, FL, USA, 15–18 May 1995.

[2] Puskas, E. Ram-Air Parachute Design Considerations and Applications. In Proceedings of the 8th Aerodynamic Decelerator and Balloon Technology Conference, Hyannis, MA, USA, 2–4 April 1984; pp. 255–259, doi:10.2514/6.1984-826.

[3] Dunker, S. Ram-air Wing Design Considerations for Airborne Wind Energy. *Airborne Wind Energy* **2013**, 517–546, doi:10.1007/978-3-642-39965-7_31.

[4] Dek, C.; Overkamp, J.L.; Toetert, A.; Hoppenbrouwer, T.; Slimmens, J.; van Zijl, J.; Rossi, P.A.; Machado, R.; Hereijgers, S.; Kilic, V.; et al. A recovery system for the key components of the first stage of a heavy launch vehicle. *Aerosp. Sci. Technol.* **2020**, *100*, 105778, doi:10.1016/j.ast.2020.105778.

[5] Mashud, M.; Umemura, A. Improvement in Aerodynamic Characteristics of a Paraglider Wing Canopy. *Trans. Jpn. Soc. Aeronaut. Space Sci.* **2006**, *49*, 154–161, doi:10.2322/tjsass.49.154.

[6] Fogell, N.A.T. Fluid-Structure Interaction Simulations of the Inflated Shape of Ram-Air Parachutes. Ph.D. Thesis, Imperial College London, London, UK, 2014, doi:10.2514/6.2013-1326.

[7] Mashud, M.; Umemura, A. Experimental Investigation on Aerodynamic Characteristics of a Paraglider Wing. *Trans. Jpn. Soc. Aeronaut. Space Sci.* **2006**, *49*, 9–17, doi:10.2322/tjsass.49.9.

[8] Kulhánek, R. Identification of a degradation of aerodynamic characteristics of a paraglider due to its flexibility from flight test. *Aircr. Eng. Aerosp. Technol.* **2019**, *91*, 873–879, doi:10.1108/AEAT-06-2018-0162.

[9] Wachlin, J.; Ward, M.; Costello, M. In-canopy sensors for state estimation of precision guided airdrop systems. *Aerosp. Sci. Technol.* **2019**, *90*, 357–367, doi:10.1016/j.ast.2019.04.036.

[10] Burdette, S.; Costello, M.; Scheuermann, E. Using an Array of In-Canopy Sensors for Guided Airdrop System State Estimation. In Proceedings of the 24th AIAA Aerodynamic Decelerator Systems Technology Conference, Denver, CO, USA, 5–9 June 2017; doi:10.2514/6.2017-3721.

[11] Coleman, J.; Ahmad, H.; Toal, D. Development and Testing of a Control System for the Automatic Flight of Tethered Parafoils. *J. Field Robot.* **2016**, 1–20, doi:10.1002/rob.21652.

[12] Gorman, C.M.; Slegers, N. Evaluation of Multibody Parafoil Dynamics Using Distributed Miniature Wireless Sensors. *J. Aircr.* **2011**, *49*, doi:10.2514/6.2011-6612.

[13] Ghoreyshia, M.; Bergeronb, K.; Jiráseka, A.; Seidela, J.; Lofthousea, A.J.; Cummingsa, R.M. Computational aerodynamic modeling for flight dynamics simulation of ram-air parachutes. *Aerosp. Sci. Technol.* **2016**, *54*, 286–301, doi:10.1016/j.ast.2016.04.024.

[14] Tanaka, K.; Tanaka, M.; Takahashi, Y.; Wang, H.O. Waypoint Following Control Design for a Paraglider Model with Aerodynamic Uncertainty. *IEEE/ASME Trans. Mechatron.* **2018**, *23*, doi:10.1109/tmech.2017.2728678.

[15] Zhang, Z.; Zhao, Z.; Fu, Y. Dynamics analysis and simulation of six DOF parafoil system. *Clust. Comput.* **2019**, *22*, 1–12, doi:10.1007/s10586-018-1720-3.

[16] Tan, P.; Sun, M.; Sun, Q.; Chen, Z. Dynamic Modeling and Experimental Verification of Powered Parafoil with Two Suspending Points. *IEEE Access* **2020**, *8*, 12955–12966, doi:10.1109/ACCESS.2020.2965541.

[17] Belloc, H.; Chapin, V.; Manara, F.; Sgarbossa, F.; Forsting, A.M. Influence of the air inlet configuration on the performances of a paraglider open airfoil. International Journal of Aerodynamics. *Indersci. Publ.* **2016**, *5*, 83–104, doi:10.1504/IJAD.2016.080510.

[18] Tao, J.; Sun, Q.; Liang, W.; Chen, Z.; He, Y.; Dehmer, M. Computational fluid dynamics based dynamic modeling of parafoil system. *Appl. Math. Model.* **2018**, *54*, 136–150, doi:10.1016/j.apm.2017.09.008.

[19] Takizawa, K.; Tezduyar, T.E.; Terahara, T. Ram-air parachute structural and fluid mechanics computations with the Space–Time Isogeometric Analysis (ST-IGA). *Comput. Fluids* **2016**, *141*, 191–200, doi:10.1016/j.compfluid.2016.05.027.

[20] Burk, S.M.; Ware, G.M. *Static Aerodynamic Characteristics of Three Ram-Air-Inflated Low-Aspect-Ratio Fabric Wings*; Technical Report NASA TN D-4182; NASA Langley, Hampton, VA, USA, 1967.

[21] Abdelqodus, A.A.; Kursakov, I.A. Optimal Aerodynamic Shape Optimization of a Paraglider Airfoil Based on the Sharknose Concept. *MATEC Web Conf.* **2018**, *221*, 05002, doi:10.1051/matecconf/201822105002.

[22] Becker, S.; Paul, B. Experimental Study of Paraglider Aerodynamics. Master's Thesis, Imperial College London, London, UK, 2017, doi:10.13140/RG.2.2.33674.16321.

[23] Mashud, M.; Umemura, A. Three-Dimensional Measurements of Aerodynamic Characteristics of Paraglider Canopy Cells. *Trans. Jpn. Soc. Aeronaut. Space Sci.* **2006**, *49*, 146–153, doi:10.2322/tjsass.49.146.

[24] Yamamori, Keitaro, Umemura, Akira, Hishida, Manabu. Experimental Study on the Wing Formation of a Paraglider Canopy Cell (Inflatable Wing). *J. Jpn. Soc. Aeronaut. Space Sci.* **2005**, *53*, 68–74, doi:10.2322/jjsass.53.68.

[25] Uddin, M.; Mashud, M. Wind Tunnel Test of a Paraglider (flexible) Wing Canopy. *Int. J. Mech. Mechatron. Eng*. *IJMME-IJENS* **2010**, *10*, 7–13.

[26] Benedetti, D.M.; Pinto, R.F.; Ferreira, R. *Paragliders Stability Characteristics*; SAE Technical Paper 2013-36-0355; Warrendale, PA, USA, October 2013; https://saemobilus.sae.org/content/2013-36-0355/ doi:10.4271/2013-36-0355.

[27] Mohammadi, M.A.; Johari, H. Computation of Flow over a High Performance Parafoil. In Proceedings of the 20th AIAA Aerodynamic Decelerator Systems Technology Conference and Seminar, Seattle, WA, USA, 4–7 May 2009, doi:10.2514/1.47363.

[28] Traub, L.; Coffman, C. Efficient Low-Reynolds-Number Airfoils. *J. Aircr.* **2019**, *56*, 1–17, doi:10.2514/1.C035515.

[29] Genç, M.; Karasu, L.; Hakan, H.; Akpolat, T. *Low Reynolds Number Aerodynamics and Transition*; Intech, Rijeka, Croatia, 2012; doi:10.5772/31131.

[30] King, R.M.; Chokani, N.; Mangalam, S.M. Control of Laminar Separated Bubbles Using an Adaptive Mechanical Turbulator. In Proceedings of the 40th AIAA Aerospace Sciences Meeting and Exhibit, Reno, NV, USA, 14–17 January 2002;doi:10.2514/6.2002-294.

[31] Lissaman, P.B.S.; Brown, G.J.; Apparent Mass Effects on Parafoil Dynamics - 12th RAeS/AIAA Aerodynamic Decelerator Systems Technology Conference and Seminar. American Institute of Aeronautics and Astronautics: London, England -1993

[32] Prakash, o.; Ananthkrishnany, N.; Modeling and Simulation of 9-DOF Parafoil-Payload System Flight Dynamics - Indian Institute of Technology - Bombay, Mumbai 400076

[33] Cochrane, C.; Lewandowski, M.; Koncar, V. A Flexible Strain Sensor Based on a Conductive Polymer Composite for in situ Measurement of Parachute Canopy Deformation. *Sensors* **2010**, *10*, 8291–8303, doi:10.3390/s100908291.

[34] Burns, D.W.; Burns, D.B. Compact, Lightweight Pressure Sensors for Aerodynamic Parachute Measurements. In Proceedings of the 19th AIAA Aerodynamic Decelerator Systems Technology Conference and Seminar, Williamsburg, VA, USA, 21–24 May 2007, doi:10.2514/6.2007-2569.

[35] McCarty, M. *The Measurement of the Pressure Distribution over the Wing of an Aircraft in Flight*; Australian Defence Force Academy, Campbell ACT 2612, Austrália, 2008.

[36] Song, P.; Ma, Z.; Ma, J.; Yang, L.; Wei, J.; Zhao, Y.; Zhang, M.; Yang, F.; Wang, X. Recent Progress of Miniature MEMS Pressure Sensors. *Micromachines* **2020**, *11*, 56, doi:10.3390/mi11010056.

[37] Milosevic, V.; Marković, B.; Stojić, D. Effects of point loads on membrane structures. *Građevinar* **2018**, *70*, 1033–1041, doi:10.14256/JCE.1670.2016.

[38] Lu, K.; Accorsi, M.; Leonard, J. Finite element analysis of membrane wrinkling. *Int. J. Numer. Methods Eng.* **2001**, *50*, 1017–1038, doi:10.1002/1097-0207(20010220)50:5<1017::AID-NME47>3.0.CO;2-2.

[39] Ibrahim, A.; Ryu, Y.; Saidpour, M. Stress Analysis of Thin-Walled Pressure Vessels. *Mod. Mech. Eng.* **2015**, *5*, 1–9, doi:10.4236/mme.2015.51001

[40] Sensirion®. Datasheet SDP3x-Digital, Version 1. Available online: https://www.sensirion.com/fileadmin/user_upload/customers/sensirion/Dokumente/8_Differential_Pressure/Datasheets/Sensirion_Differential_Pressure_Sensors_SDP3x_Digital_Datasheet.pdf - (accessed on 13 December 2017).

[41] Ferreira, G.F.L. Um Cálculo da Espessura da Camada Limite. *Revista Brasileira de Ensino de Física* **2002**, *24*, doi:10.1590/S0102-47442002000100003.

[42] Casellas, P.H. Paraglider Design Handbook—Chapter 2—Airfoils. Available online: http://www.laboratoridenvol.com/paragliderdesign/airfoils.html#5 (accessed on 20 April 2020).

[43] Macias, M.M. Estudo Experimental em Túnel de Vento de Turbinas de Eixo Horizontal. Master Dissertation, Departamento de Engenharia Mecânica, Universidade de Brasília, Brasília, DF, Brazil; Publicação ENM.DM-230 A/2016, doi:http://repositorio.unb.br/handle/10482/22013.

[44] Zovatto, L.; Pedrizzetti, G. Flow about a circular cylinder between parallel walls. *J. Fluid Mech.* **2001**, *440*, 1–25, doi:10.1017/S0022112001004608.

[45] Chang-Koon, C.; Kwon, D.K. Wind tunnel blockage effects on aerodynamic behavior of bluff body. *Wind Struct. Int. J.* **1998**, *1*, 351–364, doi:10.12989/was.1998.1.4.351.

[46] Hassanalian, M.; Rice, D.; Abdelkefi, A. Evolution of space drones for planetary exploration: A review. *Prog. Aerospace Sci.* **2018**, *97*, 61–105, doi:10.1016/j.paerosci.2018.01.003.

Appendix – A: Experimental data – Static readings

Flow Speed - V=3m/s																		
		Upper-front sensor			Upper-midle sensor			Upper-rear sensor			Botton-front sensor			Botton-midle sensor			Botton-rear sensor		
		P(1) [Pa]	s(1) [Pa]	s(1) [%]	P(2) [Pa]	s(2) [Pa]	s(2) [%]	P(3) [Pa]	s(3) [Pa]	s(3) [%]	P(4) [Pa]	s(4) [Pa]	s(4) [%]	P(5) [Pa]	s(5) [Pa]	s(5) [%]	P(6) [Pa]	s(6) [Pa]	s(6) [%]
AOA =	-20	-1,5	0,2	13%	-2,2	0,2	10%	-2,1	0,2	9%	-5,5	0,8	15%	-3,7	0,5	13%	-1,9	0,2	10%
AOA =	-15	-4,9	0,9	18%	-5,6	1,1	20%	-5,4	1,1	20%	-11,0	2,6	23%	-8,4	1,8	21%	-4,1	0,8	20%
AOA =	-10	-3,6	0,2	6%	-3,6	0,2	5%	-3,3	0,2	5%	-5,9	0,6	10%	-4,6	0,4	9%	-2,4	0,2	9%
AOA =	-5	-8,3	0,1	1%	-7,7	0,4	5%	-7,1	0,1	2%	-12,1	0,8	6%	-9,0	0,6	7%	-4,8	0,2	3%
AOA =	0	-4,4	0,0	1%	-3,8	0,2	5%	-3,0	0,1	2%	-3,9	0,4	9%	-4,0	0,1	2%	-2,2	0,0	2%
AOA =	5	-8,6	0,2	2%	-6,0	0,4	6%	-5,6	0,2	3%	-4,9	0,5	11%	-7,3	0,2	3%	-4,0	0,1	3%
AOA =	10	-10,1	0,1	1%	-6,7	0,3	5%	-6,2	0,1	2%	-5,3	0,4	7%	-7,5	0,1	1%	-4,3	0,1	2%
AOA =	15	-9,5	0,2	2%	-6,3	0,1	2%	-5,9	0,2	3%	-4,2	0,2	5%	-6,2	0,1	1%	-3,7	0,1	2%
AOA =	20	-10,1	0,9	9%	-8,0	0,8	10%	-7,0	0,6	8%	-3,6	0,3	8%	-6,2	0,5	8%	-3,9	0,3	7%

Flow Speed - V=6m/s																		
		Upper-front sensor			Upper-midle sensor			Upper-rear sensor			Botton-front sensor			Botton-midle sensor			Botton-rear sensor		
		P(1) [Pa]	s(1) [Pa]	s(1) [%]	P(2) [Pa]	s(2) [Pa]	s(2) [%]	P(3) [Pa]	s(3) [Pa]	s(3) [%]	P(4) [Pa]	s(4) [Pa]	s(4) [%]	P(5) [Pa]	s(5) [Pa]	s(5) [%]	P(6) [Pa]	s(6) [Pa]	s(6) [%]
AOA =	-20	-7,1	0,6	9%	-11,5	0,8	7%	-12,6	0,4	3%	-39,4	5,1	13%	-24,2	2,5	10%	-11,6	0,9	8%
AOA =	-15	-15,3	0,3	2%	-18,6	0,6	3%	-19,7	0,4	2%	-39,7	3,9	10%	-30,4	2,2	7%	-14,3	0,8	6%
AOA =	-10	-20,6	0,1	1%	-22,4	0,3	2%	-22,8	0,3	1%	-40,8	2,1	5%	-31,5	2,3	7%	-15,6	0,7	5%
AOA =	-5	-25,3	0,3	1%	-24,8	0,4	2%	-24,3	0,4	2%	-41,6	2,8	7%	-31,9	1,9	6%	-16,4	0,6	4%
AOA =	0	-26,0	0,2	1%	-21,6	0,4	2%	-20,8	0,3	1%	-30,4	2,0	7%	-28,8	0,5	2%	-14,5	0,3	2%
AOA =	5	-30,8	0,3	1%	-23,7	0,4	2%	-22,0	0,4	2%	-19,6	1,5	7%	-30,9	0,5	1%	-15,5	0,3	2%
AOA =	10	-33,6	0,3	1%	-24,0	1,1	5%	-21,8	0,4	2%	-18,9	1,3	7%	-28,9	0,4	1%	-15,3	0,3	2%
AOA =	15	-36,9	0,5	1%	-27,5	0,5	2%	-24,4	0,7	3%	-16,8	1,1	6%	-28,2	0,3	1%	-15,5	0,3	2%
AOA =	20	-36,4	2,1	6%	-29,9	1,7	6%	-25,9	0,9	4%	-13,2	0,6	5%	-24,9	0,3	1%	-14,6	0,3	2%

Flow Speed - V=9m/s																		
		Upper-front sensor			Upper-midle sensor			Upper-rear sensor			Botton-front sensor			Botton-midle sensor			Botton-rear sensor		
		P(1) [Pa]	s(1) [Pa]	s(1) [%]	P(2) [Pa]	s(2) [Pa]	s(2) [%]	P(3) [Pa]	s(3) [Pa]	s(3) [%]	P(4) [Pa]	s(4) [Pa]	s(4) [%]	P(5) [Pa]	s(5) [Pa]	s(5) [%]	P(6) [Pa]	s(6) [Pa]	s(6) [%]
AOA =	-20	-14,4	2,0	14%	-25,7	2,1	8%	-30,3	1,3	4%	-95,2	13,7	14%	-53,7	6,4	12%	-26,2	2,4	9%
AOA =	-15	-32,2	1,1	4%	-43,5	2,2	5%	-46,2	2,0	4%	-95,8	7,1	7%	-71,8	6,3	9%	-33,7	2,3	7%
AOA =	-10	-43,0	0,4	1%	-51,6	1,2	2%	-52,9	0,8	1%	-96,7	6,4	7%	-74,3	5,2	7%	-36,5	2,4	7%
AOA =	-5	-54,2	0,6	1%	-57,6	0,9	2%	-56,5	0,9	2%	-98,6	4,7	5%	-76,9	3,9	5%	-38,8	1,2	3%
AOA =	0	-62,4	0,4	1%	-59,1	0,6	1%	-55,6	0,7	1%	-86,9	5,2	6%	-80,1	1,4	2%	-39,3	0,8	2%
AOA =	5	-71,8	0,4	1%	-62,2	0,7	1%	-55,8	0,7	1%	-53,1	3,6	7%	-82,3	0,9	1%	-40,7	0,7	2%
AOA =	10	-76,7	0,6	1%	-60,5	2,8	5%	-53,3	0,9	2%	-45,7	0,9	2%	-74,9	0,7	1%	-38,8	0,6	2%
AOA =	15	-78,8	1,2	1%	-62,7	1,3	2%	-55,0	1,4	3%	-38,1	0,5	1%	-66,9	0,9	1%	-36,6	0,7	2%
AOA =	20	-82,0	5,3	6%	-68,6	3,9	6%	-59,5	2,2	4%	-29,4	0,6	2%	-59,2	1,2	2%	-34,6	0,8	2%

Flow Speed - V=10m/s																		
		Upper-front sensor			Upper-midle sensor			Upper-rear sensor			Botton-front sensor			Botton-midle sensor			Botton-rear sensor		
		P(1) [Pa]	s(1) [Pa]	s(1) [%]	P(2) [Pa]	s(2) [Pa]	s(2) [%]	P(3) [Pa]	s(3) [Pa]	s(3) [%]	P(4) [Pa]	s(4) [Pa]	s(4) [%]	P(5) [Pa]	s(5) [Pa]	s(5) [%]	P(6) [Pa]	s(6) [Pa]	s(6) [%]
AOA =	-20	-16,5	2,0	12%	-31,0	2,3	7%	-36,6	1,4	4%	-112,7	13,5	12%	-66,2	7,3	11%	-31,6	2,6	8%
AOA =	-15	-39,5	1,0	2%	-55,2	2,0	4%	-58,7	1,7	3%	-120,4	9,0	7%	-93,2	7,3	8%	-42,5	2,8	6%
AOA =	-10	-50,7	0,4	1%	-62,4	1,3	2%	-63,9	0,8	1%	-117,2	8,5	7%	-90,1	6,3	7%	-44,0	2,0	4%
AOA =	-5	-68,8	0,5	1%	-75,9	1,1	1%	-74,0	0,9	1%	-130,2	8,0	6%	-102,7	4,1	4%	-50,6	1,5	3%
AOA =	0	-74,1	0,6	1%	-72,0	0,8	1%	-67,4	0,8	1%	-104,2	8,7	8%	-97,8	1,7	2%	-47,7	1,0	2%
AOA =	5	-85,8	0,7	1%	-76,1	4,9	6%	-68,1	1,0	1%	-63,4	4,4	7%	-101,3	1,2	1%	-49,7	0,8	2%
AOA =	10	-94,6	0,7	1%	-76,5	1,1	1%	-66,6	1,2	2%	-57,0	2,7	5%	-94,5	1,0	1%	-48,8	0,8	2%
AOA =	15	-100,7	1,7	2%	-82,8	1,6	2%	-72,3	1,7	2%	-49,6	0,6	1%	-89,0	1,1	1%	-48,5	0,9	2%
AOA =	20	-104,2	6,2	6%	-88,2	5,4	6%	-76,5	2,8	4%	-37,5	0,7	2%	-77,6	1,3	2%	-44,8	1,0	2%